FINAL REPORT

DESIGN CONSIDERATIONS FOR INTEGRAL ABUTMENT BRIDGES IN FLORIDA

Submitted to:

Director, Research Center

Florida Department of Transportation

605 Suwannee St., MS 30

Tallahassee, Florida 32399-0450

CONTRACT No. BC - 342

By

Dr. M. Arockiasamy

Principal Investigator
Professor and Director
Center for Infrastructure and Constructed Facilities
Department of Ocean Engineering
Florida Atlantic University
Boca Raton, FL 33431

M. Sivakumar

Graduate Research Assistant

November 2003

1. Report No.	2. Government Accession No.	3. Recipient's Catalog No.
4. Title and Subtitle **Design Considerations for Integral Abutment Bridges in Florida**		5. Report Date **November 2003** 6. Performing Organization Code
7. Authors **M. Arockiasamy, and M. Sivakumar**		8. Performing Organization Report No.
Performing Organization Name and Address **Florida Atlantic University** **Center for Infrastructure and Constructed Facilities** **Department of Civil Engineering** **Boca Raton, Florida 33431**		10. Work Unit No. 11. Contracts or Grant No. **CONTRACT No. BC-342**
12. Sponsoring Agency Name and Address **Florida Department of Transportation** **605 Suwannee Street** **Tallahassee, Florida 32399-0466**		13. Type of Report and Period Covered **Final Report** 14. Sponsoring Agency Code **99500-7554-010, C-3654**
15. Supplementary Notes **Prepared in cooperation with the Federal Highway Administration**		

16. Abstract

Integral abutment bridges provide bridge engineers an economical and attractive design alternative to traditional bridges with thermal expansion joints. The study includes a comprehensive literature review of published information as well as existing practices adopted by the state departments of transportation. Analytical models and numerical procedures are developed for predicting instantaneous linear and non-linear time dependent long-term behavior of composite superstructures. The distributions of moments due to temperature change, prestressing, creep, shrinkage, and restraints provided by abutment foundation and backfill have been considered in the analyses. Illustrative numerical design examples are presented with emphasis on the pile-soil interaction with varying soil strata. Parametric studies of laterally loaded piles were made using LPILE and FB-Pier computer programs considering provision of predrilled hole, the type of fill in the predrilled hole, elevation of water table, soil type, and pile orientation. Recommendations are presented for the analysis and design of integral abutment bridges.

17. Key Words	18. Distribution Statement
Integral abutment bridges,. temperature, creep, shrinkage, non-linear time dependent behavior, laterally loaded piles	**No restrictions. This document is available to the public through the National Technical Information Service, Springfield, `Virginia 22161**

19.Security Classif. (of this report)	20. Security Classif. (of this page)	21. No. of Pages	22. Price
Unclassified	Unclassified	**173**	

Form DOT F 1700.7 (8-89)

DISCLAIMER

The opinions, findings and conclusions expressed in this publication are those of the authors who are responsible for the facts and accuracy of the data presented herein. The contents do not necessarily reflect the views or policies of the Florida Department of Transportation or the Federal Highway Administration. This report does not constitute a standard, specification or regulation.

The report is prepared in cooperation with the Florida Department of Transportation and the Federal Highway Administration.

ACKNOWLEDGEMENTS

The authors wish to express sincere thanks to Florida Department of Transportation (FDOT) for the financial support of the study. Grateful acknowledgements are due to Marc Ansley, P.E., Project Manager for the guidance and contribution to this study. They wish to express their appreciation to Dr. S. Nix, Professor and Chairman, Department of Civil Engineering, and Dr. Karl K. Stevens, Dean, College of Engineering, Florida Atlantic University for their continued interest and encouragement. In addition, the authors are grateful to N. Butrieng, graduate assistant for his assistance in the analysis and parametric studies.

SUMMARY

Provisions for longitudinal movement of bridges due to thermal expansion and contraction are made using a system of expansion joints, roller supports, and other structural releases. Integral abutment bridges provide bridge engineers an economical and attractive design alternative to traditional bridges with thermal expansion joints.

The study includes a comprehensive literature review of published information as well as existing practices adopted by the state departments of transportation. Analytical models and numerical procedures are developed for predicting instantaneous linear behavior and non-linear time dependent long-term behavior of composite superstructures used in integral abutment bridges. The distributions of moments due to temperature change, prestressing, creep, shrinkage, and restraints provided by abutment foundation and backfill have been considered in the analyses. Illustrative numerical design examples of integral abutment bridges are presented with emphasis on the pile-soil interaction with varying soil strata, temperature, creep and shrinkage effects. Parametric studies were made using LPILE and FB-Pier computer programs considering provision of predrilled hole, the type of fill in the predrilled hole, elevation of water table, soil type, and pile orientation. Based on the literature review as well as the analytical studies, recommendations are presented for the analysis and design of integral abutment bridges.

TABLE OF CONTENTS

CHAPTER 3

THEORY AND CONCEPTS

CHAPTER 4

NUMERICAL ILLUSTRATIONS AND DISCUSSIONS

CHAPTER 5

CONCLUSIONS AND RECOMMENDATIONS

LIST OF TABLES

CHAPTER 3

CHAPTER 4

LIST OF FIGURES

CHAPTER 1

CHAPTER 2

CHAPTER 3

CHAPTER 4

TABLE OF CONVERSIONS

To convert from	To	Multiply by
Length		
Inch (in.)	Millimeter (mm)	25.4
Foot (ft)	Meter (m)	0.3048
Area		
Square inch (sq. in.)	Square millimeter (sq. mm)	645.2
Square foot (sq. ft.)	Square meter (sq. m)	0.0926
Volume		
Cubic inch (cu. in.)	Cubic meter (cu. m)	0.00001639
Cubic foot (cu. ft.)	Cubic meter (cu. m)	0.02832
Cubic yard (cu. yd.)	Cubic meter (cu. m)	0.7646
Gallon (gal)	Liter	3.785
Force		
Kip	Kilogram (kgf)	453.6
Kip	Newton (N)	4448.0
Pound (lb)	Newton (N)	4.448
Pressure or Stress		
Kip/square inch (ksi)	Megapascal (MPa)**	6.895
Pound/square inch (psi)	Megapascal (MPa)**	0.006895
**One Pascal equals one Newton/square meter		
Mass		
Pound	Kilogram (kg)	0.4536
Ton (short, 2000 lb)	Kilogram (kg)	907.2
Mass (weight per length)		
Kip/linear foot (klf)	Kilogram/meter (kg/m)	0.001488
Pound/linear foot (plf)	Kilogram/meter (kg/m)	1.488
Pound/linear foot (plf)	Newton/meter (N/m)	4.593

CHAPTER 1

INTRODUCTION

1.1 Introduction

Traditionally, a system of expansion joints, roller supports, and other structural releases are provided on bridges to prevent damage caused by the longitudinal movement of bridges due to thermal expansion and contraction of the superstructure.

The joints and bearings are expensive to install and require constant maintenance. In due course, the water, debris, and seepage from deicing chemicals passing through them cause deterioration of superstructure as well as the joints. The clogged debris prevent the joints from free movement of the superstructure, causing damage and distress to the superstructure. Thus, expansion joints have negative economic impact on design and construction and all phases of highway-bridge service life.

In order to reduce the maintenance cost and avoid problems associated with bridge deck joints and improve the structural efficiency, integral construction is being used by many state

departments of transportation. Continuous deck bridges with joints only at abutments, called “jointless bridges”, and bridges with no joints even at the abutments called “Integral abutment bridges”, are two major types of integral constructions being adopted.

Integral abutment bridges accommodate superstructure movements without conventional expansion joints. Integral abutment bridges typically have its superstructure rigidly connected to the substructure with flexible substructure piling, permitting the superstructure expansion and contraction. Approach slabs are connected to the abutment and deck slab with reinforcement, and move along with the superstructure. At the junction with the approach pavement, the approach slabs are supported by a sleeper slab. If a sleeper slab is not utilized, the superstructure movement is accommodated using flexible pavement joints.

Some of the advantages of integral construction are better seismic resistance due to the continuity between superstructure and sub-structure developing higher energy dissipation and improved live-load capacity. Even though continuity will subject superstructures to secondary stresses, the damage and distress caused by the use of joints is more significant than the secondary stresses caused by continuity for short and medium span bridges. Construction of integral abutment bridges is simpler and less time consuming. Conversion of existing jointed bridges into jointless bridges has been successful and shown to improve the performance of the bridge.

The disadvantages associated with integral constructions are the effects of connections at integral abutments. Integral bridges may operate at very high stress levels that cannot be

quantified easily. Only very limited design and construction specifications are available in the American Association of State Highway Transportation Officials Specifications for Highway Bridges (AASHTO). There are no unified design guidelines or procedures available nationwide to follow and hence lack of enthusiasm for using integral abutment bridges for long spans. The integral bridges differ from regular rigid frame bridges in the manner of distribution of stresses due to temperature change, prestressing, creep, shrinkage, and restraints provided by abutment foundation and backfill. States that use integral abutments rely on their own experience, empirical formulae, and simplified design assumptions rather than theoretical calculations to limit span lengths.

1.2 Background

The integral abutment bridge concept is based on the theory that thermal stresses are transferred to the substructure by way of a rigid connection between the superstructure and substructure and thermal movements are accommodated by the flexibility of the piling. A connection at the ends of the girders is provided by rigidly connecting the girders by encasing them in reinforced concrete abutment. This provides a full transfer of forces due to temperature variation and live load rotational displacement to the abutment piling.

In order to analyze the integral abutment bridges, important parameters that influence the behavior and performance need to be identified and studied. The following are some of the vital and basic parameters:

- Effects of superstructure – substructure connection,

- Effects of time dependent concrete creep, shrinkage, temperature,
- Effects of soil properties, types of foundation, soil settlement, and connection details between the foundation and the abutment,
- Effect of approach slab and its connection to the abutment, and
- Effect of approach slab and the pavement connection

Fig. 1.1 shows the details of cross section of a typical integral abutment bridge. The typical cross section of integral abutment is shown in Fig. 1.2.

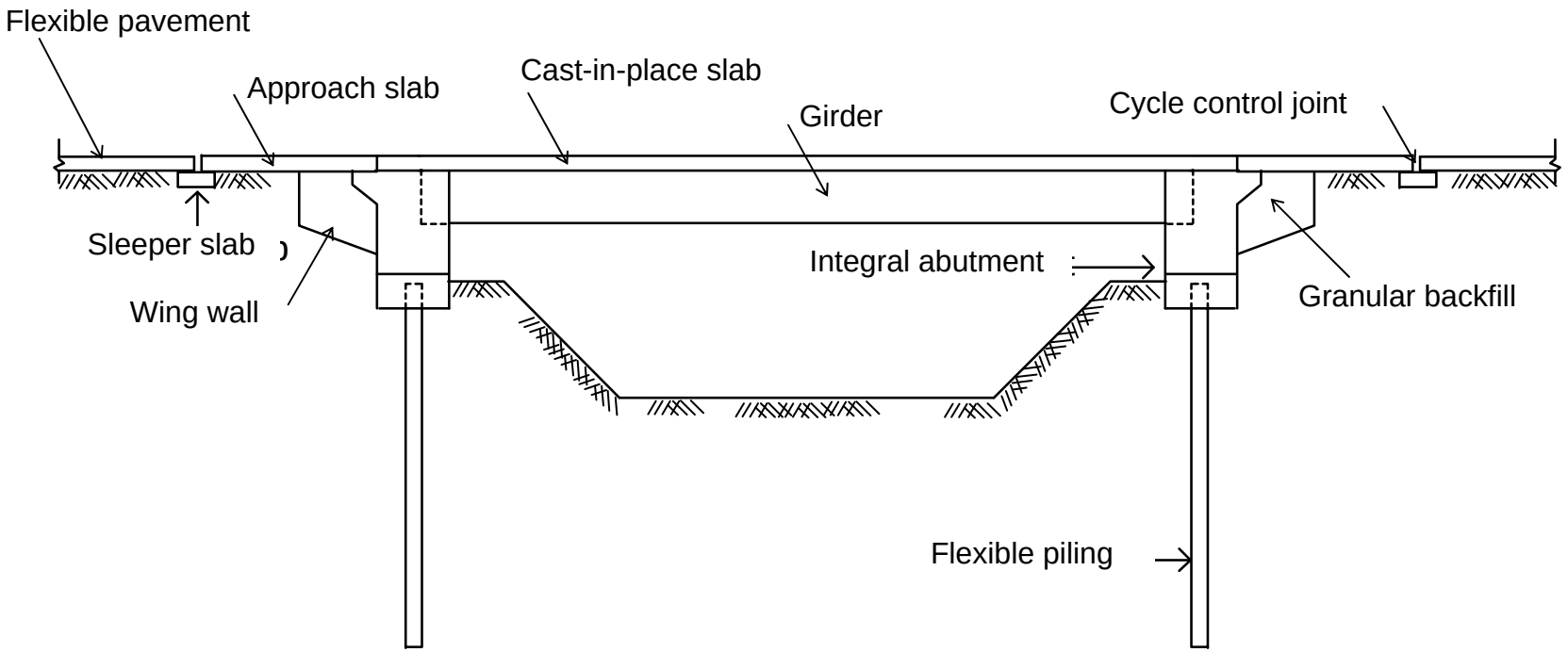

Fig. 1.1 Cross section of integral abutment bridges

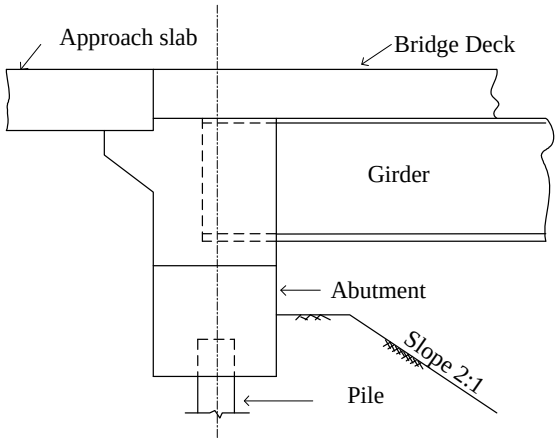

Fig. 1.2 Typical cross section of integral abutment

1.3 Objective and Scope

The objective of this study is to identify the design considerations for integral abutment bridges. The following are the scope of the present investigation:

- Literature review including the existing methods of analysis and design adopted by the various State Departments of Transportation.
- Temperature effects in the movement of integral bridges
- Creep and shrinkage effects
- Evaluation of abutment stiffness, soil pressure, pile capacity and analysis of laterally loaded piles
- Development of analysis and design procedures

A detailed research on various aspects that influence the behavior of integral abutment bridges were conducted at the Center for Infrastructure and Constructed facilities, Florida

Atlantic University. The current practices adopted by various State Departments of Transportation (State DOT) are evaluated to arrive at a rational design procedure for integral abutment bridges. An analytical model and numerical procedure are developed to predict instantaneous linear behavior and non-linear time dependent long-term behavior of uncracked and cracked composite superstructures used in integral abutment bridges. Partial rigidity provided by the substructure system is included in the analysis by modeling the abutment-wingwall-pile substructure system using discrete springs for translational and rotational degrees of freedom. Illustrative numerical design examples of integral abutment bridges are presented with emphasis on the pile-soil interaction, temperature, creep and shrinkage effects and varying soil strata. A parametric study was conducted on the important design parameters that were identified concerning the selection and design of pile, use of predrilled hole, the type of fill in the predrilled hole, elevation of water table, soil type, and pile orientation. The effect of these parameters was analyzed using LPILE and FB-Pier computer programs.

1.4 Report Organization

Chapter 1 deals with the introduction, objectives and scope of the research on the integral abutment bridges. Some of the important advantages and disadvantages associated with the integral bridges are stated in this chapter along with the vital parameters that influence the behavior of integral abutment bridges. **Chapter 2** reviews the available literature regarding the assumptions made in the design and current practices adopted for the construction of integral abutment bridges by various state departments of transportation. **Chapter 3** discusses the theory and assumptions involved in the analyses of integral abutment bridges, in particular the

superstructure – abutment – substructure interaction, creep, shrinkage and temperature effects, behavior of laterally loaded piles. Detailed numerical illustrations on the analysis and design of a typical bridge for the creep, shrinkage and temperature effects on superstructure and laterally loaded piles based on the rational design procedure is presented in **Chapter 4**. A summary of the results of the parametric studies on laterally loaded piles is also presented. **Chapter 5** presents the design considerations and recommendations.

CHAPTER 2

LITERATURE REVIEW

2.1 Introduction

Bridges must be designed to accommodate the movements and stresses caused by thermal expansion and contraction. In general, bridge designers accommodate these movements by using bridge deck expansion joints and expansion bearings. Use of deicing chemicals to maintain dry pavements throughout the winter season has a significant effect on the durability and integrity of bridges built with deck joints. Joints allow deck drainage, contaminated with deicing chemicals and wash over supporting beams, on to the bearings and bridge seats. The resulting corrosion and deterioration was serious enough that some bridges have collapsed and others had to be closed to traffic to prevent their collapse (Burke, 1990). Maintenance problems that have developed at the movement of joints and bearings of bridges have often been far worse than the problems they were intended to avoid (Loveall, 1985).

Single and multiple span continuous jointless integral abutment bridges have been used to overcome these shortfalls. Integral abutment bridges are constructed as a rigid connection of the deck and primary support members of the superstructure to a pile supported substructure (NY DOT, 1999). These bridges have no movement joints between the deck and the abutments or between spans. The justification for jointless integral bridge construction is based on the recognition that for short and medium span bridges more damage will occur in terms of problems associated with bearings due to the provision of deck joints than by the secondary stresses caused by thermal expansion and contraction (Burke, 1989). Integral bridges receive very high rankings on economic grounds and are strongly recommended for 60-ft and 100 ft span ranges (Gangarao, 1988).

Advantages

In addition to the maintenance free structure, integral bridges provide added redundancy and capacity for all types of catastrophic events. Tests in Japan have demonstrated that significant improvements in damping capacity are realized when integral abutments are used. When abutments move rapidly, passive pressure that develop absorbs significant amounts of energy. This mobilized damping force is increased by the soil/pile interaction and remains effective throughout each full cycle of seismically induced movement (Kunin, 2000). A comparative study has been made on integral abutment bridges vs armored compression-seal joints bridges (Wasserman, 1996). It has been shown that jointless bridges have better performance records than those with conventional joints. It confirms that integral bridges and jointless decks are preferable to conventional bridges wherever possible. Integral abutment

bridges provide fixity between the superstructure and substructure, and provide greater protection against translation and uplift than conventional bridges (NJDOT 1987). Current design and construction practices have been reviewed and presented in a state-of-the-art of integral abutment bridges (M. Arockiasamy et al., 2003).

A comprehensive review of published literature and the reported surveys concerning the use of integral abutment bridges is made to identify the factors considered in the design practices currently followed in the US.

Components of integral abutment bridges

The integral abutment bridges do not have an expansion joint between the abutments and the bridge superstructure. Typical integral abutments are shown in Figs 2.1-1 – 2.1-3.

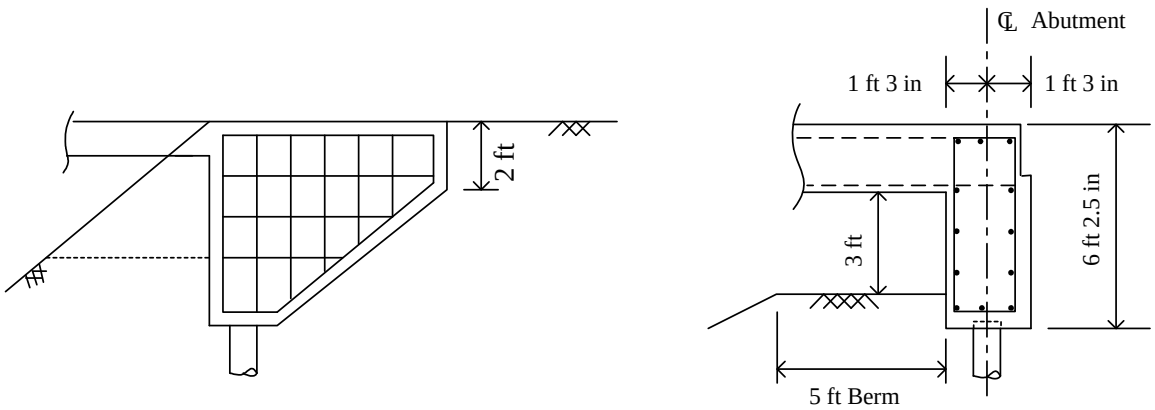

Slab bridge

Fig. 2.1-1 Solid slab integral abutment

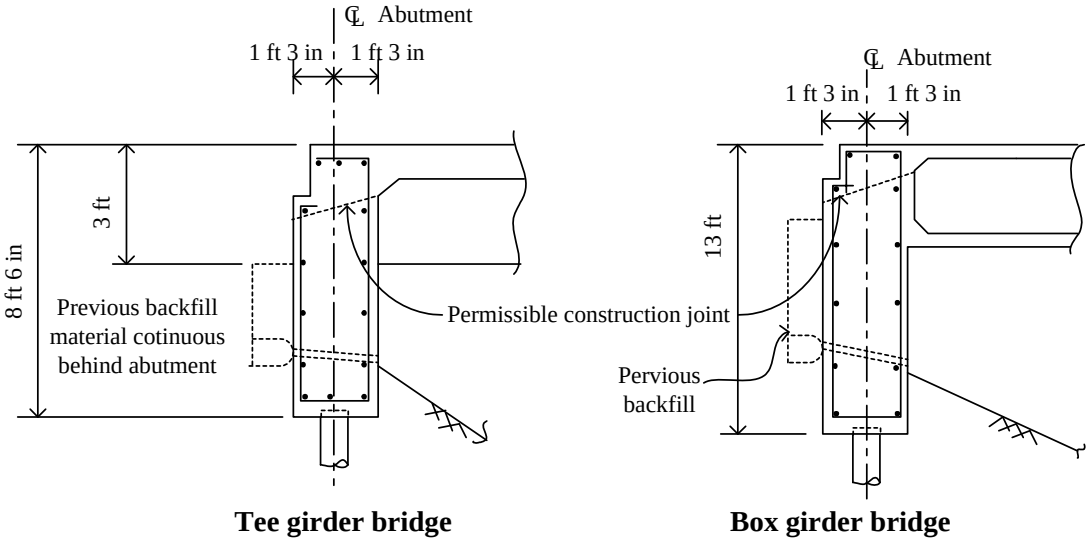

Fig. 2.1-2 Cast in place concrete (California DOT)

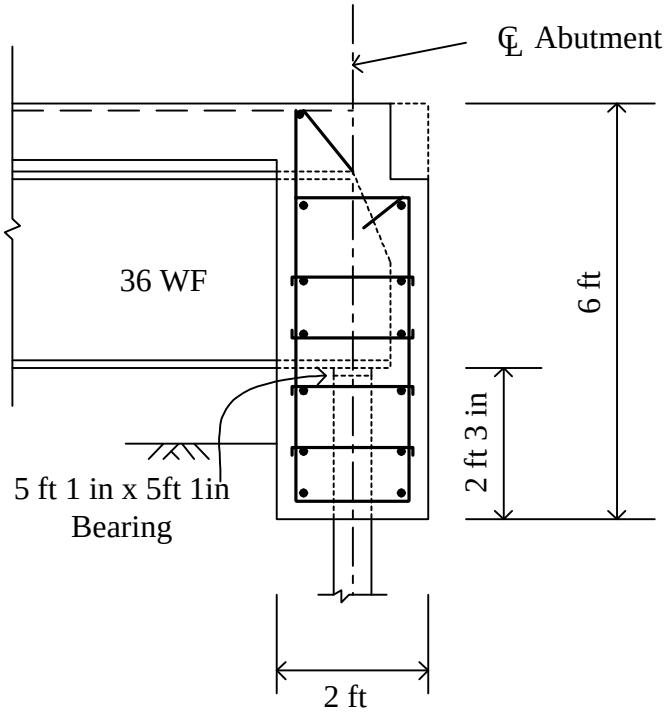

Fig. 2.1-3 Steel girder integral abutment bridges (Missouri DOT)

Bridge movements caused by the thermal expansion or contraction and concrete creep and shrinkage induce bending stresses in the piling that supports the abutments, which must be resisted by the bridge and its substructure (Abendorth, 1989). The concrete abutment contains sufficient bulk to be considered as a rigid mass. A positive connection with the ends of the beams or girders is provided by rigidly connecting the beams or girders and by encasing them in reinforced concrete; thus, the bridge girders are rigidly connected to substructure. This provides for full transfer of temperature variation and live load rotational displacement to the abutment piling (NJDOT, 1987). Therefore, the substructures must absorb thermally induced movements of the superstructure. The supporting foundation, therefore, has to be flexible enough to accommodate superstructure deformation due to volume changes caused by temperature, creep and shrinkage (Kamel, 1996). The required flexibility is provided by the use of a stub abutment supported by a single row of piles. Essentially all lateral and longitudinal loads applied to the superstructure of integral bridges are distributed directly to abutment.

Approach slabs, also called as run-on slabs, are needed to span the area immediately behind integral abutments. The approach slab spans over the backfill that is affected by passive movements, and it prevents traffic compaction of material, where the fill is partially disturbed by abutment movement. The uncompacted backfill behind abutments can yield passively during thermal expansion while still providing sufficient resistance to longitudinal braking forces. Different types of backfill used by various states include granular, cohesive, pervious, roadway fill, free draining granular fill, and select granular fill (Wolde-Tinsae, 1988). Approach slabs are anchored with reinforcing steel to the abutment and superstructure (Hambly, 1997) so that they move with the abutments during thermal and volume changes due to shrinkage and creep.

Parallel, flared, and U type wing walls are the different types of wing walls adopted for integral abutment bridges. The size of structures that must move with integral abutments shall be kept to a minimum. They are either poured monolithically with abutment or rigidly connected to abutment with reinforcement. Active and passive earth pressures are considered in designing the wing wall (Kunin, 2000).

Piers are the elements in bridge structures that transmit the loads from the superstructure to the foundation. The type of selection of pier depends on the form of the superstructure, clearance requirements, soil conditions and aesthetics. If the situation warrants, piers also can be made integral with the superstructure. Integral piers are more redundant and aesthetic than conventional piers. It also eliminates one row of bearings (Tabsh, 1996).

Composite deck, either prestressed concrete girder system with cast in place deck or steel stringers with cast in-situ deck slab constitutes the superstructure. In some states existing bridges with simply supported spans have been made continuous to become integral bridges by simply filling the gaps between the ends of the beams with concrete and adding a continuous reinforced overlay to the deck slab (Hambly, 1997).

2.2 Factors Influencing the Behavior of Integral Abutment Bridges

In addition to the primary effects due to dead load, live load, etc., integral bridges are subjected to secondary effects due to

- creep and shrinkage,

- thermal gradients,
- differential settlement and differential deflections,
- pavement relief pressures when moisture and sustained high temperatures trigger pavement growth, and
- soil-pile interaction

2.2.1 Creep and Shrinkage

Both creep and shrinkage are time dependent. Creep and shrinkage effects are important parameters in integral abutment bridges. Since integral abutment bridges do not have joints at abutment or along its span, the axial shortening and rotation at the girder ends will induce stresses in the continuous deck. The season when concrete is cast and loaded, cement type, concrete composition, and size of the member affect creep and shrinkage of concrete. Creep is a source of inelasticity in concrete (Samra R.M., 1997). Creep and shrinkage are commonly thought of as components that introduce forces into a structure, but they can also act as relieving mechanism for stresses developed from thermal gradients. Fig. 2.2-1 shows the distribution of moment and axial forces along the span of continuous composite bridge due to differential shrinkage and creep. The interaction of creep and shrinkage with temperature and humidity variations may aid in relieving stresses caused by annual temperature variations. Shrinkage partially offsets the effects of creep, passive pressure, and thermal gradients (Loveall B.M., 1985).

Shrinkage creates shear forces between old and new members thus producing axial forces and bending moments. Shrinkage has its effects more on positive moments of single span and on continuity connection at abutments of continuous span than on negative moments at piers.

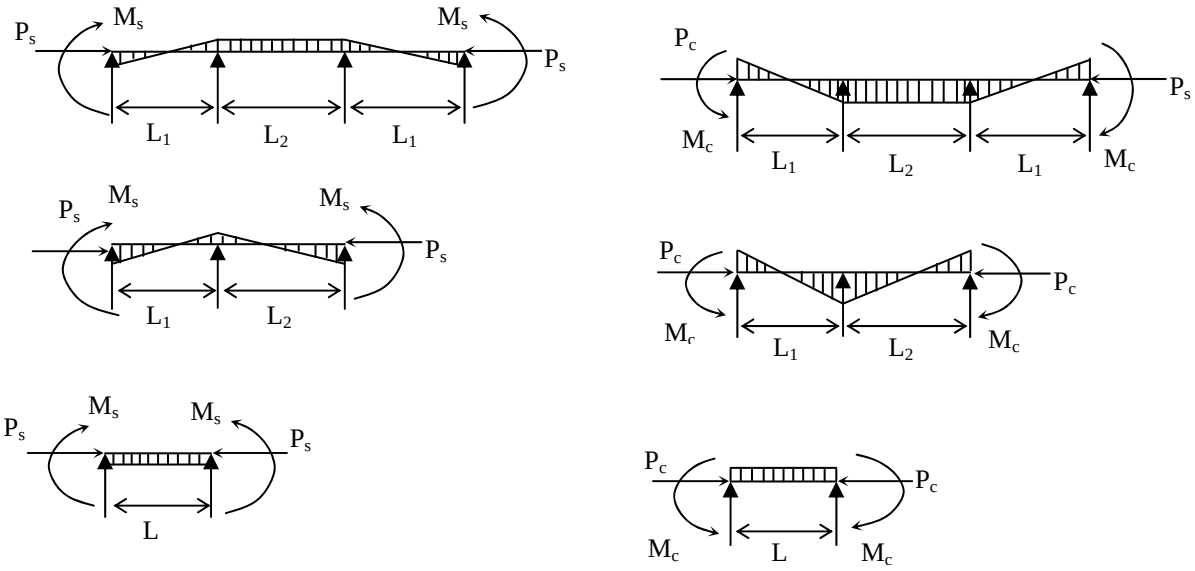

(a) (b)

Fig. 2.2-1 Shrinkage and creep effects in single and multispan continuous integral bridges; a) differential shrinkage effects of composite concrete bridges; b) creep effects for composite prestressed concrete bridges

A method based on incremental analysis of the behavior of viscoelastic composite member is presented for the numerical analysis of creep, shrinkage and relaxation in concrete bridges using classic finite beam element (Desterbecq, 2001). Time dependent viscoelastic analysis procedure for composite steel-concrete beams with flexible shear connectors is presented including the slip at the steel-concrete interface (Tarantino, 1992, Dezi, 1993). The stress in the concrete slab depends on the stiffness of the connection system. Due to creep and

shrinkage, the shear force per unit length on the connectors tends to decrease with time, but the stiffness connectors have less influence on the deflections. An interaction between creep, shrinkage and slip is reported by Bradford (1991, and 1992). Smeared finite element model is proposed based on an improved cracking criterion, which is derived from principles of fracture mechanics. It is concluded that bond-slip increases with loading, while tension stiffening does not and hence both effects are to be included to get consistent results. Effect of bond-slip outweighs the contribution of tension stiffening in heavily reinforced concrete members (Hyo-Gyoung, 1997).

Bradford (1989) Gilbert (1995) used a simplified approach to evaluate creep and shrinkage effects in steel-concrete composite beam with rigid or deformable connections, based on the age-adjusted effective modulus to model the constitutive material relationship for concrete. Aging coefficient, χ is introduced in the method. It was demonstrated that residual stress of typical magnitudes result in increased curvatures and decreased stiffness, but only at sustained loads close to that causing first yield of the joist. Generally at typical service loads, the effects of creep and shrinkage will dominate the reduction in stiffness, with the effects of residual stress being only minor An analytical model with layer approach is used to account for the variation in the material property across the section (Hyo-Gyoung, 2000). An analytical model and numerical procedure was presented to predict instantaneous linear and non-linear time dependent long-term behavior of composite superstructure in integral abutment bridges (M.Sivakumar and M. Arockiasamy, 2002).

Consideration of the geometric and material nonlinearities allows the structural response to be traced through the elastic, cracked, and ultimate load level, providing valuable information about the influence process on the short- and long-term carrying capacity of the structure. Step-by-step model for the nonlinear and time-dependent analysis of reinforced concrete, prestressed concrete and composite steel-concrete planar frame structures, traces the structural response during the construction of the structure and throughout its service life (Cruz, 1998).

A three dimensional model is developed and utilized for nonlinear creep and shrinkage analysis of composite integral bridges. The rate of creep method is employed. The results are compared with two-dimensional model based on age-adjusted modulus. The results show that creep stresses are smaller in steel component compared to concrete, which is about 26-49 % of dead load stresses. Creep causes a small increase in positive stresses at the bottom of steel stringers and a reduction in the tensile and compressive stresses at the top of concrete deck. This reduction in compressive stress may reverse them into tensile, in which case steel reinforcement is necessary at the top in the deck slab (Siros K.A and Spyrakos C.C, 1995).

2.2.2 Thermal Gradients

Thermal movements in the bridge structure cause serious problems, if not adequately considered in the design and maintenance of the bridges. Skewed bridges sometimes display transverse as well as the longitudinal movements for which they are designed (Roeder, 1990). The uncertainty of the direction of movement in some curved and skewed bridges provides increased incentive for the engineers to use integral construction or other forms of jointless

construction. One such example is the bridge carrying Tennessee State Route 50 over Happy Hollow Creek (PCI, IB-01).

Temperature distribution in the bridge is obtained based on three basic heat flow components, namely, radiation, convection, and conduction. The parameters that influence the temperature distribution in the bridges are cloud cover, air temperature, wind speed, the solar position angles, the orientation of the structure with respect to the sun, and the geometry and materials of the bridge.

One-dimensional models are adequate for many slab-girder bridges. Concrete box girder bridges or concrete girder bridges with thick beam webs may require a two dimensional heat flow model to accurately estimate the temperature distribution within the bridge. Three dimensional heat flow models are required only in very unusual circumstances where the temperature is expected to vary significantly along the length of the bridge. Skewed or curved bridges required the refined methods much more frequently than straight bridges (Moorty and Roeder 1992).

Temperature gradients through the depth of the bridge beams generate secondary bending moments due to the fact that the centroid of the temperature distribution curve and the centroid of the cross-section of the bridge beams may not coincide. The most important factors in the temperature distribution through bridge beams are

- the maximum temperature differential and
- the distribution of this differential across the depth of the beams.

Moments induced by thermal gradients are similar to those due to shrinkage and creep. However, the direction depends on the ambient temperature (Burke, 1993). Most of the state agencies refer to AASHTO article 3.16 to determine the temperature ranges and use the following equation to estimate thermal movement (Kunin, 2000):$\Delta l = l\,\alpha\,\Delta t$.

Where, Δl = change in length, l = length of the bridge, α = coefficient of thermal expansion and Δt = change in temperature.

Employing two-dimensional finite element analysis, Elbardy and Ghali (1983) show that bridges with larger depths have larger eigen stresses. Churchward and Sokal (1981) described a three-year experimental program aimed at finding the vertical temperature gradient across sections of a prestressed post tensioned concrete bridge. Attempt has been made to establish analytical criteria for prediction of average temperatures, which are responsible for the longitudinal deformation of the bridge and the vertical differential temperature profiles responsible for the bending deformations in the vertical plane.

Lawver (2000) evaluated the field performance of integral abutment bridge. The effects from the environmental loading due to solar radiation and changing ambient temperature were found to be as large as or larger than live load effects. The abutment was found to accommodate superstructure expansion and contraction through horizontal translation instead of rotation. The abutment piles appeared to be deforming in double curvature, with onset of yielding.

2.2.3 Differential Settlements and Deflections

Settlement of abutments of multiple span integral bridges induces bending moments similar to those induced by shrinkage. Settlement of piers induces moments similar to those induced by creep. Integral bridges should not be used unless the probability of appreciable abutment settlement is remote (Burke, 1993 and Arsoy et.al., (1999). AASHTO (1994) provides simple procedures to estimate differential settlements.

2.2.4 Pavements and Pavement Pressure Relief Joints

The kernel of integral bridge design is the abutment/ backfill/ pavement interface. The strained growth of all jointed rigid pavements can generate irresistible longitudinal forces. Since the longitudinal compressive force will be transmitted to the bridge through the approach slabs, it will be eccentric with respect to the composite neutral axis of the superstructure and will induce bending moments throughout the superstructures similar to those due to shrinkage (Burke, 1993) When integral bridges adjoin concrete pavements, movement joints have to be inserted between the deck and the highway pavement in order to accommodate longitudinal movements of the bridge to protect bridge superstructures. If there are no joints, the thermal expansion of the deck can cause very high thrusts within the concrete pavement and possibly bursting (Hambly, 1997). A case of severe abutment damage was documented for a bridge without pressure relief joints. The numerical stress analysis indicated that the damage was caused by the longitudinal growth of continuous reinforced concrete pavement, causing excessive longitudinal pressures on the abutments. Increase in internal stresses in the approach slabs has been reported as the main cause

of bridge failures in some bridges (Soltani, 1992). Pressure relief joints, such as asphaltic plug joints provided in bridge approaches can accommodate movements occurring between concrete abutments and flexible pavement. Pavement pressures transmitted through these joints should be considered in the design of the superstructure (Burke, 1993).

2.2.5 Soil-Pile Interaction

Piles in integral abutment bridges are subjected to lateral movement due to thermal expansion and contraction of the superstructure. This leads to reduction in vertical load-carrying capacity of the pile. The behavior of the soil-pile interaction for a laterally loaded pile is non-linear. The laterally loaded pile may be modeled as an equivalent beam column without transverse loads between the member-ends and with a base fixed at a specific soil depth. Either a fixed head or pinned head for the beam column approximates the actual rotational restraint at the pile head (Abendroth, 1983).

2.3 Design Considerations

2.3.1 Abutment

Although the majority of bridges with integral abutment bridges perform adequately, many of them operate at high stress levels. Some failures of continuous concrete frame bridges are attributed to its stiffness and resistance to shrinkage and contraction of the bridge deck. Failures of this type emphasize the necessity of achieving flexibility in substructure design and

conservative reinforcement to withstand secondary stresses induced by foundation restraint and superstructure shortening (Burke, 1990). Abutment stiffness must be considered, because the large horizontal movement of a structure at the abutments tend to be more damaging to bridge superstructures. In the abutment and pile design, it is assumed that the girders transfer all moments and vertical and horizontal forces that are produced by the superimposed dead load, live load plus impact, earth pressure, temperature, shrinkage, creep and seismic loads. The transfer of the forces shall be considered to be achieved after the rigid connection to the abutments is made. The rigid connection shall be detailed to resist all applied loads (NJDOT, 1987).

2.3.2 Pile Behavior

The ability of the piles to accommodate lateral displacements is a significant factor in determining the maximum possible length of integral bridges. In order to build longer integral bridges, pile stresses should be kept low. Steel, timber, concrete cast in drilled holes, concrete cast in thin steel shells, and precast concrete piles are used in integral abutment bridges. Most of the states prefer to use steel H-piles. To reduce flexural resistance of piles to lateral movement, the piles are often oriented for weak axis bending and placed in predrilled holes filled with fine sand or pea gravel or a cohesive mud (which flows under long term creep shortening) (Colorado DOT) to better accommodate bridge displacements (Burke, 1993). The pile stresses are assumed to be relieved that may permit longer allowable lengths of integral abutment bridges. However it is interesting to note that most of the states do not use predrilled holes. For a given deflection, weak-axis bending generates smaller stress in the piles than with strong-axis bending, but

Washington State DOT typically alternates pile orientation from one pile to the next pile (Kunin, 2000).

Full continuity is assumed at pile abutment connection. Consequently, bending moments high enough to initiate plastic yielding of steel piles are produced at the pile ends due to temperature variations and live loads (Emmanuel, 1978, Loveall, 1985, Burke, 1987, Abendroth, 1989, and Girton, 1991). Repetitive temperature cycle and effect of live load may cause additional fatigue in piles (Burke, 1989). A hinge connection between pile and abutment may prevent such a potentially destructive problem (Dicleli, 2000). The assumption made by the different state transportation agencies include various boundary conditions for the pile-abutment joint: – hinged, partially restrained, fixed, free translation, free rotation, and roller (Wolde-Tinsae, 1988).

Abendroth et.al., (1989) presented two design alternatives for the pile capacity. Alternative one, involving elastic behavior, is recommended for piles with insufficient moment-rotation capacity, while alternative two, based on inelastic behavior, is recommended for piles having a moment-rotation capacity that exceeds the moment-rotation demand at plastic hinge locations.

Alternative one accounts for the stresses induced in the pile caused by thermal expansion or contraction of the bridge superstructure. This design alternative is based on elastic behavior and neglects plastic redistribution of internal forces. Failure is assumed to occur when any internal stress reaches the yield value. Therefore, unlike the plastic collapse theory, alternative

one can be expected to show a dramatic reduction in member strength associated with lateral displacement of the pile head.

Alternative two was developed to permit plastic redistribution of forces induced by thermal movements. Applying first-order plastic theory, the stresses in the pile due to longitudinal displacement of the bridge superstructure are neglected. However, the strains induced by this movement are considered and must satisfy a pile ductility requirement. Also, for fixed-headed piles, the pile flexural stresses and rotations caused by the gravity loads are considered in the evaluation of the pile strength. When the design of an abutment pile in an integral abutment bridge is governed by the capacity of the pile as a structural member, alternative one is recommended for piles that have limited ductility, such as timber, concrete, and steel sections having insufficient moment-rotation capacity. Alternative two is recommended when the piles have a moment-rotation capacity that exceed the moment-rotation demand at the plastic hinge locations. The ductility requirements for alternative two are specified. When the piles have sufficient ductility, alternative two will permit the safe design of integral abutment bridges with longer span than those designed using alternative one.

A detailed parametric study was reported considering provision of predrilled hole, the type of fill in the predrilled hole, elevation of water table, soil type, and pile orientation (M. Arockiasamy et al., 2003). Kamel et al., (1996) conducted a feasibility study of using precast, prestressed concrete piles in jointless bridges The results showed that concrete piles have limited flexibility for lateral loads with current pile-abutment details, so they can be used only in short span integral abutment bridges. Greimann and Wolde-Tinse (1988) presented a simplified design

method for analyzing piles in integral abutment bridges. Two failure modes are examined for a pile: i) the slip mechanism, where the pile slips through the soil; and ii) the lateral mechanism where the failure of the soil-pile system is associated with lateral movement of the pile. The design method gives conservative results for the ultimate load capacity of the pile. Only structural integrity of the pile is considered in the design. The effects of the abutment movement on the approach slab and fill, and the effects of the induced axial stresses in the superstructure are not included in this study. It was suggested that these factors have a relatively small effect on shorter bridges and for long bridges with integral abutments.

Kunin (1983) discussed a field study of the behavior of abutment piles in an integral bridge due to thermal movement. The study concluded that these changes did not result in equal abutment movements at each end of the bridge, and the maximum abutment movements resulted in stresses at the top of the piles sufficient to initiate yield stress in the steel but not sufficient to form a plastic hinge. An analytic model was used to predict stresses in the abutment piles due to thermal movement of the abutment. The two parameters that have the most influence on the pile stresses are the amount of abutment movement and the modulus of subgrade reaction near the upper portion of the pile.

2.3.3 Approach Slab

The approach system of an integral bridge consists of the backfill, the approach fill, and the foundation soil. An approach slab and a sleeper slab, if used, are also part of the approach system. Both jointed and integral bridges are vulnerable to differential settlement between the

approach system and the bridge abutment. This problem is often referred to as the "bump at the end of the bridge". Causes for the bump problem, include the following (Briaud, 1997):

- Compression of the fill material,
- Settlement of the natural soil under the embankment,
- Poor construction practices,
- High traffic loads,
- Poor drainage,
- Poor fill material, and
- Loss of fill by erosion

The "bump" problem is further complicated for integral bridges by the cyclic compression and decompression of the backfill due to temperature cycles. When approach slabs are used, a void between the backfill and the abutment is likely to develop as the abutments move back and forth. The "bump at the end of the bridge" is pushed out to the end of the approach slab, when approach slabs are used (Schafer, 1992).

The intended functions of approach slabs are (Briaud, 1997) the following:

- span the void that may develop below the slab,
- provide a ramp for the differential settlement between the abutment and the embankment and
- provide a better seal against water percolation and erosion of the backfill material.

It is often argued that the length of the zone of surface deformation extends from the abutment a distance equal to twice the height of the abutment, and that the approach slab, should be made two to three times the height of the abutment. This argument is based on the fact that displacing an abutment causes movement of a wedge of the backfill with a height equal to the height of the abutment and a length equal to tan $(45+\phi/2)$ times the height of the abutment, which is about twice the abutment height, where ϕ = soil friction angle.

The approach slab must be anchored into the abutment back-wall so that it moves in concert with the bridge as shown in the Fig 2.3-1. Otherwise, cyclic expansions force the slab to move with the bridge without a mechanism to pull it back when the bridge contracts. As debris fills the resulting opening, repeated cycles will ratchet the slab off its support. The anchorage used to fasten the approach slab should be detailed to act as a hinge so that the slab can rotate downward without distress as the embankment settles (AISI, 1996). In some states, the approach slabs are tied to the abutment with dowels, and hence moves back and forth with superstructure, whereas approach slab is provided only for bridges greater than 200-ft.long in certain other cases. Some states detail reinforcing steel connecting corbel or lip of the abutment to the approach slab. In some cases, approach slabs simply rest on the corbel or lip. Approach slabs shall always be a separate pour from the superstructure slab, but shall be joined together. The approach slab shall be cast on two layers of four mil thick polyethylene sheets. It shall be designed as a structural slab that is supported at each end. The excavation for the sleeper slab shall be made after the compacted abutment backfill is placed. The sleeper slab shall be founded on undisturbed compacted material. No loose backfill may be used (NJDOT, 1987).

The three expansion control methods include i) expansion joint at the far end of the approach slab, ii) joint between the abutment and approach slab, and iii) no expansion joints at any place (Kunin, 2000). Some European countries do not provide approach slab (Hambly, 1997).

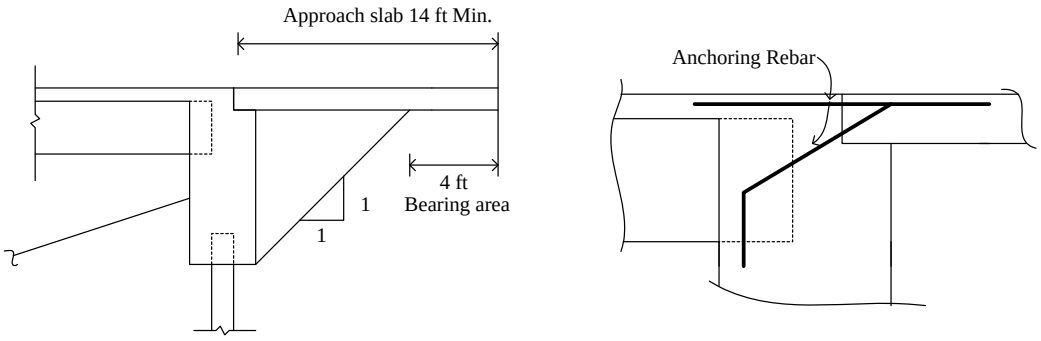

Fig. 2.3-1 Approach slab

2.3.4 Backfill Earth Pressure

When the bridge contracts due to decrease in temperature, abutment will be subjected to active earth pressure. When there is an increase in temperature, passive pressure will develop. Depending on the magnitude of temperature induced displacement of the abutments, earth pressures can be as low as the minimum active or as high as the maximum passive pressures. The mode of displacement of the abutment involves both translation and rotation. Experiments conducted by Thomson and Lutenegger (1998), and Rowe (1954), show that both the deformation mode and the magnitude of the deformation affect the magnitude and distribution of the earth pressure.

Some agencies assume active pressure for contraction and passive for expansion. Some states do not consider earth pressure at all but some others take into account earth pressures only for certain larger size abutments. Uniform, triangular, and Rankine load distributions are used in design for soil pressure. Many bridge engineers prefer to use Rankine or Coulomb passive pressure theories because of their simplicity. Rankine and Coulomb passive pressure calculations are conservative for bridge abutment applications. A study by Oesterle, (1998) reported that Rankine passive pressures are in good agreement with experiments. Occasionally, the actual passive earth pressures can exceed the design values as in the case of 98-meter long bridge located in Virginia (Hoppe, 1996). It was reported that the bending moments induced by passive pressures on abutments counteracted the dead and live load bending moments in simple spans. Therefore, overestimating passive pressures is not a conservative approach for such bridges.

The porous granular soil is generally used as the backfill. The selection of this type of backfill has two advantages of easy compaction in close spaces, and drainage of water away from the abutments. Well-graded material is desirable. Uniformly graded material does not compact well and provides less interlocking of particles, thus acting more like marbles (AISI, 1996). Some state DOTs use loose, uncompacted back fill, which in some cases attributed to settlement of sleeper slabs. Illinois reports excellent results using uncompacted, porous, granular embankment with an underdrain. Some states used a soil reinforced fill with gap at the structure wall. High-density foam backing is also used in one bridge (Kunin, 2000). As the backfill is acted upon for several cycles, the backfill becomes remolded. Several structures with tall integral abutments have been built with a gap between the abutment and reinforced fill to reduce earth pressures (Colorado DOT).

The ultimate or maximum passive pressure P_{pu} generated in abutment back fill at a depth H due to bridge elongation and backfill compression can be idealized as

$$P_{pu} = \gamma \tan^2\left(45 + \frac{\phi}{2}\right) H + 2c \tan^2\left(45 + \frac{\phi}{2}\right) \quad \text{.....(2.3-1)}$$

where:

P_{pu} = ultimate passive pressure (psf [N/m^2])

γ = unit soil weight (pcf [N/m^3])

ϕ = angle of internal friction (degrees)

H = depth below approach slab (ft. [m])

c = soil cohesion (psf [N/m^2])

Total passive pressure on the structure will depend on the area of abutment exposed to pressure and hence the depth of abutment H is made as small as possible. Granular fill is specified to minimize ϕ values. Magnitude of passive pressure is related to the magnitude of soil compression. Approach slabs are used to minimize consolidation of back fill and eliminate live load surcharge on backfill (Burke, 1993).

The orientation of the wing-walls can also affect the magnitude of the passive earth pressures. Tests by Thomson and Lutenegger (1998) showed that turn-back (U shaped) wing-walls result in greater earth pressures than transverse wing-walls. This suggests that transverse wing-walls could be used to reduce the magnitude of passive pressures. The turn back wing-wall cantilevered off from the abutment with no special foundation support has the advantage that it reduces approach fill settlements. When the required wingwall length exceeds the length for a

practical wing cantilevered off the abutment, a retaining wall shall be used along with a nominal length of cantilevered wing to provide the needed wingwall length (Colorado DOT).

2.3.5 Intermediate Piers

Piers are designed only for vertical superstructure, pier loads and lateral loads that may be applied directly to the piers assuming that the unbalanced horizontal soil pressure forces resulting from unsymmetrical configurations, if any, are transferred directly to the approach embankments with no effects on piers. But this assumption holds good only for structures that are fully symmetrical and the soil pressure at both sides are in equilibrium (Burke 1993, Husain, 1996).

2.3.6 Superstructure

Adjacent prestressed box beams, prestressed concrete girders and structural steel beams may be used as superstructure. The bridge deck is designed treating integral bridge as a continuous beam with simply supported ends. To accomplish continuity, in a prestressed girder bridge, a common diaphragm is used to join both the ends of the girders in adjacent spans and cast in place slab. New continuity details using high strength threaded rods are developed to connect the simple girders and make it continuous (Ma, 1998, Saleh, 1995). The deck is modeled as a continuous frame only for the design of deck-abutment joints. Piers and abutments are replaced with simple supports thus eliminating continuity of the structure at the deck-pier and deck-abutment. The effect of axial force in the deck due to earth pressure loads is neglected. But

this force will cause shortening of the prestressed concrete girders due to elastic deformation and creep, resulting in the loss of prestressing force. Frame action is ignored when analyzing the superstructure for superimposed dead and live loads (Burke, 1993). Deck-abutment joints are designed assuming full composite action between the slab, girders and abutments only and with maximum passive earth pressure condition (Hambly, 1997, Soltani, 1992, Burke, 1993, Husain, 1996.).

A positive connection with the ends of the beams or girders is provided by rigidly connecting the beams or girders and by encasing them in reinforced concrete; thus, the bridge girders are rigidly connected to substructure. Steel superstructures may have their girders directly attached to the piles through the use of welded plates. Other type connections, such as bolting the girder to the abutment, may also be used. Prestressed girders may be connected by doweling them to the abutments. The superstructure design shall include a check for the adverse effects of fixity. The connection between the abutments and the superstructure shall be assumed to be pinned in the superstructure design and analysis (NJDOT, 1987). The connection between the superstructure and abutment is normally assumed pinned for girder design and analysis (Husain I and Bagnariol D, 1996).

The stress distribution in concrete deck slabs on composite steel beams used with integral bridges is studied using finite element method. The results are compared with corresponding stresses induced in the slab of equivalent jointed bridges. The results showed that integral bridges distribute the loads in the deck slab more uniformly than their jointed counterparts (Mourad, 1999).

Continuity of precast prestressed spliced-girder bridges under seismic loads has been studied experimentally with two 40% scale model bridge structures. They were tested under fully reversed simulated seismic forces and displacements in the longitudinal direction. Integral column-superstructure bent cap design is presented together with its performance. The performance of the model bridge structure exceeded the design requirements during tests (Holombo, 2000). A 1:2 scale model of a two span continuous bridge was tested in order to study its behavior during the construction process and under permanent loads. Time dependent concrete properties, as well as support reactions, deflections and strains in concrete and steel were measured for 500 days. Important time dependent redistribution of stresses and internal forces throughout the bridge were also measured. The results are used to validate a numerical model (Mari, 2000). Positive anchorage of integral abutments to the superstructure is strongly recommended (FHWA, 1980).

2.3.7 Construction Sequence

The following sequence is recommended when constructing steel bridges with integral abutments to reduce the effects of thermal movements on fresh concrete and control moments induced into the supporting pile system (AISI, 1996):

- Drive the piling and pour the pile cap to the required bridge seat elevation. Install one of the desired anchoring systems and pour the pile caps for the wingwalls concurrently.
- Set the beams/girders and anchor them to the abutment. Slotted holes in the bottom flanges are recommended to aid in the erection since the temperature will

vary from the time that the anchors are set in the cap to the time that the girders are fully erected. Do not fully tighten the anchor nuts at this time; instead, leave free play for further dead-load rotations.

- Pour the bridge deck in the desired sequence excluding the abutment back-wall/diaphragm and the last portion of the bridge deck equal to the back-wall/diaphragm width. In this manner, all dead-load slab rotations will occur prior to lock-up, and no dead-load moments will be transferred to the supporting piles.
- Tighten the anchor nuts and pour the back-wall/diaphragm to the full height. Since no backfilling has occurred to this point, the abutment is free to move without overcoming passive pressures against the back-wall/ diaphragm. The wingwalls may also be poured concurrently.
- Place the vertical drain system and backfill in 152-mm (6 in.) lifts until the desired sub-grade elevation is reached. Place a bond breaker on the abutment surfaces in contact with the approach pavement.
- Pour the approach pavement starting at the end away from the abutment and progressing toward the back-wall. Approach pavements may be poured in the early morning so that the superstructure is expanding, and therefore, not placing the slab in tension.
- A construction joint should be located at a distance of 150 mm (492 in.) from the back of the back-wall between the approach slab and bridge slab. This will provide a controlled crack location rather than allowing a random crack pattern to develop. Corrosion coated dowels shall pass through the joint and shall be

located near the bottom of the slab. This will keep the joint tight but still allow the approach slab to settle without causing tension cracking in the top of the slab.

- The excavation for the approach slabs shall be carefully made after compacted abutment embankment material is in place. The slabs shall be founded on undisturbed compacted material. No loose backfill will be allowed. To permit unhindered longitudinal movement of the approach slab, the surface of the sub-base course must be accurately controlled to follow and be parallel to the roadway grade and cross slope.
- A filter fabric or some type of bond breaker such as polyethylene sheets shall be placed on the finished sub-base course to the full width of the roadway prior to placement of approach slab reinforcement.
- A lateral drainage system should be provided at the end of the approach slab adjacent to the sleeper slab. Suitable description should be provided on the plans to incorporate these construction procedures.

CHAPTER 3

THEORY AND CONCEPT

3.1 Superstructure

3.1.1 Creep and Shrinkage

If the ends of a structural member are held in position by stiff supports or adjacent members and are thereby prevented from relative longitudinal movement, the members will be subjected to significant tension N(t) as shrinkage strains develop with time Fig. 3.1-1 (L. Vandewalle, 2000). The magnitude of this restraining tensile force depends on the stiffness of the

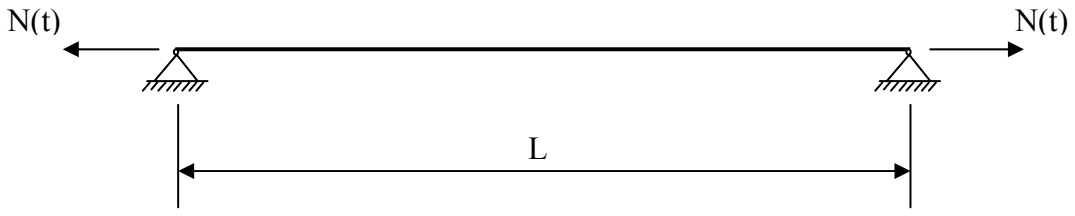

Fig. 3.1-1. Restrained shrinkage

member and therefore, tends to be highest prior to cracking when the member stiffness is maximum. When cracking occurs and the stiffness of the member reduces, the restraining force, which caused the cracking, is relieved to some extent.

Creep, Aging Coefficients, and Shrinkage Strain

The creep, aging coefficients and shrinkage strains for the analysis of long-term behavior of integral abutment bridges are based on ACI Committee 209 (1992) CEB –FIP model code (1990) and AASHTO (1998) recommendations.

3.1.1.1 ACI committee 209 (1992) recommendations

Creep: The coefficient for creep at time *t* for age at loading τ_0 is given by:

$$\phi(t,\tau_0) = \frac{(t-\tau_0)^{0.6}}{10+(t-\tau_0)^{0.6}}\phi_u \qquad \text{.....(3.1-1)}$$

where ultimate creep $\phi_u = \phi(\tau_\infty, \tau_0) = 2.35\gamma_c$

γ_c = a correction factor = $K_C\ K_H\ K_T\ K_S\ K_F\ K_A$

$$K_C = \begin{cases} 1.25\tau_0^{-0.118} & \text{for moist cured concrete} \\ 1.13\tau_0^{-0.094} & \text{for steam cured concrete} \end{cases}$$

$K_H = 1.27 - 0.0067\ h_e \qquad h_e \geq 40\%$

$$K_T = \begin{cases} 1.14 - 0.023T_M & \text{for} \leq 1 \text{ year} \\ 1.10 - 0.017T_M & \text{for ultimate value} \end{cases}$$

$K_S = 0.82 + 0.067\ S_c$

$K_F = 0.88 + 0.0024\ F_a$

$$K_A = \begin{cases} 1.00 & \text{for } A_c \le 6\% \\ 0.46 + 0.09A_c & \text{for } A_c > 6\% \end{cases}$$

Aging coefficient: Aging coefficient $\chi\ (t,\tau_0)$ is calculated based on the ultimate creep value $\phi(t_\infty, 7)$ from the table provided by ACI Committee 209 (Table 5.1.1, ACI-209).

Shrinkage: For moist cured concrete, the free shrinkage which occurs between $\tau_0 = 7$ days and any time t

$$\varepsilon_{sh}(t,\tau_0) = \frac{(t-\tau_0)}{35+(t-\tau_0)}(\varepsilon_{sh})_u \qquad \text{.....(3.1-2)}$$

where ultimate shrinkage coefficient $(\varepsilon_{sh})_u = 0.000780\ S_H\ S_T\ S_S\ S_B\ S_F\ S_A$

$$S_H = \begin{cases} 1.40 - 0.01h_e & 40\% \le h_e \le 80\% \\ 3.00 - 0.03h_e & 80\% \le h_e \le 100\% \end{cases}$$

$$S_T = \begin{cases} 1.23 - 0.038T_M & \text{for} \le 1 \text{ year} \\ 1.17 - 0.029T_M & \text{for ultimate value} \end{cases}$$

$S_S = 0.89 + 0.041\ S_C$

$S_B = 0.75 + 0.034\ B_S$

$$S_F = \begin{cases} 0.30 + 0.014F_a & \text{for } F_a \le 50\% \\ 0.90 + 0.002F_a & \text{for } F_a \ge 50\% \end{cases}$$

h_e = relative humidity (%)

T_M = minimum thickness (in.)

S_c = slump (in.)

F_a = fine aggregate % by weight

A_c = air content in % of volume of concrete

B_s = number of 94 lb sacks of cement per cubic yard of concrete

3.1.1.2 CEB – FIP recommendation

Creep coefficient: The modified CEB-FIP equation for creep coefficient is given by,

$$\phi(t,\tau_0) = \phi_0 \beta_c(t,\tau_0)\beta_E(\tau_0) \qquad \text{.....(3.1-3)}$$

where $\phi_0 = \phi_{RH}\beta(f_{cm})\beta(\tau_0)$

$$\phi_{RH} = 1 + \frac{1 - \left(\frac{RH}{RH_0}\right)}{0.46\left(\frac{h}{h_0}\right)^{\frac{1}{3}}}$$

$$\beta(f_{cm}) = \frac{5.3}{\sqrt{(f_{cm}/f_{cm0})}}$$

$$\beta(\tau_0) = \frac{1}{0.1 + (\tau_0/t_1)^{0.2}}$$

$$\beta(t-\tau_0) = \left[\frac{(t-\tau_0)/t_1}{\beta_H + (t-\tau_0)/t_1}\right]^{0.3}$$

$$\beta_H = \frac{150h}{h_0}\left[1 + \left(1.2\frac{RH}{RH_0}\right)^{18}\right] + 250 \le 1500 \text{ mm}$$

$$\beta_E(\tau_0) = \frac{E_c(\tau_0)}{E_c(28)}$$

Shrinkage: Shrinkage or the swelling at any time τ_0 (days) may be estimated by:

$$\varepsilon_{cs}(t,\tau_s) = \varepsilon_{cs0}\beta_s(t-\tau_s) \qquad \text{.....(3.1-4)}$$

where $\varepsilon_{cs0} = \varepsilon_s(f_{cm})\beta_{\mathrm{RH}}$

$$\varepsilon_s(f_{cm}) = \left[160 + 10\beta_{sc}\left(9 - \frac{f_{cm}}{f_{cm0}}\right)\right]10^{-6}$$

$$\beta_{sc} = \begin{cases} 4 \text{ for slow hardening cement} \\ 5 \text{ for normal or rapid hardening cements} \\ 8 \text{ for rapid hardening high - strength cement} \end{cases}$$

$$\beta_{RH} = \begin{cases} -1.55\left[1 - \left(\frac{RH}{RH_0}\right)^3\right] & \text{for } 40\% \le \mathrm{RH} \le 99\% \\ +0.25 & \text{for } \mathrm{RH} \ge 99\% \end{cases}$$

$$\beta_s(t - \tau_s) = \left(\frac{(t - \tau_s)/t_1}{350(h/h_0)^2 + (t - \tau_s)/t_1}\right)^{0.5}$$

RH = relative humidity of the ambient environment (%)

h = 2 A_c / u

A_c = cross sectional area of the structural member (mm^2)

u = perimeter of the structural member in contact with the atmosphere (mm)

f_{cm} = mean compressive strength of concrete at the age of 28days (MPa)

t = age of concrete at the moment considered (days)

τ_0 = age of concrete at loading (days)

τ_s = age at which curing is stopped (days)

RH_0 = 100 %

h_0 = 100 mm

f_{cm0} = 10 MPa

t_1 = 1 day

3.1.1.3 AASHTO recommendations

AASHTO LRFD Bridge Design Specifications recommend the following expressions for creep and shrinkage of concrete:

Creep coefficient: The creep coefficient is calculated from [art. 5.4.2.3.2]

$$\psi(t,t_i) = 3.5 k_c k_f \left(1.58 - \frac{H}{120}\right) t_i^{-0.118} \left(\frac{(t-t_i)^{0.6}}{10+(t-t_i)^{0.6}}\right) \quad \text{.....(3.1-5)}$$

where

k_c = factor for the effect of the volume-to-surface ratio of the component specified in Fig. 3.1-2

k_f = factor for the effect of concrete strength given by $k_f = \frac{62}{42+f'_c}$

H = relative humidity (percent)

t = maturity of concrete (day)

t_i = age of concrete when load is initially applied (day)

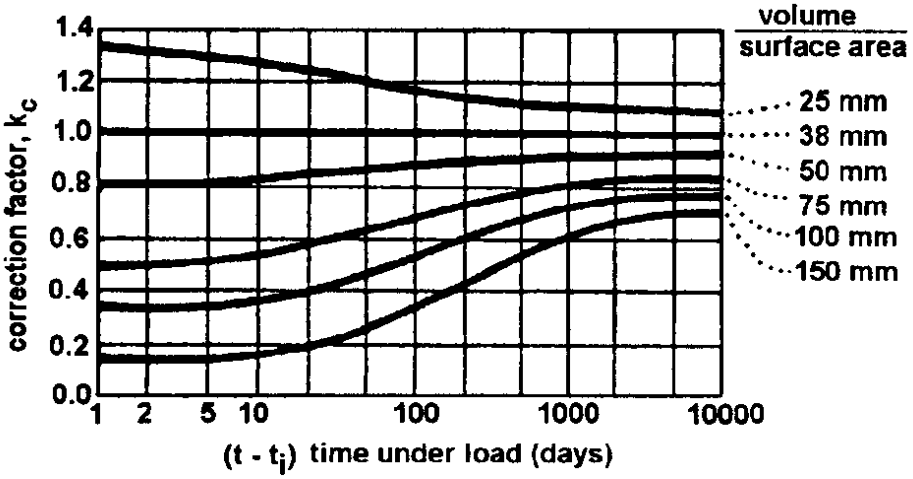

Fig. 3.1-2 Factor k_c for volume to surface ratio (AASHTO, 1998)

Shrinkage: for moist cured concretes devoid of shrinkage-prone aggregates, the strain due to shrinkage, ε_{sh}, at time t, is calculated as [5.4.2.3.3]

$$\varepsilon_{sh} = -k_s k_h \left(\frac{t}{35.0 + t} \right) 0.51 \times 10^{-3} \qquad \text{.....(3.1-6)}$$

where t = drying time (day)

k_s = size factor specified in Fig. 3.1-3

k_h = humidity factor as shown in Table 3.1-1

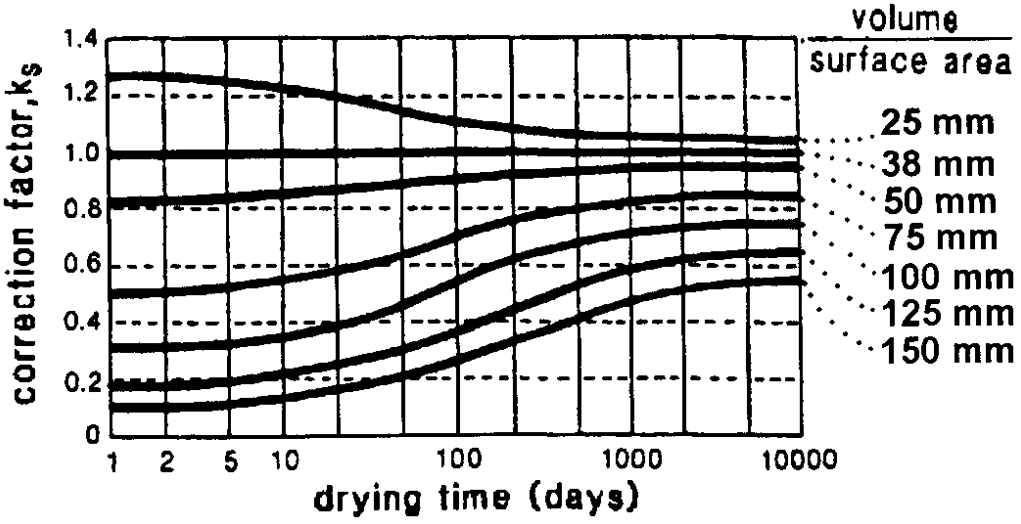

Fig. 3.1-3 Factor k_s for volume to surface ratio (AASHTO, 1998)

Table 3.1-1 Factor k_h for relative humidity

Average Ambient Relative Humidity %	k_h
40	1.43
50	1.29
60	1.14
70	1.00
80	0.86
90	0.43
100	0.00

A rational approach for the computation of deflections of composite superstructure would be based on

- Equilibrium

- strain compatibility
- stress – strain relationship.

3.1.2 Temperature Effects

Two types of temperature is included in the analysis of the superstructure:

- a uniform temperature change where the entire superstructure changes in temperature by a constant amount. This variation causes an expansion or contraction of the structure as shown in Fig. 3.1-4(a). Since the integral abutment bridges are constrained, this change in length develops forces in the structure.
- a gradient or non-uniform heating or cooling of the superstructure across the depth. If this non-uniform temperature variation across the cross section is assumed as non-linear or piecewise linear, then internal stresses are produced even if the structure is unrestrained as shown in the Fig. 3.1-4(b). In integral abutment bridges, since the end supports are assumed restrained, self-equilibrating statically indeterminate reactions develop, introducing statically indeterminate internal forces and corresponding stresses.

Field observations reveal that generally one-dimensional analysis is adequate for obtaining temperature distributions and the maximum bridge temperature ranges (Moorty, S., and Roeder, C. W., 1992).

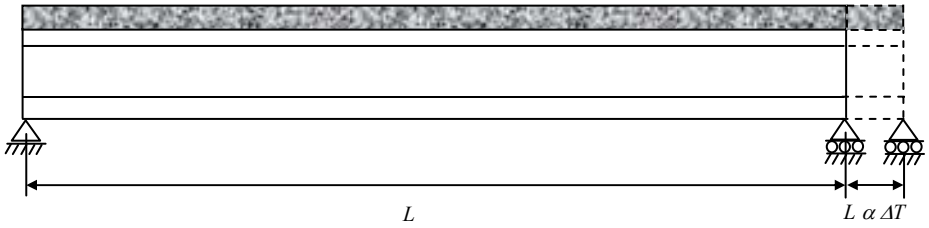

Fig. 3.1-4 (a) Expansion of the structure due to uniform temperature change

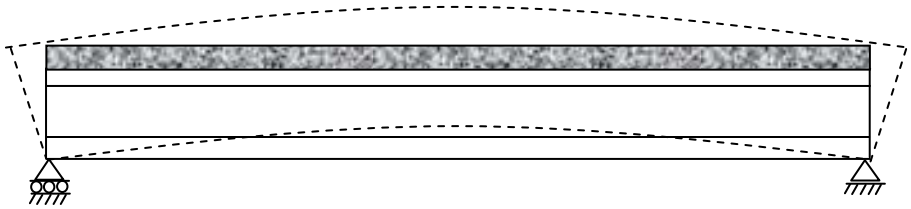

Fig. 3.1-4 (b) Curvature of the structure due to temperature gradient across the depth

In the absence of more precise information on the uniform temperature variations, AASHTO [3.12.2.1] recommends a range of temperature as specified in the Table 3.1-2 to calculate thermal deformation effects.

Table 3.1-2 Temperature ranges

Climate	Steel or Aluminum	Concrete	Wood
Moderate	-18° to 50° C	-12° to 27° C	-12° to 24° C
Cold	-35° to 50° C	-18° to 27° C	-18° to 24° C

Positive temperature gradient values for different zones, recommended by AASHTO [3.12.3], are given in Table 3.1-3. Negative temperature values can be obtained by multiplying the values specified by – 0.30 for plain concrete decks and – 0.20 for decks with an asphalt overlay.

Table 3.1-3 Temperature gradients

Zone	T_1(° C)	T_2(° C)
1	30	7.8
2	25	6.7
3	23	6
4	21	5

The vertical temperature gradients in concrete and steel superstructure with concrete decks are taken as shown in Fig. 3.1-5. Dimension A in Fig.3.1-5 is taken as:

- 300 mm – for concrete superstructures that are 400 mm or deeper
- 100 mm less than the actual depth – for concrete superstructures that are less than 400 mm deep

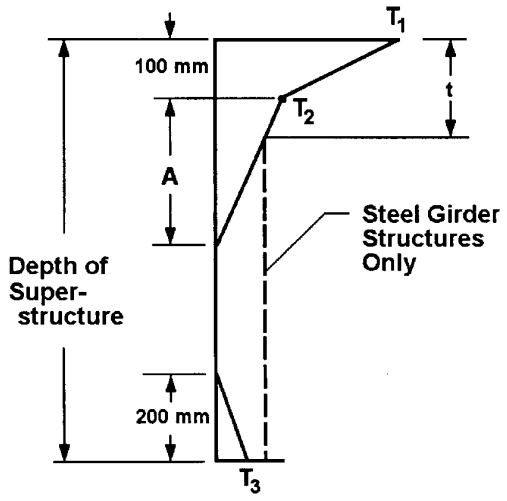

Fig. 3.1-5 Positive vertical temperature gradient in concrete and steel superstructures (AASHTO 1998)

For steel superstructures, the distance "t" is taken as the depth of the concrete deck. Value of T_3 is taken as 0° C, unless a site-specific study is made to determine an appropriate value, but not to exceed 3° C.

3.2. Substructure

The two different methods of modeling for obtaining the forces in the pile-soil system are presented below:

i) In the first method the substructure is modeled by assuming discrete translational and rotational springs for the entire substructure system, i.e., abutment, wing wall, pile cap piles, and backfill soil. The spring stiffness are used in the conventional structural analysis to obtain the forces coming on the laterally loaded piles.

ii) In the second method the piles are idealized as equivalent cantilevers with bases fixed at some distance below the ground. With conventional frame analysis, the forces coming on the laterally loaded piles are obtained.

3.2.1 Discrete Spring Model

3.2.1.1 Introduction

In jointless bridges with integral abutments, the substructure must absorb the induced movements of the superstructure. The supporting foundation, therefore, has to be flexible enough to accommodate superstructure deformation due to volume changes caused by temperature, creep and shrinkage. The required flexibility can be provided by the use of a stub abutment supported by a single row of piles. The analysis of superstructure-abutment-substructure interface is highly complex due to non-linear soil, and the material properties. Since the structural components of the integral abutment bridge - the abutment, wing wall, piles, abutment backfill behave as a

single component, it is difficult to model, without simplifications. One such simplification is to model the bridge as frame with substructure components replaced with translational and rotational springs.

3.2.1.2 Sub-structure stiffness

A typical integral abutment bridge consists of abutment, wing walls and piles supporting the abutment as shown in Fig. 3.2-1. The abutments may be considered as rigid due to their physical configuration and restraint provided by the backfill. The abutment walls, footings and piles reacting against the soil, will provide the total abutment stiffness (Wilson, 1988). The abutment is monolithically connected to the bridge deck. Therefore there will not be any relative movement between the abutment and the deck.

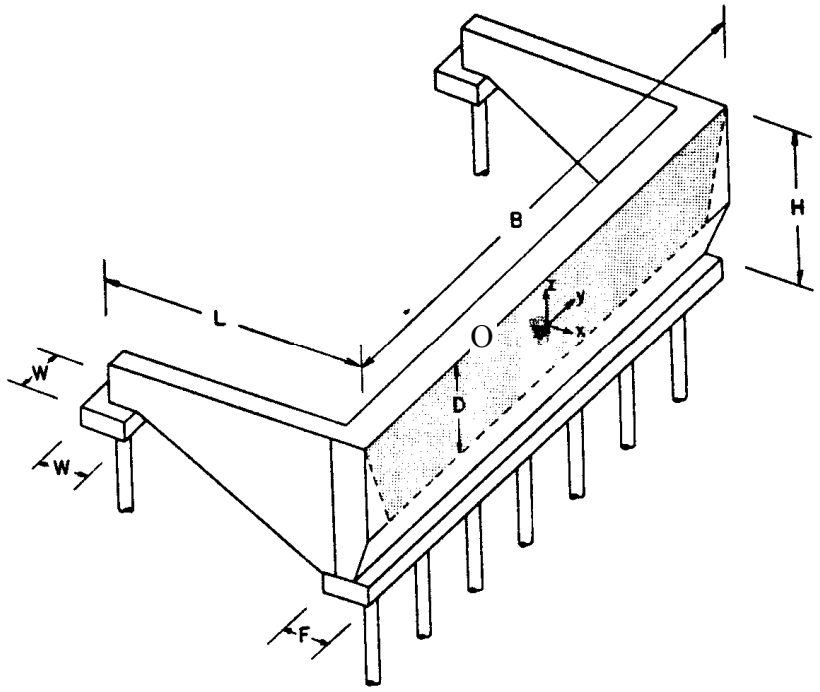

Fig. 3.2-1 Structural elements of a typical highway bridge abutment (Wilson, 1988)

The height of the wing wall is assumed to be same as the total depth of the bridge deck. The abutment and the pile cap are integrally connected without any joint and hence no relative movements between the pile foundation and the abutment exist. Similarly the pile heads are rigidly fixed to the pile caps to prevent rotation of the pile head relative to the cap. Since a rigid connection is assumed, this model will be reasonably good for concrete and steel piles. Piles replaced by equivalent translational and rotational springs are shown in Fig. 3.2-2. For timber piles, it may be more realistic to assume a pinned connection between pile and pile cap. The backfill soil is assumed to be linear elastic material with a constant soil modulus, E_s.

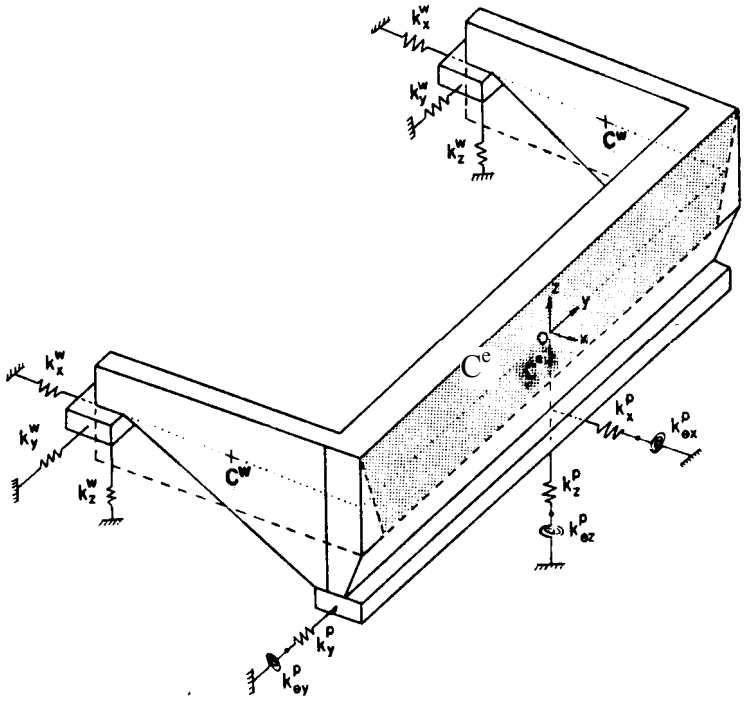

Fig. 3.2-2 Representation of piles by equivalent translational and rotational springs (Wilson, 1988)

The abutment and the backfill soil are assumed to be bonded together in order to provide equal resistance both in compression and tension, i.e. during thermal cycles and material rheological

behavior. Thus, the abutment and backfill interaction lead to combined stiffness effects of the abutment and the backfill.

3.2.1.3 Soil stiffness

Spring constants represent a linear relation between applied load and displacement of the foundation, which implies a linear stress-strain relation for the soil. Since the backfill soil is assumed to be linearly elastic material with constant soil modulus, E_s, which is constant with depth, the backfill can be represented with a linear spring. The abutment and backfill are assumed bonded to provide equal resistance in compression and tension induced from the loads normal to the walls. This assumption may overestimate the abutment stiffness, where the system cannot resist tensile loads. The vertical stiffness of the backfill can be found by equating the force equilibrium of resistance offered by the backfill to the applied load.

Vertical displacement for a rectangular area (l x b) is given by (Poulos and Davis, 1974)

$$\rho_z = \frac{\left(1-\nu^2\right)}{E_s} pbI \qquad \text{(3.2-1)}$$

where p = uniform load per unit area of the rectangle

ν = Poisson's ratio, which can be taken as 0.3

I = influence factor depends on the ratio of l/b which lies between 1.0 and 3.0

Applied force in vertical direction $= p\ l\ b$

Spring force $= k_z\ \rho_z$

by equilibrium of forces, and substituting ρ_z, $k_z = \frac{E_s l}{\left(1-\nu^2\right)I}$ (3.2-2)

where k_z = equivalent vertical stiffness for vertically loaded area such as pile caps, and

l = the longer side of the rectangle.

The equivalent vertical stiffness for vertically loaded area such as pile caps can be determined using Eqn. (3.2-2). However, for integral abutment bridges, the horizontal displacement plays a vital role. Hence, finding the horizontal soil stiffness is of primary concern. The stiffness coefficients for horizontal displacement can be found using the same concept adopted in finding the vertical stiffness (Eqn. 3.2-2) (Wilson, 1988). Rotational stiffness are assumed to be due to the result of the translational stiffness and derived based on the computed translational stiffness being applied uniformly over the length of the abutment as shown in Fig 3.2-3.

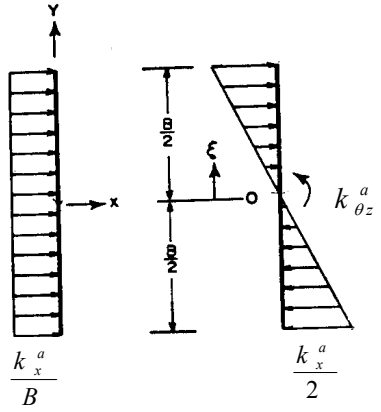

Fig. 3.2-3 Uniform distribution of translational Stiffness k_x^a / B for computation of rotational stiffness of the abutment $k_{\theta z}^a$

Thus,

$$k_{\theta z}^a = 2\int_0^{\frac{B}{2}} k_x^a \xi^2 \mathrm{d}\xi = \frac{k_x^a B^2}{12} \qquad \text{(3.2-3)}$$

Recommended spring constants (Richart, et al., 1970) obtained from the theory of elasticity for rectangular footings resting on the surface of the elastic half-surface (Table 3.2-1) can also be used. These expressions have been obtained for rigid footings except for the case of horizontal motion, for which the spring constant was obtained by assuming a uniform distribution of shearing stress on the contact area and computing the average horizontal displacement of this area.

Table 3.2-1 Spring constants for rigid rectangular footing resting on elastic half-space**

Motion	Spring Constant
Vertical	$k_z = \frac{G}{1-\nu}\beta_z\sqrt{4cd}$
Horizontal	$k_x = 4(1+\nu)G\beta_x\sqrt{cd}$
Rocking	$k_\psi = \frac{G}{1-\nu}\beta_\psi 8cd^2$

**G = modulus of elasticity in shear

ν = Poisson's ratio

The coefficients β_z, β_x, and β_ψ for rectangular footings are given in Fig. 3.2-4 for various values of d/c.

3.2.1.4 Abutment stiffness

The force from the deck is assumed to be transferred to the abutment at the centroid of the cross-section of the deck. Soil forces developed normal to the abutment due to translations and rotations of the abutment and wing wall about the reference point *O* are assumed to act at the

geometric center of abutment and wing wall respectively. The frictional forces between the

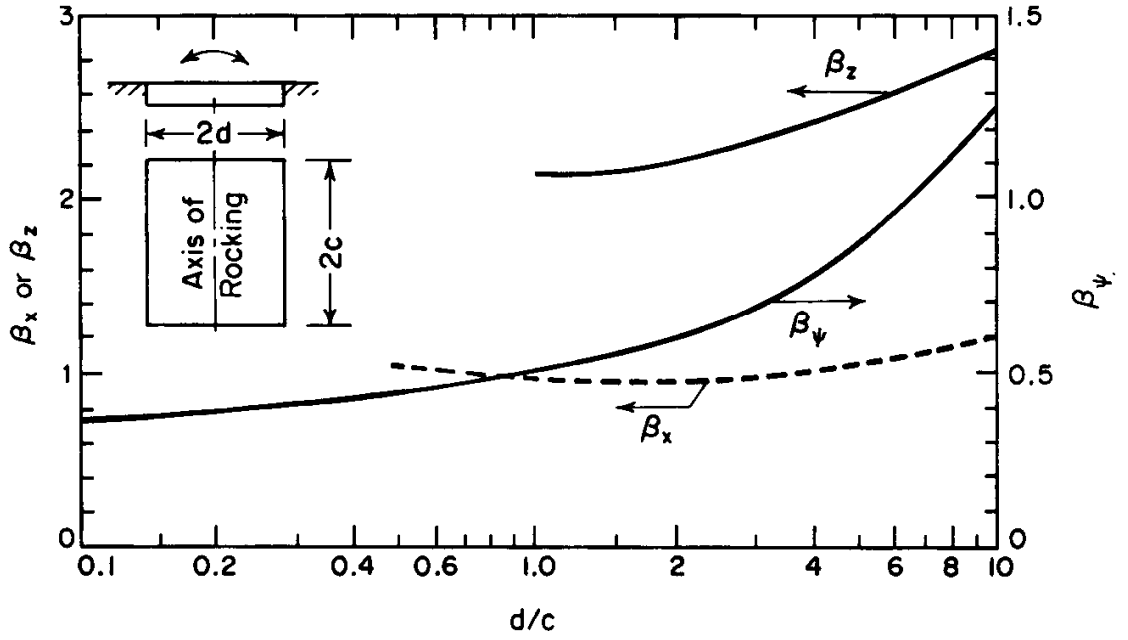

Fig.3.2-4 Coefficients β_z, β_x, and β_ψ for rectangular footings (Whitman and Richart, 1967)

abutment wall, wing wall and backfill are neglected. The axial and lateral stiffness at the pile head were included; rotational stiffness of each pile head was not considered. By this approach, the total effect of the pile stiffness can be replaced with a set of discrete springs. For example, the axial stiffness (z-direction) of the abutment piles can be modeled by an equivalent vertical translational spring, k_z^p attached to the abutment footing vertically below point O. For rotation about the x-axis, however, the stiffness k_z^p is assumed to be uniformly distributed along the length of the footing and represented as a rotational spring of stiffness $k_{\theta x}^p$ calculated by the Eqn.3.2-3. The stiffness coefficients that contribute to translational and rotational stiffness along and about x-axis are discussed below:

3.2.1.4.1 Longitudinal translational stiffness k_{xx}

A unit displacement applied to the substructure system (abutment, wingwall, pile cap, backfill, pile system) at point *O* (Fig.3.2-1) results in development of a normal force on the abutment due to backfill resistance, in addition to the pile forces k_x^p and k_x^w from the lateral stiffness in the *x*-direction of the abutment and wingwall piles, respectively. Thus,

$$k_{xx} = \frac{E_s B}{\left(1-\nu^2\right) I^a} + k_x^p + 2k_x^w \qquad (3.2\text{-}4)$$

where I^a is the influence coefficient for the rectangular abutment. The unit displacement in *x*-direction will also produce cross-coupled terms in the stiffness matrix between translations in the *x*-direction and rotations about the *y*- axis, because the resultant of the soil and pile forces acts below point *O* on the abutment. Hence, a $k_{\theta yx}$ term will appear in the stiffness matrix.

3.2.1.4.2 Torsional rotational stiffness, $k_{\theta x}$

The abutment system resists a unit rotation about the *x*-axis by a moment produced by the abutment footing, given by,

$$m^{af} = \frac{E_s B^3}{12\left(1-\nu^2\right) I^{af}} \qquad (3.2\text{-}5)$$

where I^{af} is the influence factor for the abutment footing.

Similarly, the total moment produced by the two wingwall footings is,

$$m^{wf} = \frac{E_s W B^2}{2\left(1-\nu^2\right) I^{wf}} \qquad (3.2\text{-}6)$$

where I^{wf} is the influence factor for the wingwall footing.

The lateral stiffness of the abutment piles in the *y*-direction, acting at a distance ($H - D/2$) from point *O*, contributes to a moment of

$$m^p = k_y^p \left(H - \frac{D}{2} \right)^2 \quad \text{(3.2-7)}$$

and the axial stiffness of the two sets of wingwall piles contributes a total moment of

$$m^w = k_z^w \frac{B^2}{2} \quad \text{(3.2-8)}$$

Rotation about the x-axis is also resisted by the axial stiffness of the abutment piles. This effect can be accounted for by using equivalent rotational spring stiffness $k_{\theta x}^p$.

Therefore, the torsional rotational stiffness is then given by superposition of rotational stiffness of abutment footing, wingwall footing, abutment piles, wingwall pile, and the axial stiffness of the abutment pile, given by,

$$k_{\theta x} = \frac{E_s B^3}{12\left(1-\nu^2\right) I^{af}} + \frac{E_s W B^2}{2\left(1-\nu^2\right) I^{wf}} + k_y^p \left(H - \frac{D}{2} \right)^2 + k_z^w \frac{B^2}{2} + k_{\theta x}^p \quad \text{(3.2-9)}$$

Cross-coupling of x-rotation with y-translation creates a term $k_{\theta xy}$. Similarly, the translational and rotational stiffness coefficients along and about y and z-axes can be obtained. The complete stiffness coefficients are as follows:

$$k_{xx} = \frac{E_s B}{\left(1-\nu^2\right) I^a} + k_x^p + 2k_x^w \quad \text{(3.2-10)}$$

$$k_{yy} = \frac{E_s L}{\left(1-\nu^2\right) I^w} + k_y^p + 2k_y^w \quad \text{(3.2-11)}$$

$$k_{zz} = \frac{E_s B}{\left(1-\nu^2\right) I^{af}} + \frac{2E_s W}{\left(1-\nu^2\right) I^{wf}} + k_z^p + 2k_z^w \quad \text{(3.2-12)}$$

$$k_{\theta x} = \frac{E_s B^3}{12\left(1-\nu^2\right) I^{af}} + \frac{E_s W B^2}{2\left(1-\nu^2\right) I^{wf}} + k_y^p \left(H - \frac{D}{2} \right)^2 + k_z^w \frac{B^2}{2} + k_{\theta x}^p \quad \text{(3.2-13)}$$

$$k_{\theta y} = \frac{E_s B}{12\left(1-\nu^2\right) H I^a} \left[\frac{D^3}{24} + \frac{1}{3} \left(H - \frac{D}{2} \right)^3 \right] + \frac{2 E_s W L^2}{\left(1-\nu^2\right) I^{wf}} + k_x^p \left(H - \frac{D}{2} \right)^2 + 2 k_z^w L^2 \quad \text{(3.2-14)}$$

$$k_{\theta z} = \frac{E_s B^3}{12\left(1-\nu^2\right) I^a} + \frac{2 E_s L^3}{3\left(1-\nu^2\right) I^w} + 2 k_y^w L^2 + k_z^w \frac{B^2}{2} + k_{\theta z}^p \quad \text{(3.2-15)}$$

where E_s = modulus of elasticity of the soil,

k_x^p, k_y^p and k_z^p = stiffness of abutment piles in the *x*, *y* and *z*, directions respectively,

k_x^w, k_y^w, and k_z^w = stiffness of wingwall piles in the *x*, *y* and *z*, directions respectively,

$k_{\theta x}^p, k_{\theta y}^p$, and $k_{\theta z}^p$ = equivalent rotational spring stiffness of abutment pile in the *x*, *y* and *z*, directions respectively

I^a = influence factor for abutment,

I^{af} = influence factor for abutment footing (pile cap),

I^w = influence factor for wingwall,

I^{wf} = influence factor for wingwall footing (wingwall pile cap),

ν = Poisson's ratio.

B = width of the abutment,

H = height of the abutment,

D = total depth of the bridge deck, and

L = length of the wingwall

For the substructure system, the force-deflection relationship $\{F\} = [K]\{\Delta\}$ can be written as

$$\begin{Bmatrix} f_{xx} \\ f_{yy} \\ f_{zz} \\ f_{\theta x} \\ f_{\theta y} \\ f_{\theta z} \end{Bmatrix} = \begin{bmatrix} k_{xx} & & & \text{Symmetric} & & \\ 0 & k_{yy} & & & & \\ 0 & 0 & k_{zz} & & & \\ 0 & k_{\theta xy} & 0 & k_{\theta x} & & \\ k_{\theta yx} & 0 & k_{\theta yz} & 0 & k_{\theta y} & \\ 0 & k_{\theta zy} & 0 & 0 & 0 & k_{\theta z} \end{bmatrix} \begin{Bmatrix} \delta_{xx} \\ \delta_{yy} \\ \delta_{zz} \\ \delta_{\theta x} \\ \delta_{\theta y} \\ \delta_{\theta z} \end{Bmatrix} \quad \text{(3.2-16)}$$

Thus the joint between superstructure and substructure of an integral abutment bridge can be modeled using discrete springs to represent the translational and rotational degrees of freedom of the substructure. The spring stiffness value for each degree of freedom of the substructure component may be developed by considering the resistance provided by soil to statically applied displacements of each component of substructure. Fig. 3.2-5 shows discrete springs for translational and rotational degrees of freedom.

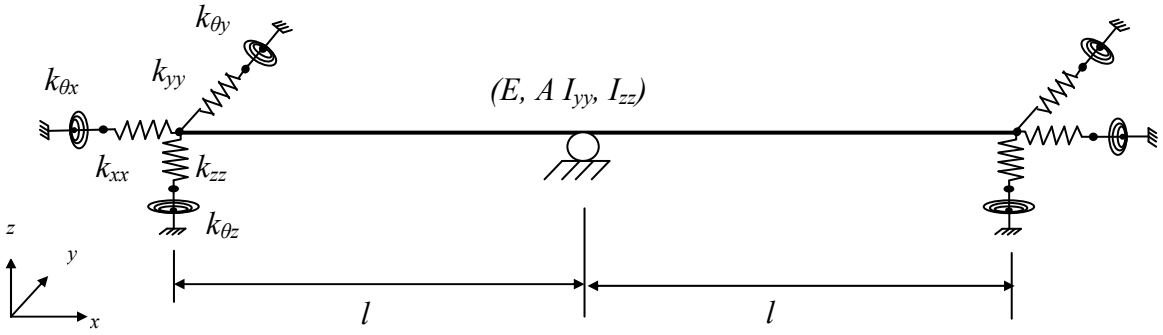

Fig. 3.2-5 Modeling of abutment and pile as translational and rotational springs (Wilson, 1988)

The translational stiffness of the abutment mainly depend on its width B. The rotational stiffness about y-axis for a given soil modulus depends on the abutment size. Once the stiffness coefficients of the substructure system are evaluated from the equations 3.2-10 – 3.2-15, the bridge structure then can be analyzed by conventional structural analysis procedure considering the moments obtained from the time dependent analysis applied at the superstructure-abutment joint.

3.2.2 Equivalent Cantilever Idealization

3.2.2.1 Equivalent cantilever length

Piles are idealized as equivalent cantilevers with bases fixed at some distance below the ground surface (Fig. 3.2-6). The equivalent cantilever length, l_e, of embedded piles is the depth from the soil surface to the fixed base of the equivalent cantilever. For a long pile embedded in soil, the horizontal displacements at the pile head have negligible effects below a certain depth, called critical length, l_c. Beyond this length, lateral displacements and bending moments are a small percentage (about 4%) of those at the pile head. This is a parameter of the pile and soil system and is not a physically identifiable length. If a pile is longer than l_c, the pile behaves as if it is infinitely long. Most piles used in practice are longer than their critical length and behave as "flexible" piles. For a soil with a uniform sub-grade reaction modulus, k_h, the critical length is selected as

$$l_c = 4R \qquad \text{.....(3.2-17)}$$

where the relative stiffness factor R is given by

$$R = \sqrt[4]{\frac{EI}{k_h}} \qquad \text{.....(3.2-18)}$$

and EI = the stiffness of the pile.

The procedure described here is discussed in detail in the literature (Greimann et al., 1987).

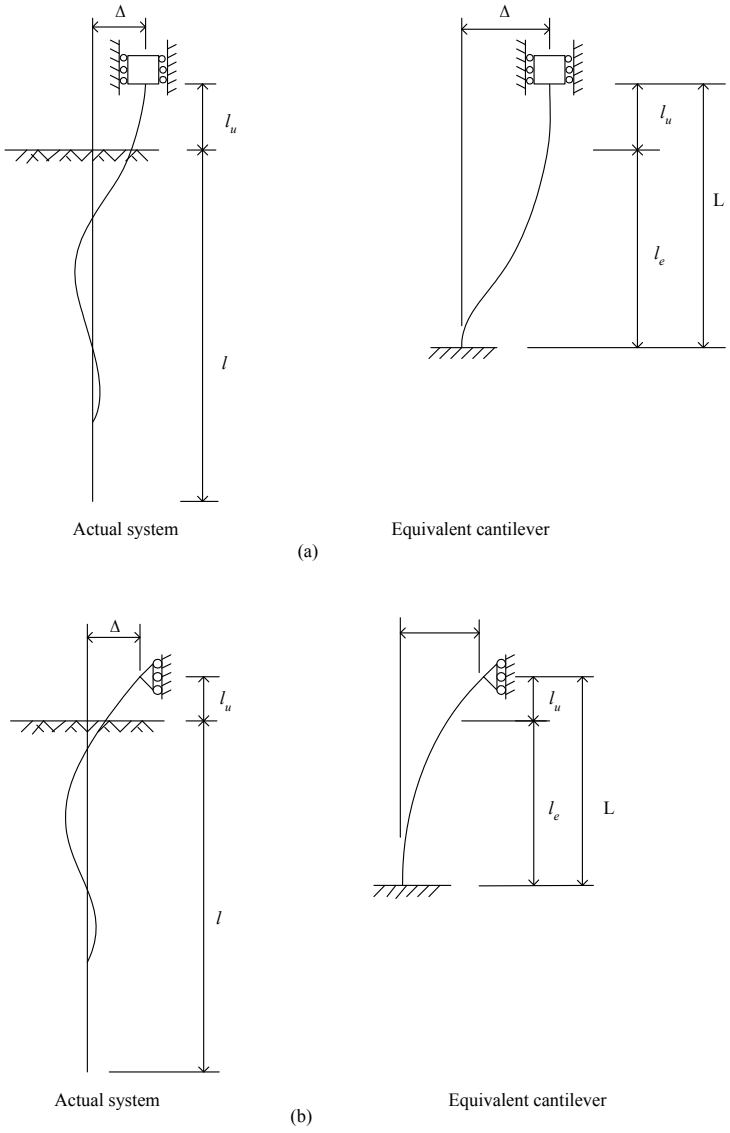

Fig. 3.2-6 Cantilever idealization of the pile: (a) fixed-head condition (b) pinned-head condition

Equivalent cantilevers are used to calculate the forces in the pile and the bridge substructure. For example, an equivalent cantilever can be determined such that its maximum moment would be equal to the maximum moment in real pile. However, the complete moment diagram below the ground surface could not be determined with the same equivalent cantilever. Three different equivalencies were considered in the development of the design method. They are based on

(i) the horizontal stiffness of the soil-pile system,

(ii) the maximum moment in the pile, and

(iii) the elastic buckling load of the pile.

For each equivalency, the boundary condition at the pile head can be either fixed (no rotation) or pinned (no moment). The horizontal displacement, Δ at the top of the equivalent system corresponds to the longitudinal expansion or contraction of the bridge superstructure at the integral abutment (Fig. 3.2-6).

Equivalent embedded length for fixed head and pinned-head piles embedded in a uniform soil are shown in a non-dimensional form in Fig. 3.2-7 and 3.2-8, respectively. The equivalent embedded length is approaching a constant value for l_u/l_c greater than one, which implies that, an unfilled predrilled hole of length l_u can significantly reduce the equivalent embedded length and there by the forces.

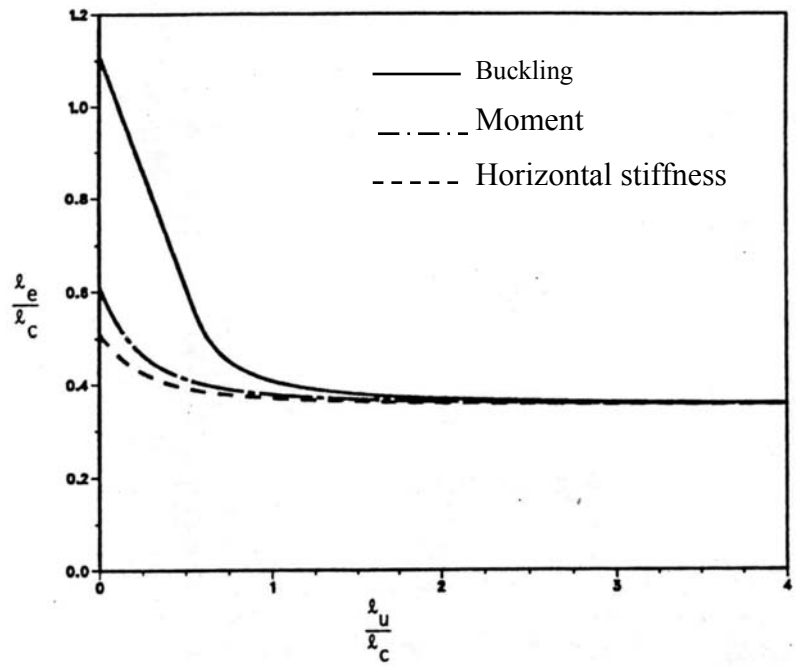

Fig. 3.2-7 Equivalent cantilever for fixed-head piles embedded in uniform soil (Greimann et. al., 1987)

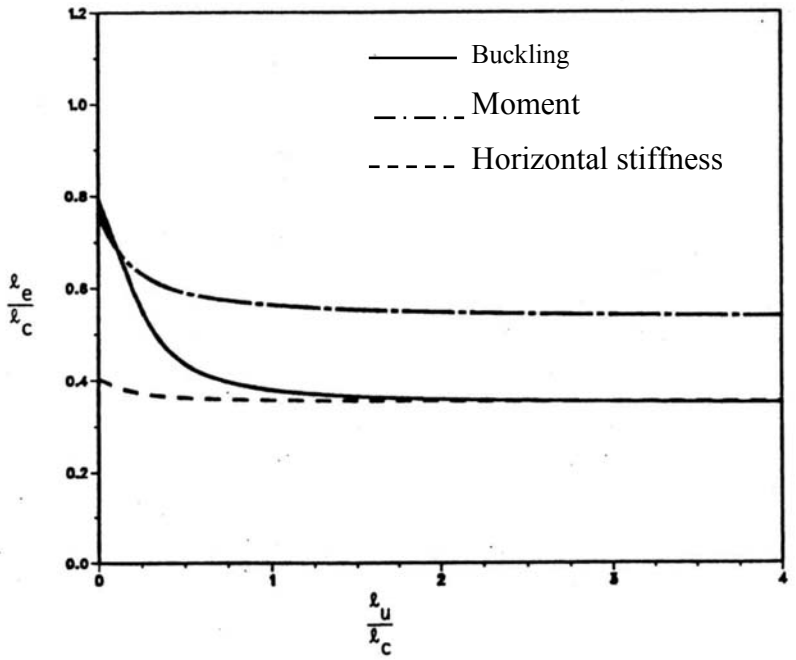

Fig. 3.2-8 Equivalent cantilever for pinned-head piles embedded in uniform soil (Greimann et. al., 1987)

3.2.2.2 Equivalent uniform soil stiffness k_h

For a pile embedded in a non-uniform soil with a stiffness, $k_h(x)$, as a function of depth x, an equivalent uniform soil stiffness, k_e, (Fig. 3.2-9) is determined using an iterative procedure.

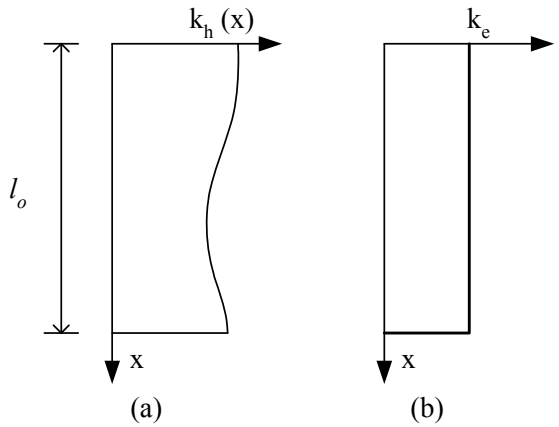

Fig. 3.2-9 Piles in non-uniform soil: (a) actual variation of stiffness (b) equivalent uniform stiffness

The equivalent uniform stiffness is determined using the following procedure:

Step i) Assume a value for the k_e.

Step ii) Calculate $l_o = 2\left(\sqrt[4]{\frac{EI}{k_e}}\right)$

Step iii) Calculate I_k by taking second moment of area about the reference axis as shown in Fig. 3.2-10.

Step iv) Determine new $k_e = \frac{3I_k}{l_o^3}$.

Step v) Repeat calculation of k_e, i.e. repeat calculations from step (ii).

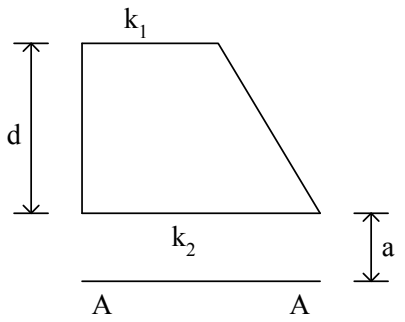

$$I_k = k_1\left[\frac{d^3}{36} + \frac{d}{2}(a + \frac{2d}{3})^2\right] + k_2\left[\frac{d^3}{36} + \frac{d}{2}(a + \frac{d}{3})^2\right]$$

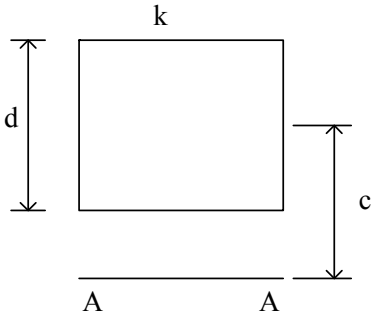

$$I_k = k\left[\frac{d^3}{12} + dc^2\right]$$

Fig. 3.2-10 Second moment about reference line A – A

3.2.3 Longitudinal Temperature Distribution

A constant temperature distribution is assumed. The horizontal displacement due to variation in temperature is calculated as $\Delta_t = \alpha_t \Delta T L_b$, where α_t is the coefficient of thermal expansion, ΔT is the temperature range and L_b is the total length of the bridge. Fifty percent of this displacement is apportioned to each of the abutments. This horizontal displacement induces moment of $6EI\Delta_t/L^2_p$ and a horizontal force of $12EI\Delta_t/L^3_p$ on the pile head.

Stress developed in the pile due to the longitudinal displacement of the superstructure is assumed to have no significant effect on the pile capacity; however, secondary P-Δ effect is

accounted for. For an equivalent cantilever with a horizontal head displacement (Δ), (Fig. 3.2-11) the combined effects of moment (M) and shear (H) balance the overturning moment (PΔ).

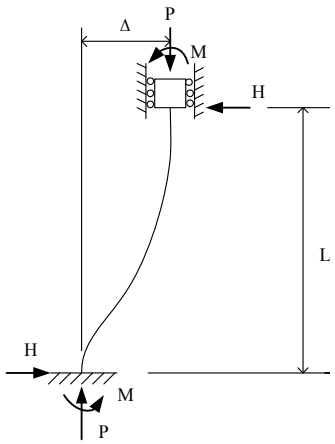

Fig. 3.2-11 Equivalent cantilever: for a fixed-head condition

3.3 Analysis of Laterally Loaded Piles

3.3.1 Introduction

Piles in an integral abutment bridge are subjected to lateral movement resulting from temperature and shrinkage effects. Several methods based on linear elastic behavior, ultimate load and nonlinear *p-y* curve have been used to analyze laterally loaded piles.

The *p-y* curve describes the soil resistance, *p* as a function of depth and pile deflection, *y*. The three factors that have the most influence on a *p-y* curve are the soil properties, the pile geometry, and the nature of loading. The principal dimension of a pile affecting the soil response is its diameter. If the cross section of the pile is not circular, the width of the pile perpendicular to the direction of loading is usually taken as the diameter (Greimann et al., 1987).

3.3.2 Soil Characterization

The Winkler soil model is used for the analysis of the soil-pile interaction. The model assumes that the soil can be represented as a series of vertical and lateral springs along the length of the pile as shown in Fig. 3.3-1. Also, the model assumes that there is no interaction between the different soil springs as the pile is displaced.

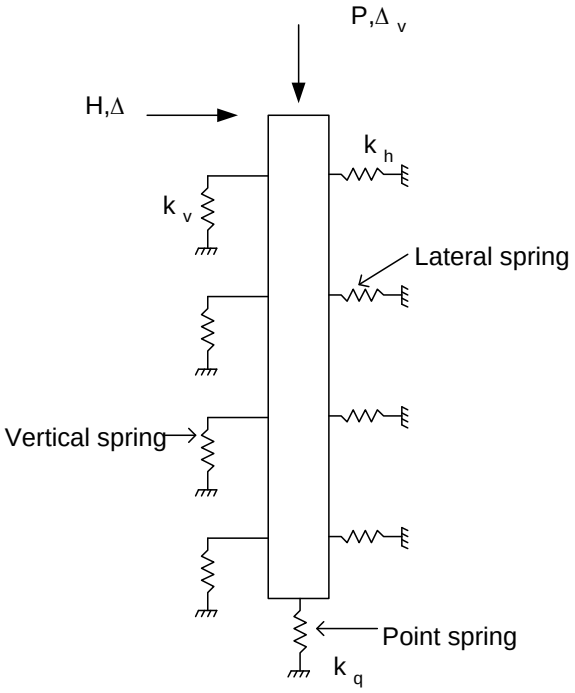

Fig. 3.3-1 Design model of soil-pile system

The characteristics of each of the three types of springs can be described by soil resistance and displacement curves:

i) *p-y* curves, which describe the relationship between the lateral soil pressure (horizontal force per unit length of pile) and the corresponding lateral pile displacement.

ii) *f-z* curves, which describe the relationship between skin friction (vertical force per unit length of pile) and the relative vertical displacement between the pile and the soil.

iii) *q-z* curves, which describe the relationship between the bearing stress (vertical force on effective pile tip area) at the pile tip and the pile tip settlement.

All three types of curves assume the soil behavior to be nonlinear. Again, the Winkler model assumes that these springs are uncoupled, which implies that motion at one spring does not affect another. For the design method used in the present study, a simplified elastic, perfectly plastic behavior is assumed.

The modified Ramberg-Osgood model is used to approximate the *p-y*, *f-z*, and *q-z* soil resistance and displacement curves:

$$p = \frac{k_h y}{\left[1 + \left|\frac{y}{y_u}\right|^n\right]^{1/n}} \qquad \text{.....(3.3-1)}$$

$$y_u = \frac{p_u}{k_h} \qquad \text{.....(3.3-2)}$$

Where

k_h = initial stiffness

p = generalized soil resistance

p_u = ultimate soil resistance

n = shape parameter

y = generalized displacement

For practical purposes, k_h is often assumed to be constant or to vary linearly with depth. For the parameters presented in Table 3.3-1, the subgrade-reaction moduli for clay soils are assumed to be constant within a soil layer and to vary linearly for granular soils.

Table 3.3-1 Parameters for p-y curve

Case	n	p_u (use lesser value)	k_h
Soft clay	1.0	$p_u = 9c_uB$ $p_u = \left(3 + \frac{\gamma}{c_u}x + \frac{0.5}{B}x\right)c_uB$	$\frac{p_u}{y_{50}}$
Stiff clay	1.0	$p_u = 9c_uB$ $p_u = \left(3 + \frac{\gamma}{c_u}x + \frac{0.5}{B}x\right)c_uB$	$\frac{p_u}{y_{50}}$
Very stiff clay	2.0	$p_u = 9c_uB$ $p_u = \left(3 + \frac{\gamma}{c_u}x + \frac{2.0}{B}x\right)c_uB$	$\frac{p_u}{2y_{50}}$
Sand	3.0	$p_u = \gamma x\left[B\left(k_p - k_a\right) + xk_p \tan\alpha \tan\beta + xk_o \tan\beta(\tan\phi - \tan\alpha)\right]$ $p_u = \gamma x\left[k_p^3 + 2k_p^2k_o \tan\phi - k_a\right]B$	$\frac{J\gamma x}{1.35}$

Note:

ε_{50} = Axial strain at one-half peak stress difference from laboratory triaxial test, or use , 0.02 for soft clay, 0.01 for stiff clay, 0.005 for very stiff clay

c_u = undrained cohesion indicated for an unconsolidated, undrained laboratory test

B = pile width

γ = effective unit soil weight

x = depth from soil surface

ϕ = angle of internal friction

$k_p = \tan^2\left(45° + \frac{\phi}{2}\right)$

$k_a = \tan^2\left(45° - \frac{\phi}{2}\right)$

$k_o = 1 - \sin\phi$

$\alpha = \frac{\phi}{2}$ for dense or medium sand, $\frac{\phi}{3}$ for loose sand

$\beta = 45° + \frac{\phi}{2}$

J = 200 for loose sand, 600 for medium sand, 1500 for dense sand

y_{50} = displacement at one-half ultimate soil reaction: 2.5 $B\varepsilon_{50}$ for soft and stiff clay, 2.0 $B\varepsilon_{50}$ for very stiff clay.

3.4 Analysis of Continuous Integral Abutment Bridges

3.4.1 Introduction

This section presents the concepts for the analysis of time-dependent behavior of continuous integral abutment bridges. Age-adjusted effective modulus method with relaxation procedure is used to include the creep behavior of concrete. The partial restraint provided by the abutment-pile-soil system is included.

Theoretical model

The constitutive materials are assumed to carry uniaxial stress only. A constant force and sectional area is assumed to act in the prestressing tendon. Stress-relieved tendons suffer loss in the prestressing force due to constant elongation with time. The magnitude of this loss called stress relaxation, depends on both the duration of the sustained prestressing force as well the ratio (f_{pi} / f_{py}) of initial stress immediately after prestressing to the yield strength of the tendon. Stress relaxation in the prestressing tendon with time is considered in the model and the remaining prestress at any time *t* after relaxation f_{pR} , is expressed as;

$$\frac{f_{pR}}{f_{pi}} = 1 - \left(\frac{\log t_2 - \log t_1}{10} \right) \left(\frac{f_{pi}}{f_{py}} - 0.55 \right) \qquad \text{.....(3.4-1)}$$

where f_{py} = stress at 1% elongation, and t = time after initial prestressing in hours.

3.4.2 Time-dependent Strain and Curvature

The total uniaxial concrete strain, $\varepsilon_c(t)$ at any time, *(t)* is assumed to be the sum of the instantaneous strain caused by service loads and the time dependent strain due to creep and shrinkage, and strain produced due to the temperature gradient across the cross-section. Under the sustained stress, the strain increases with time due to creep and the total strain including the instantaneous and creep strains at any time *(t)* is

$$\varepsilon_c(t) = \frac{\sigma_c(t_0)}{E_c(t_0)} \left[1 + \varphi(t, t_0) \right] \qquad \text{.....(3.4-2)}$$

where $\varphi(t, t_0)$ is the ratio of creep strain to instantaneous strain and a function of the age at loading, t_0 and the age *t* for which the strain is calculated.

This linear relationship, which is true within the range of stresses under sustained loads, allows superposition of the strain due to changes in stresses and shrinkage. Thus, the total strain in concrete due to applied stress and shrinkage is given by

$$\varepsilon_c(t) = \sigma_c(t_0)\frac{1+\varphi(t,t_0)}{E_c(t_0)} + \int_0^{\Delta\sigma_c(t)} \frac{1+\varphi(t,\tau)}{E_c(\tau)}\,\mathrm{d}\sigma_c(\tau) + \varepsilon_{cs}(t,t_0) \qquad \text{.....(3.4-3)}$$

A reduced creep coefficient can be used to calculate the creep strain, if the stress is applied gradually. With this simplification, the integral equation can be eliminated and Eqn.(3.4-3) can be modified as

$$\varepsilon_c(t) = \sigma_c(t_0)\frac{1+\varphi(t,t_0)}{E_c(t_0)} + \Delta\sigma_c(t)\frac{1+\chi\varphi(t,t_0)}{E_c(t_0)} + \varepsilon_{cs}(t,t_0) \qquad \text{.....(3.4-4)}$$

where χ is the concrete aging coefficient to account for the effects of aging on the ultimate value of creep for stress increments or decrements occurring gradually after the application of the corresponding load.

The total strain at any fiber at any time t is the sum of the instantaneous strain (ε_{oi}), time-dependent strains ($\Delta\varepsilon_o$) and strain due to self equilibrating force due to temperature effects ($\Delta\varepsilon_{oT}$) and given by:

$$\varepsilon_{ot} = \varepsilon_{oi} + \Delta\varepsilon_o + \Delta\varepsilon_{oT} \qquad \text{.....(3.4-5)}$$

and the total curvature at time t is

$$\kappa_t = \kappa_i + \Delta\kappa + \Delta\kappa_T \qquad \text{.....(3.4-6)}$$

In a statically indeterminate structure under sustained load, internal forces due to creep, shrinkage and temperature change due to gradual redistribution of moments over the period of time. The moment redistribution produces an additional time-dependent increment in the

moment. The total top fiber strain including the increment of strain $\delta\varepsilon_t$ due to incremental moment is given by:

$$\varepsilon_{ot} = \varepsilon_{oi} + \Delta\varepsilon_o + \varepsilon_{oT} + \Delta\varepsilon_{oT} + \delta\varepsilon_t \quad \text{.....(3.4-7)}$$

and the total curvature including the curvature increment $\delta\kappa_t$ is

$$\kappa_t = \kappa_i + \Delta\kappa + \Delta\kappa_T + \delta\kappa_t \quad \text{.....(3.4-8)}$$

3.4.2.1 Instantaneous analysis

The instantaneous strain ε_{ai} at any point a on the section at a distance y from the reference fiber (y is considered positive when measured down from the reference point) is defined in terms of reference fiber strain ε_{oi} and the initial curvature κ_i (Fig. 3.4-1 (c))

$$\varepsilon_{ai} = \varepsilon_{oi} + y\kappa_i \quad \text{.....(3.4-9)}$$

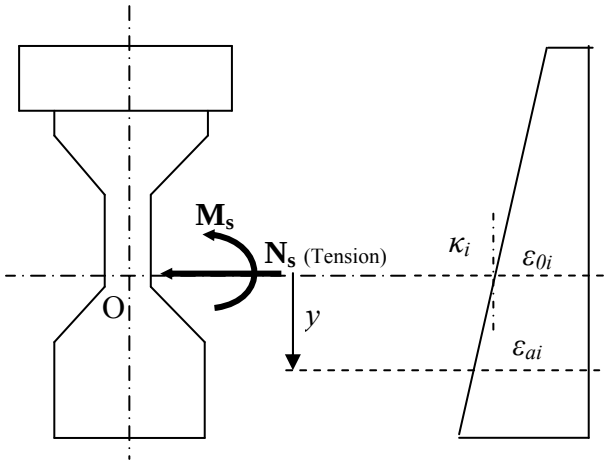

Fig.3.4-1 Details of composite integral abutment bridge system: cross-section and strain diagram

If the concrete under short-term load is assumed linear elastic, the initial stress distribution is

$$\sigma_{ai} = E_{ref}\varepsilon_{ai} \qquad \text{.....(3.4-10)}$$

$$\sigma_{ai} = E_{ref}\left(\varepsilon_{oi} + y\kappa_i\right) \qquad \text{.....(3.4-11)}$$

The resultant initial axial force N_i is found by integrating the stress block over the depth of the section. In general

$$N_i = \int \sigma_i dA \qquad \text{.....(3.4-12)}$$

$$N_i = E_{ref}\left(\varepsilon_{oi}A + \kappa_i B\right) \qquad \text{.....(3.4-13)}$$

where $A = \int dA$ = area of transformed cross section,

$B = \int ydA$ = first moment of transformed area about top fiber

E_{ref} = modulus of elasticity of reference layer

The initial bending moment about the reference surface M_i is determined by integrating the first moment of the stress block about the reference line.

$$M_i = \int \sigma_i y dA \qquad \text{.....(3.4-14)}$$

$$M_i = E_{ref}\left(\varepsilon_{oi}B + I\kappa_i\right) \qquad \text{.....(3.4-15)}$$

where $I = \int y^2 dA$ = the second moment of the transformed section about the top surface of the section.

Writing equation (3.4-13) and (3.4-15) in matrix form,

$$\begin{Bmatrix} N_i \\ M_i \end{Bmatrix} = E_{ref}\begin{bmatrix} A & B \\ B & I \end{bmatrix}\begin{Bmatrix} \varepsilon_{Oi} \\ \kappa_i \end{Bmatrix} \qquad \text{.....(3.4-16)}$$

For any applied moment and axial force, the short-term strain distribution is obtained from

$$\begin{Bmatrix} \varepsilon_{oi} \\ \kappa_i \end{Bmatrix} = \frac{1}{E_{ref}\left(AI - B^2\right)} \begin{bmatrix} I & -B \\ -B & A \end{bmatrix} \begin{Bmatrix} N_i \\ M_i \end{Bmatrix} \quad \text{.....(3.4-17)}$$

Once the initial strain ε_{oi} and curvature, κ_i are found from the transformed cross section, stress across the depth of the composite section for instantaneous analysis will be

$$\sigma_{cij} = E_{cj}\left(\varepsilon_{oi} + y_{cj}\kappa_i\right) \quad \text{.....(3.4-18)}$$

$$\sigma_{sij} = E_{sj}\left(\varepsilon_{oi} + y_{sj}\kappa_i\right) \quad \text{.....(3.4-19)}$$

where σ_{cij} = instantaneous stress at j^{th} layer of concrete

σ_{sij} = instantaneous stress at j^{th} layer of steel

3.4.2.2 Time dependent analysis including creep and shrinkage

Assuming the strain distribution to remain unchanged in any time interval, i.e., the total strain is assumed held constant and the creep and shrinkage components change, then the instantaneous component of strain must also change by an equal and opposite amount. When the instantaneous strain changes, the concrete stress also changes. The stress on the cross section is, therefore, allowed to vary freely due to relaxation. Consequently, the internal actions change and equilibrium is not maintained. To restore equilibrium, an axial force ΔN and ΔM must be applied to the section. The change of strain due to creep and shrinkage may be considered to be artificially prevented by restraining actions of $-\Delta N$ and $-\Delta M$. When ΔN and ΔM are applied to the section, the restraining actions are removed and equilibrium is restored. The restraining forces ΔN and ΔM are calculated as follows:

Creep: If creep were not restrained in any way, the top fiber strain and curvature would increase to $\phi(t,\tau_0)\varepsilon_{Oi}$ and $\phi(t,\tau_0)\kappa_i$ respectively, during the time interval (t,τ_0), where $\phi(t,\tau_0)$, ε_{Oi}, and κ_i are the creep coefficient, the initial strain and the initial curvature respectively. The restraining forces required to prevent this deformation are

$$\Delta N_{creep} = -\sum_{j=1}^{n} \overline{E}_{ej}\phi_j\left(A_{cj}\varepsilon_{Oi} + B_{cj}\kappa_i\right) \qquad \text{.....(3.4-20)}$$

$$\Delta M_{creep} = -\sum_{j=1}^{n} \overline{E}_{ej}\phi_j\left(B_{cj}\varepsilon_{Oi} + I_{cj}\kappa_i\right) \qquad \text{.....(3.4-21)}$$

where A_{cj} = area of the j^{th} concrete element

B_{cj} and I_{cj} are first and second moments of the area of j^{th} concrete element about the reference level respectively. The initial strain ε_{Oi} and curvature, κ_i are found from the transformed area of cross-section.

$\overline{E}_e$ = The age adjusted effective modulus of one of the concrete elements ($\overline{E}_{e1}$, say the girder) is selected as the modulus of age adjusted section. The age adjusted effective modulus is calculated using the following equation:

$$\overline{E}_e(t,\tau_0) = \frac{E_c(\tau_0)}{1+\chi(t,\tau_0)\phi(t,\tau_0)} \qquad \text{.....(3.4-22)}$$

where $\chi(t,\tau_0)$ is the concrete aging coefficient, which accounts for the effect of aging on the ultimate value of creep for stress increments or decrements occurring gradually after the application of the initial load. The value of the aging coefficient varies between 0.6 and 1.00, and is typically about 0.8 for long time intervals.

Shrinkage: If the shrinkage is assumed uniform over the depth of the section and completely unrestrained, the shrinkage induced top fiber strain which develops during the time interval (t,τ_0) is $\varepsilon_{sh}(t,\tau_0)$ and curvature is zero. The restraining forces required to prevent this uniform deformation is given by

$$\Delta N_{shrinkage} = -\sum_{j=1}^{n} \overline{E}_{ej}\left(A_{cj}\varepsilon_{shi}\right) \qquad \text{.....(3.4-23)}$$

$$\Delta M_{shrinkage} = -\sum_{j=1}^{n} \overline{E}_{ej}\left(B_{cj}\varepsilon_{shi}\right) \qquad \text{.....(3.4-24)}$$

Relaxation: For a prestressed concrete section, restraining forces required to prevent the reduced relaxation in the tendon must also be included. The restraining forces required to prevent the tensile creep in the steel (which causes relaxation) are

$$\Delta N_{relaxation} = \sum_{k=1}^{n} A_{psk}\Delta\sigma_{prk} \qquad \text{.....(3.4-25)}$$

$$\Delta M_{relaxation} = \sum_{k=1}^{n} A_{psk}\Delta\sigma_{prk}y_{psk} \qquad \text{.....(3.4-26)}$$

Temperature Gradient: Uniform or linearly varying temperature over the depth of the cross-section of a member of a statically determinate structure does not produce any stresses. However, if the temperature variation is multi-linear or non-linear, then self-equilibrating stresses are produced. The resultant restrained forces required to prevent deformation due to temperature gradient can be derived by integrating the stress produced by the hypothetical strain that would occur at any fiber, if it were free.

$$\Delta N_T = -\int E\varepsilon_{Tj}\,\mathrm{d}A \qquad \text{.....(3.4-27)}$$

$$\Delta M_T = -\int E\varepsilon_{Tj}\,y\,\mathrm{d}A \qquad \text{.....(3.4-28)}$$

ΔN_T and ΔM_T are applied to the age-adjusted transformed section.

The restraining forces are calculated as the sum of the four terms:

$$\begin{Bmatrix}\Delta N\\ \Delta M\end{Bmatrix} = \begin{Bmatrix}\Delta N\\ \Delta M\end{Bmatrix}_{creep} + \begin{Bmatrix}\Delta N\\ \Delta M\end{Bmatrix}_{shrinkage} + \begin{Bmatrix}\Delta N\\ \Delta M\end{Bmatrix}_{relaxation} + \begin{Bmatrix}\Delta N\\ \Delta M\end{Bmatrix}_{temp.gradient} \qquad \text{.....(3.4-29)}$$

The increments of strain $\Delta\varepsilon_o$ in reference fiber and curvature $\Delta\kappa$ produced by the axial force ΔN and moment ΔM, gradually applied about the reference level, may be obtained from,

$$\begin{Bmatrix}\Delta\varepsilon_o\\ \Delta\kappa\end{Bmatrix} = \frac{1}{\overline{E}_e\left(\overline{A}_e\bar{I}_e - \overline{B}_e^{\,2}\right)}\begin{bmatrix}\bar{I}_e & -\overline{B}_e\\ -\overline{B}_e & \overline{A}_e\end{bmatrix}\begin{Bmatrix}-\Delta N\\ -\Delta M\end{Bmatrix} \qquad \text{.....(3.4-30)}$$

where $\overline{A}_e =$ area of age adjusted transformed section

$\overline{B}_e =$ first moment of area $\overline{A}_e$ about reference fiber

$\bar{I}_e =$ second moment of area $\overline{A}_e$ about reference fiber

Age adjusted effective modulus $\overline{E}_e$ and corresponding modular ratio are used in these equations, since ΔN and ΔM are gradually applied.

The change of stress $\Delta\sigma$, at a point in the j^{th} concrete element at a depth y below the reference fiber is equal to the sum of the stress loss due to relaxation of the age-adjusted transformed section, when creep and shrinkage are fully restrained, and the stress which results when ΔN and ΔM are applied to the cross section.

$$\Delta\sigma_c = \overline{E}_{ej}\left[\phi_j\left(\varepsilon_{0i} + y\kappa_i\right) + \varepsilon_{shj} - \left(\Delta\varepsilon_0 + y\Delta\kappa\right)\right] \qquad \text{.....(3.4-31)}$$

The stress change with time in the j^{th} layer of steel is

$$\Delta\sigma_{sj} = E_{sj}\left(\Delta\varepsilon_0 + y_{sj}\Delta\kappa\right) \quad \text{.....(3.4-32)}$$

Based on the principle of superposition, the total concrete strain at any time is assumed to be the sum of instantaneous strain due to applied load and strains due to time effects consisting of creep, shrinkage of concrete, relaxation of prestress and temperature effects. In addition to the time-dependent effects, if the structure is statically indeterminate, time effects cause a gradual distribution of redundant moment δM over the period the load is sustained. Hence, each cross section will be subjected to a time-dependent increment of moment δM along with the initial moment M.

3.4.3 Analysis of Two Span Bridge with Restraints at the Integral Abutments

3.4.3.1 Precast prestressed composite continuous integral abutment bridge

A two span prestressed concrete (PSC) composite girder (Fig. 3.4-2) is modeled as a continuous structure with fixity at the abutments. The structure is analyzed at four different stages of construction. These stages are the following:

i) precast girder immediately after the transfer of prestress;

ii) precast girder prior to casting of the deck;

iii) precast girder immediately after casting of deck slab; and

iv) composite girder after the hardening of deck slab.

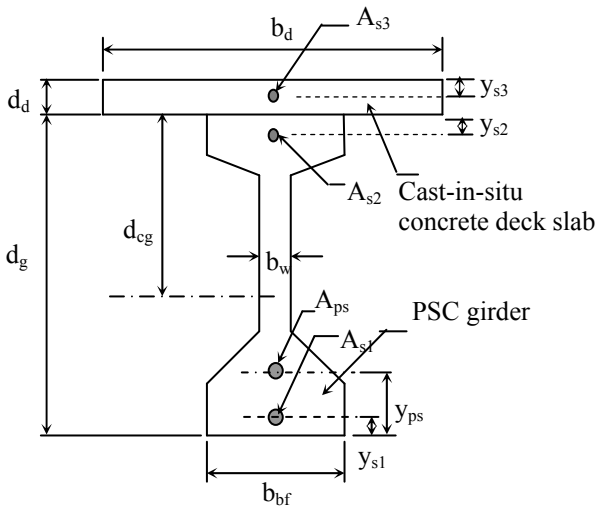

Fig. 3.4-2 Cross-section of PSC composite section

In stage I, the pre-cast girder is cast and pre-stressing force is applied, before casting of the deck slab. By the time the girder is placed in position for casting of slabs, the PSC girders undergo time-dependent changes in the internal stresses due to the sustained dead load and the pre-stressing force. In the proposed model, in stage I, PSC girder is assumed to be simply supported. In stage II, the slab is cast and additional superimposed dead loads are introduced. The girder is assumed to be simply supported for instantaneous application of dead load from the deck slab and other imposed dead loads. Composite action is assumed three days after casting of deck slab. For the time dependent analysis the slab is assumed to attain sufficient strength to be considered as a composite section with distinct characteristic strengths each for girder and slab. An internal redistribution of forces takes place due to creep, shrinkage and relaxation of prestressing steel of the girder, differential creep and shrinkage of the deck slab caused due to difference in age of concrete in the girder and the slab. The composite girder is assumed continuous over supports for time dependent analysis. The changes of forces are expressed in

terms of the unknown strains and curvature considering the equilibrium and compatibility conditions.

Stage I Instantaneous response (at t_1=3 days)

In stage I, the pre-cast girder is cast and pre-stressing force is applied, before casting of the deck slab (Fig.3.4-3). By the time the girder is placed in position for casting of slabs, the PSC girders undergo time-dependent changes in the internal stresses due to the sustained dead load and the pre-stressing force.

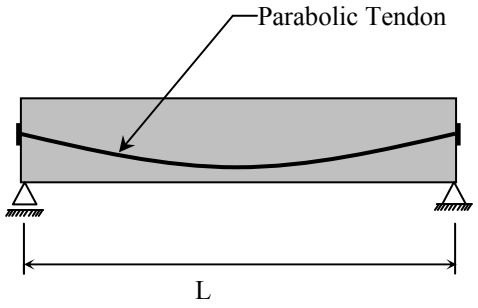

Fig.3.4-3 PSC girder with simple supports at stage I

The instantaneous strain in the reference fiber can be derived by substituting appropriate cross sectional properties and corresponding M_1 and N_1.

where M_1 = moment at any cross section along the simply supported structure and

N_1 = initial prestressing force immediately after transfer.

By equivalent load approach, the moment at any section along the span is given by

$$M_1 = \frac{1}{2}\left(w_g - \frac{8Pe_c}{L^2} \right)\left(Lx - x^2\right) \quad \text{.....(3.4-33)}$$

and $N_1 = -P$ .....(3.4-34)

By integrating twice the curvature from Eqn. (3.4-17) and utilizing the boundary conditions, (deflection is zero at both the supports), the equation for deflection is obtained along the span. The deflection at the midspan (Y_1) of the simple supported prestressed girder is given by

$$Y_1 = \left(\frac{5e_c}{48}\alpha_1 - \frac{1}{8}\beta_1 \right)PL^2 - \frac{5}{384} w_g L^4 \alpha_1 \quad \text{.....(3.4-40)}$$

where $\alpha_1 = \dfrac{A_{g1}}{E_{g1}\left(-A_{g1}I_{g1} + B_{g1}{}^2 \right)}$ .....(3.4-41)

and $\beta_1 = \dfrac{B_{g1}}{E_{g1}\left(-A_{g1}I_{g1} + B_{g1} \right)}$ .....(3.4-42)

Stage II Change in stress and strain occurring between t=3 days and t=60 days

After prestressing of the girder, the girder undergoes time-dependent stresses due to sustained prestress, creep and shrinkage. Restraint forces develop in the girder due to creep, shrinkage of concrete and relaxation of prestressing steel during the period from t_1=3 days to t_2=60 days. Using the Eqns. 3.4-29 the total restraining forces are calculated and the corresponding stress at various fibers are determined from Eqns. 3.4-31 – 3.4-32. The cumulative strain at reference fiber O at any time t, ($t_1 < t < t_2$), is the sum of the strain at time t_1 and strain at t_2. Similarly the total curvature up to time t_2 is the sum of curvature at time t_1 and the curvature

due to time dependent effects till time t_2. By integrating twice the curvature from Eqn. 3.4-30 and utilizing the boundary conditions, the equation for deflection along the span is obtained for any time t_2.

The deflection induced due to the creep, shrinkage and temperature gradients across the cross section at time t_2 is given by:

$Y_2 = Y_{cr\ wg} + Y_{cr\ P} + Y_{relax\ ps} + Y_{sh}$ .....(3.4-38)

Where

$Y_{cr\ wg}$,the deflection component from the creep effect (ϕ_2) due to sustained girder dead load w_g, is given by

$$Y_{cr\,wg} = -\frac{5w_g L^4 \phi_2}{384 E_{g1}} \left({}_g I_1 \alpha_{12} + {}_g A_1 \beta_{12} \right), \qquad \text{.....(3.4-39)}$$

$Y_{cr\ P}$, the deflection component from the creep effect (ϕ_2) due to sustained prestressing force P, is given by

$$Y_{cr\,P} = \frac{PL^2 \phi_2}{E_{g1}} \left[\frac{5e_c}{48} \left(- {}_g I_1 \alpha_{12} - {}_g A_1 \beta_{12} \right) + \frac{1}{8} \left(- {}_g I_1 \gamma_{12} - {}_g A_1 \delta_{12} \right) \right], \qquad \text{.....(3.4-40)}$$

$Y_{relax\ ps}$,the deflection component due to the effect of relaxation of prestressing force ($\Delta\sigma_{pr}$), is given by,

$$Y_{relax\,ps} = \frac{A_{ps} \Delta\sigma_{pr} L^2}{E_{g2}} \left[\frac{5e_c}{48} \left(-\alpha_{12} I_{g1} + \gamma_{21} \beta_{g1} \right) + \frac{1}{8} \left(\delta_{12} A_{g1} - \beta_{12} B_{g1} \right) \right], \qquad \text{.....(3.4-41)}$$

Y_{sh} ,the deflection component due to the effect of concrete shrinkage (ε_{sh}), is given by,

$$Y_{sh} = \frac{1}{8} L^2 \varepsilon_{sh2} \left(\delta_{12\ g} A_1\ A_{g1} + \beta_{12\ g} A_1\ B_{g1} \right), \qquad \text{.....(3.4-42)}$$

where $\alpha_{12} = \frac{A_{g1}A_{g2}}{\left(A_{g1}I_{g1} - B_{g1}^{\ 2}\right)\left(A_{g2}I_{g2} - B_{g2}^{\ 2}\right)}$, ...(3.4-43)

$\beta_{12} = \frac{B_{g1}B_{g2}}{\left(A_{g1}I_{g1} - B_{g1}^{\ 2}\right)\left(A_{g2}I_{g2} - B_{g2}^{\ 2}\right)}$, ...(3.4-44)

$\gamma_{12} = \frac{B_{g1}A_{g2}}{\left(A_{g1}I_{g1} - B_{g1}^{\ 2}\right)\left(A_{g2}I_{g2} - B_{g2}^{\ 2}\right)}$, ...(3.4-45)

and $\delta_{12} = \frac{I_{g1}B_{g2}}{\left(A_{g1}I_{g1} - B_{g1}^{\ 2}\right)\left(A_{g2}I_{g2} - B_{g2}^{\ 2}\right)}$ .....(3.4-46)

Stage III Instantaneous response due to increment of load (at t_3=60 days)

At this point of time, the deck slab is cast, but the slab has not gained sufficient strength, to provide composite action. Hence, the girders are still statically determinate, and the girders are now subjected to additional superimposed dead load due to deck slab (w_3) for the time upto t_3.

Instantaneous strain and curvature of the girder at instant of time t_3 = 60 days, due to the dead load of the slab and any other superimposed load at this point of time can be calculated from the Eqn.3.4-20. The girder concrete is assumed to gain its full strength and the corresponding modulus of elasticity of concrete (E_g (28)) should be used. The transformed area should correspond to this higher modulus value.

Only gravity loads are considered since no additional prestressing force is applied and hence N_3 = 0 in Eqn. 3.4-20. $M_3 = (w_3\, x\, /2)\, (L - x)$, moment at any section x along the span, due to the newly introduced dead load from deck slab and superimposed dead loads on the simply

supported girder. Strain at reference fiber O at end of time t_3, is the sum of the strains up to time t_2 and at t_3. Similarly, the curvature at the end of time t_3 is the sum of curvatures up to time t_2 and at time t_3.

The deflection induced due to the self-weight of the slab and superimposed dead loads across the cross section is given by

$$Y_3 = \frac{5}{384} w_3 L^4 \alpha_3 \qquad \text{.....(3.4-47)}$$

where $\alpha_3 = \dfrac{A_{g3}}{E_{g3}\left(A_{g3} I_{g3} - B_{g3}{}^2\right)}$ .....(3.4-48)

Stage IV *Changes in stress and strain due to creep, shrinkage and relaxation during the period t_{4i}= 63 days to t_4 = infinity.*

The deck slab is assumed to attain strength and the girder and slab start acting together as a composite section. The properties of composite section are to be considered in calculating the cross sectional properties. Since the abutment and the deck are integrally cast, the end supports are no longer simple supports. The simple support condition seizes to exist. Now the structure becomes statically indeterminate (Fig. 3.4-4). Two end moments and one interior support reaction are taken as the redundants. Taking advantage of the symmetry of the structure and loading, the redundants reduce to two. In addition to the time effects, redundancy will also cause a redistribution of moments. The problem can be divided into two parts:

i) Analysis of the new stage of the structure, i.e. statical indeterminacy of the composite section with w_g along with the prestress P and w_3 assumed to act together.

ii) Time effects on the composite section for time $t > t_3$.

Composite action effect: The reaction at the internal support and the moment at the left support are selected as redundants, considering the symmetry of the structure.

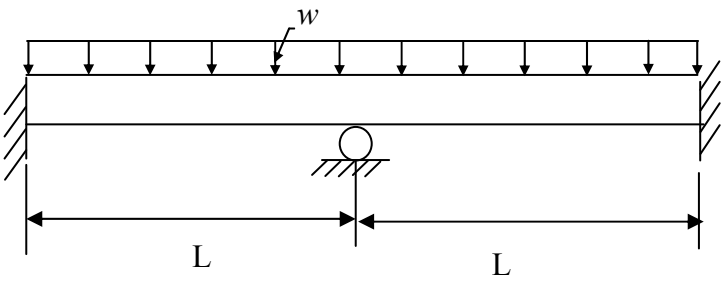

Fig. 3.4-4 Two span composite PSC girder

The total moment *M (x)* at any section at a distance *x* from left support in the left span is

$$M_4 = \frac{w_4 x}{2}(2L - x) - R_c \frac{x}{2} + M_A \qquad \text{.....(3.4-49)}$$

where, $w_4 = w_g - w_b + w_3$

Using the principle of virtual work, the redundant forces are determined with the conditions that the deflection at the internal support and the rotation at the left support are zero.

$$R_C = (w_g + w_3)L - \frac{8Pe_c}{L} \qquad \text{.....(3.4-50)}$$

and $$M_A = \frac{2}{3}Pe_c - (w_g + w_3)\frac{L^2}{12} \qquad \text{.....(3.4-51)}$$

Strain and curvature of the girder at instant of time t_{4i} = 63 days, due to the dead load of the girder, slab and any other superimposed load can be calculated from the Eqn.3.4-20. The corresponding modulus of elasticity of concrete for girder (E_g) and deck slab (E_d) are used, in

which the girder concrete is taken as the reference material. The transformed area is based on the girder modulus, E_g. The deflection of the composite cross section at mid-span is given by

$$Y_4 = \left(\frac{(w_g + w_3)L^4}{384} - \frac{PL^2 e_c}{48} \right) \alpha_{4i} + \frac{PL^2}{8} \beta_{4i} \quad \text{.....(3.4-52)}$$

where $\alpha_{4i} = \frac{A_{c4i}}{E_{g4i}\left(A_{c4i} I_{c4i} - B_{c4i}{}^2\right)}$ .....(3.4-53)

and $\beta_{4i} = \frac{B_{c4i}}{E_{g4i}\left(A_{c4i} I_{c4i} - B_{c4i}{}^2\right)}$ .....(3.4-54)

The time effects in the statically indeterminate structure: For the time dependent analysis, the slab is assumed to attain sufficient strength to the composite section with distinct characteristic strengths for the girder and slab. Age difference between the girder and the slab are also to be considered in the time-dependent analysis. The composite girder is assumed continuous over supports for time-dependent analysis.

During the period of sustained load, the structure is subjected to change in redundant forces. The redundant reactions R_c and M_A change by an amount δR_c and δM_A causing a change in moment in the left span, δM_x given by

$$\delta M_x = -\frac{\delta R_c x}{2} + \delta M_A \quad \text{.....(3.4-55)}$$

Addition of this time-dependent increment of the redundant moment to the applied moment, gives the total moment at any time t_4. The change in the redundant forces δR_{ci} and δM_{Ai} are derived again using the principle of virtual work and time-dependent cross sectional and material properties. Moment in the composite section at any section x from left support at time t_4

$$M_4 = \frac{w_4 x}{2}(2L - x) - R_c \frac{x}{2} + M_A - \frac{\delta R_c x}{2} + \delta M_A \quad \text{.....(3.4-56)}$$

$$\delta Rc = 0, \quad \text{.....(3.4-57)}$$

$$\text{and } \delta M_A = \frac{\beta_{4i}}{\alpha_4} P \quad \text{.....(3.4-58)}$$

$$\text{where } \beta_{4i} = -\frac{B_{c4i}}{E_{g4i}\left(A_{c4i} I_{c4i} - B_{c4i}^{\ 2}\right)} \quad \text{.....(3.4-59)}$$

$$\alpha_4 = \frac{A_{c4}}{E_{g4}\left(A_{c4} I_{c4} - B_{c4}^{\ 2}\right)} \quad \text{.....(3.4-60)}$$

Then the long term redundant R_c and M_A are expressed as

$$R_c = R_{ci} + \delta R_c \quad \text{.....(3.4-61)}$$

$$\text{and } M_A = M_{Ai} + \delta M_A \quad \text{.....(3.4-62)}$$

The change in moment, strain, curvature, stresses on any section due to time dependent increment in the redundant moment may be determined from the above formulations.

In addition, the composite girder undergoes time-dependent stresses due to sustained dead loads, prestress, creep and shrinkage. Restraint forces develop in the composite section due to creep, shrinkage of concrete and relaxation of prestressing steel during the period from t_{4i} = 63 days to t_4 = infinity. The restraining forces are computed using Eqns. 3.4-29 and the corresponding strain and curvature calculated using Eqn. 3.4-30. Strain at any time $t > t_{4i}$ is given by the sum of strain at time t_{4i} and the time effects in the composite section. Curvature at any time $t > t_{4i}$ is the sum of curvature at time t_{4i} and the time effects in the composite section

The variation in displacement with respect to time at any point along the composite PSC concrete girder can be found by double integration of the corresponding curvature at any given

time interval. Performing the integration and using the boundary conditions, the deflection at the mid-span is obtained as:

$$Y_4 = Y_{cr\ wg} + Y_{cr\ P1} + Y_{cr\ P2} + Y_{relax\ ps} + Y_{sh} \quad \text{.....(3.4-63)}$$

Where

$$Y_{cr\,wg} = \left(\frac{\left(w_g + w_3\right)L^4}{384}\right)\left[\left(-\alpha_{4i}\beta_{4\ g}B_4 + \beta_{4i}\beta_{4\ g}A_4 - \beta_{4i}\alpha_{4\ g}B_4 + \alpha_{4i}\alpha_{4\ g}I_4\right)\phi_{4g} + \left(-\alpha_{4i}\beta_{4\ d}B_4 + \beta_{4i}\beta_{4\ d}A_4 + \beta_{4i}\alpha_{4\ d}B_4 + \alpha_{4i}\alpha_{4\ d}I_4\right)\mu_4\,\phi_{4d}\right] \quad \text{.....(3.4-64)}$$

$$Y_{cr\,P1} = \left(-\frac{Pe_cL^2}{48}\right)\left[\left(-\alpha_{4i}\beta_{4\ g}B_4 + \beta_{4i}\beta_{4\ g}A_4 - \beta_{4i}\alpha_{4\ g}B_4 + \alpha_{4i}\alpha_{4\ g}I_4\right)\phi_{4g} + \left(-\alpha_{4i}\beta_{4\ d}B_4 + \beta_{4i}\beta_{4\ d}A_4 + \beta_{4i}\alpha_{4\ d}B_4 + \alpha_{4i}\alpha_{4\ d}I_4\right)\mu_4\ \phi_{4d}\right] \quad \text{.....(3.4-65)}$$

$$Y_{cr\,P2} = \left(-\frac{PL^2}{8}\right)\left[\left(\alpha_4\delta_{4i\ g}B_4 + \beta_{4i}\beta_{4\ g}B_4 - \beta_{4i}\alpha_{4\ g}I_4 - \delta_{4i}\beta_{4\ g}A_4\right)\phi_{4g} + \left(-\delta_{4i}\alpha_{4\ d}B_4 - \beta_{4i}\alpha_{4\ d}I_4 - \delta_{4i}\beta_{4\ d}A_4 + \beta_{4i}\beta_{4\ d}B_4\right)\mu_4\,\phi_{4d} + \left(-\beta_{4i}\beta_4B_{c4} + \beta_{4i}\alpha_4I_{c4}\right)\right] \quad \text{(3.4-66)}$$

$$Y_{relax\,ps} = \left(\frac{A_{ps}\Delta\sigma_{pr}L^2\eta_4}{48}\right)\left[\left(-\alpha_{4i}\alpha_4I_{c4i} + \beta_{4i}\alpha_4B_{c4i}\right)5e_c + \left(\alpha_{4i}\beta_4I_{c4i} - \beta_{4i}\beta_4B_{c4i}\right)\ 6\right] \quad \text{.....(3.4-67)}$$

$$Y_{sh} = \left(\frac{E_{g4i}L^2}{8}\right)\left[\left(-\beta_{4i}\beta_{4\ g}A_4B_{c4i} - \beta_{4i}\alpha_{4\ g}B_4B_{c4i} + \alpha_{4i}\alpha_{4\ g}B_4I_{c4i} - \alpha_{4i}\beta_{4\ g}A_4I_{c4i}\right)\varepsilon_{sh4g} + \left(-\beta_{4i}\alpha_{4\ d}B_4B_{c4i} + \beta_{4i}\beta_{4\ d}A_4B_{c4i} - \alpha_{4i}\beta_{4\ d}A_4I_{c4i} + \alpha_{4i}\alpha_{4\ d}B_4I_{c4i}\right)\mu_4\,\varepsilon_{sh4d}\right] \quad \text{(3.4-68)}$$

$$\delta_{4i} = -\frac{I_{c4i}}{E_{g4i}\left(A_{c4i}I_{c4i} - B_{c4i}{}^2\right)} \quad \text{.....(3.4-69)}$$

$$\mu_4 = \frac{E_{de4}}{E_{ge4}} \quad \text{.....(3.4-70)}$$

$$\eta_4 = \frac{E_{ge4i}}{E_{ge4}} \quad \text{.....(3.4-71)}$$

3.4.3.2 Composite steel-concrete integral abutment bridge

This section presents the detailed derivation of redundant forces in the integral abutment bridges. The expressions for the bending moment, strain, curvature, stresses, and deflection of a two span continuous composite integral abutment bridge are also included in this section.

A two span composite steel/concrete girder is analyzed as a continuous structure with fixed ends as shown in Fig 3.4-5. A typical cross-section is shown in Fig 3.4-6. The reaction at the internal support R_c and the moment at the left support M_A are selected as redundants. Due to the symmetry of the load and geometry, the total bending moment changes from negative to positive at two locations x_a and x_b from the left and interior supports respectively as shown in Fig 3.4-5.

For a uniformly distributed load w, the total moment M_x at any section x is given by

$$M_x = wlx - \frac{R_c x}{2} - \frac{wx^2}{2} - M_A \quad \text{for} \quad 0 \le x \le l \qquad \text{.....(3.4-72)}$$

$$M_x = wlx + \frac{R_c x}{2} - \frac{wx^2}{2} - M_A - R_c l \quad \text{for } l \le x \le 2l \qquad \text{.....(3.4-73)}$$

The redundant forces are determined using the principle of virtual work, and using the boundary conditions that the deflection at the internal support and the rotation at the left support are zero.

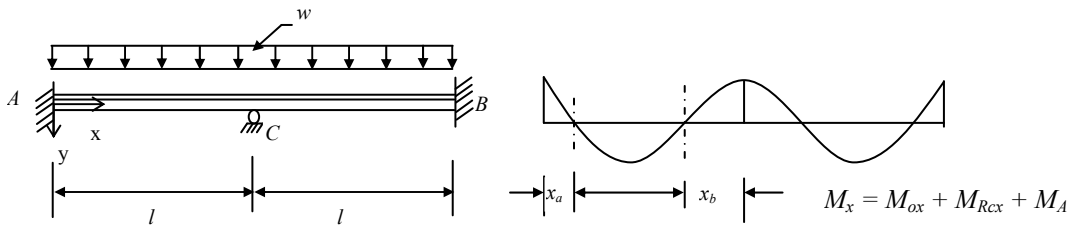

Fig. 3.4-5 Two span composite steel/concrete girder

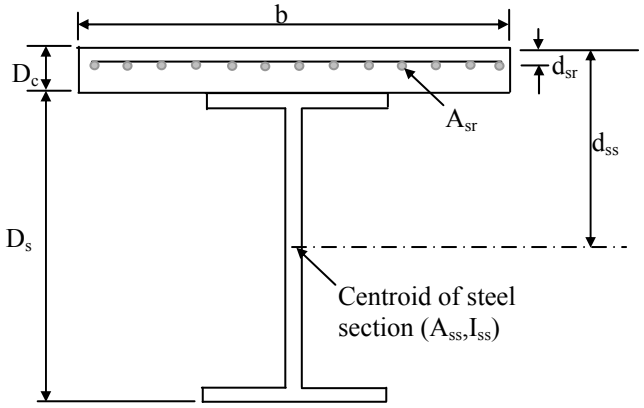

Fig 3.4-6 Typical cross-section of steel-concrete composite girder

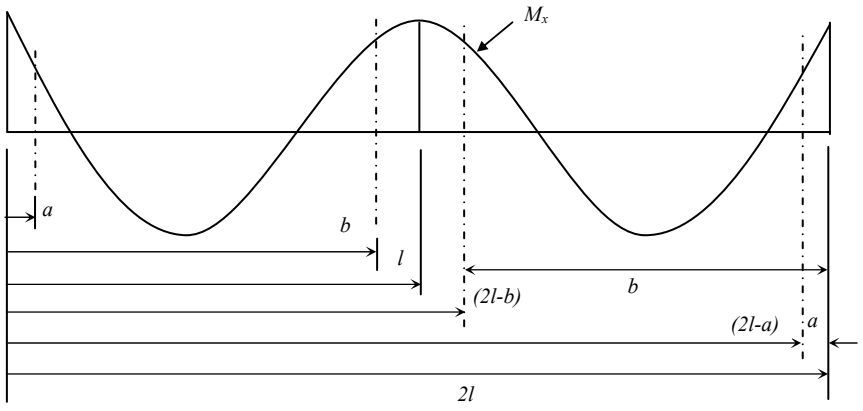

Fig. 3.4-7 Extent of cracked region along the span

It is assumed that the concrete in the negative moment region cracks (Fig. 3.4-7) and no creep will develop, since no stress is carried by the concrete.

Redundant reactions

Using the principle of virtual work, the redundant forces R_c and M_A are determined with the condition that the deflection of the structure at interior support and the rotation at the left support are zero.

$$Rc = w\,l \qquad \text{.....(3.4-74)}$$

$$M_A = \left(\frac{w}{12}\right)\left[\frac{\left(l^3 - 6la^2 + 4a^3\right)b_1 + \left(6la^2 + 4a^3\right)b_2}{\left(l - 2a\right)b_1 + 2\,b_2 a}\right] \qquad \text{.....(3.4-75)}$$

When the cracked region lengths a = 0, Eqns. 3.4-74 and 3.4-75 yield the following linear elastic solutions:

$$R_c = wl \qquad \text{.....(3.4-76)}$$

$$M_A = \frac{wl^2}{12} \qquad \text{.....(3.4-77)}$$

With the initial values of the redundant forces R_c and M_A, the elastic moment can be calculated using Eqns.3.4-74 and 3.4-75. The top fiber stress in concrete can be calculated and compared with the tensile strength of concrete. If the fiber stress in the concrete at any section exceeds the tensile strength limit, then the first estimate is made of the distance of the a from the left support. An iterative procedure is carried out using modified stiffness neglecting the contribution of concrete in the cracked region of the beam to determine the modified values of R_c and M_A.

Due to the sustained load, the structure is subjected to change in redundant reactions R_c and M_A by an amount ΔR_c and ΔM_A causing a time-dependent increment in moment of statically determinate structure, $\Delta M'_x$.

$$\Delta M'_x = \frac{\Delta R_c x}{2} + \Delta M_A \qquad \text{for } 0 \le x \le l \qquad \text{.....(3.4-78)}$$

$$\text{and } \Delta M'_x = \frac{\Delta R_c x}{2} + \Delta M_A - \Delta R_c l \qquad \text{for } l \le x \le 2l \qquad \text{.....(3.4-79)}$$

where ΔR_c = the time-dependent change in redundant reaction at the interior support and ΔM_A = the time-dependent change in redundant moment at the left support.

The change in the redundant forces ΔR_c and ΔM_A are derived as described above using the principle of virtual work and time dependent cross sectional and material properties. The unknown reaction ΔR_c and moment ΔM_A are determined as

$$\Delta R_c = \frac{C_{tR1} R_c + C_{tR2} w}{D_{tR1}} \qquad \text{.....(3.4-80)}$$

$$\text{and} \quad \Delta M_A = \frac{C_{tM1} M_A + C_{tM2} R_c + C_{tM3} w + C_{tM4}}{D_{tM1}} \qquad \text{.....(3.4-81)}$$

where

$$C_{tR1} = (8a^3 - 12\,la^2 + 6\,l^2a - l^3)\,b_1 + (-8\,a^3 + 12\,la^2 - 6\,l^2a)\,b_2 \qquad \text{.....(3.4-82)}$$

$$C_{tR2} = -\,l\,[C_{tR1}] \qquad \text{.....(3.4-83)}$$

$$D_{tR1} = (-8\,a^3 + 12\,la^2 - 6\,l^2a + l^3)\,c_1 + (8a^3 - 12\,la^2 + 6\,l^2a)\,c_2 \qquad \text{.....(3.4-84)}$$

$$C_{tM1} = [(192a^4 - 384\,la^3 + 288\,l^2a^2 - 96\,l^3a + 12\,l^4)\,c_1 + (-192a^4 + 384\,la^3 - 288\,l^2a^2 + 72\,l^3a)\,c_2]\,b_1 + [(-192\,a^4 + 288\,la^3 - 144\,l^2a^2 + 24\,l^3a)\,c_1 + (192\,a^4 - 288\,la^3 + 144\,l^2a^2)\,c_2]\,b_2 \qquad \text{.....(3.4-85)}$$

$$C_{tM2} = (24\,l^2a^3 - 36\,l^3a^2 + 12\,l^4a)\,c_2b_1 + (-24\,l^2a^3 + 36\,l^3a^2 - 12\,l^4a)\,c_1b_2 \qquad \text{.....(3.4-86)}$$

$$C_{tM3} =[(32\ a^6 – 96\ la^5 + 96\ l^2a^4 – 32\ l^3a^3 – 6\ l^4a^2 + 6\ l^5a – l^6)c_1 + (– 32\ a^6 + 96\ la^5 – 96\ l^2a^4 + 4\ l^3a^3 + 48\ l^4a^2 – 18\ l^5a)\ c_2]\ b_1 +[(- 32\ a^6 + 96\ la^5 – 96\ l^2a^4 + 64\ l^3a^3 – 42\ l^4a^2 + 12\ l^5a)\ c_1 + (32\ a^6 – 96\ la^5 + 96\ l^2a^4 – 36\ l^3a^3)\ c_2]\ b_2 \quad (3.4\text{-}87)$$

$$C_{tM4} = [(- 192\ a^4 + 384\ la^3 – 288\ l^2a^2 + 96\ l^3a – 12\ l^4)\ (a_1+T_1) + (192\ a^4 – 288\ la^3 + 144\ l^2a^2 – 24\ l^3a)\ (a_2+T_2)]\ c_1 + [(192\ a^4 – 384\ la^3 + 288\ l^2a^2 – 72\ l^3a)\ (a_1+T_1) + (-192\ a^4 + 288\ la^3 – 144\ l^2a^2)\ (a_2+T_2)]\ c_2 \quad (3.4\text{-}88)$$

$$D_{tM1} =12\ [(16\ a^4 – 32\ la^3 + 24\ l^2a^2 – 8\ l^3a + l^4)\ c_1^2 + (- 32\ a^4 + 56\ la^3 – 36\ l^2a^2 + 8\ l^3a)\ c_1c_2 + (16\ a^4 – 24\ la^3 + 12\ l^2a^2)\ c_2^2] \quad (3.4\text{-}89)$$

The changes in moment, strain, curvature, stresses in steel and concrete on any section due to time effects are determined from the above formulations. If the redistribution of concrete stress due to creep and shrinkage, together with the change in stress caused by the gradual change in the redundant R_{ct} and M_{At}, is such that cracking occurs on a previously uncracked section, the lengths of the cracked sections a and b are revised and new values of R_{ct} and M_{At} calculated, using an iterative process until required accuracy is achieved.

The variation in displacement at any point along the beam can be found by double integration of the corresponding curvature at any given time interval. Performing the double integration and using the boundary conditions that the slope and deflection at the left and interior supports are zero, the deflections are obtained as

$$y(x) = Y_1(x) \qquad \text{for } 0 \le x \le a \quad (3.4\text{-}90)$$

$$y(x) = Y_2(x)+C_2(x)\ x+D_2(x) \quad \text{for } a \le x \le b \quad (3.4\text{-}91)$$

where

$$Y_1(x) = (a_2 + T_2)\frac{x^2}{2} + b_2\left(\frac{wlx^3}{6} - \frac{R_c x^3}{12} - \frac{wx^4}{24} - \frac{M_A x^2}{2}\right) + c_2\left(\frac{-\Delta R_c x^3}{12} + \frac{\Delta M_A x^2}{2}\right) \quad \text{(3.4-92)}$$

$$Y_2(x) = (a_1 + T_1)\frac{x^2}{2} + b_1\left(\frac{wlx^3}{6} - \frac{R_c x^3}{12} - \frac{wx^4}{24} - \frac{M_A x^2}{2}\right) + c_1\left(\frac{-\Delta R_c x^3}{12} + \frac{\Delta M_A x^2}{2}\right) \quad \text{(3.4-93)}$$

$$C_2(x) = -(a_1 + T_1)\frac{l}{2} - b_1\left(\frac{5wlx^3}{48} - \frac{R_c l^2}{16} - \frac{M_A l}{2}\right) + c_1\left(\frac{\Delta R_c l^2}{16} - \frac{\Delta M_A l}{2}\right) \quad \text{(3.4-94)}$$

$$D_2(x) = \frac{a^2}{2}(a_2 - a_1) + \left(\frac{wla^3}{6} - \frac{R_c a^3}{12} - \frac{wa^4}{24} - \frac{M_A a^2}{2}\right)(b_2 - b_1) + \left(\frac{\Delta R_c a^3}{12} - \frac{\Delta M_A a^2}{2}\right)(c_1 - c_2)$$

$$+ (a_1 + T_1)\frac{la}{2} - b_1\left(\frac{-5wal^3}{48} + \frac{R_c al^2}{16} + \frac{M_A al}{2}\right) - c_1\left(\frac{\Delta R_c al^2}{16} - \frac{\Delta M_A al}{2}\right) \quad \text{(3.4-95)}$$

CHAPTER 4

NUMERICAL ILLUSTRATIONS AND DISCUSSIONS

4.1 Analysis Considering Creep, Shrinkage and Temperature Gradients

4.1.1 Pre-cast Pre-stressed Composite Concrete Continuous Integral Bridges

4.1.1.1 Superstructure analysis for creep, shrinkage and temperature gradient

A two-span continuous integral abutment bridge of span 82 ft. (25 m) each (Fig. 4.1.1-1a and b) with prestressed concrete composite deck is analyzed to illustrate the analytical procedure developed in section 3.4. The analysis includes the time dependent deformations of composite cross section due to creep, shrinkage and temperature. American Concrete Institute (ACI) and American Association of State Highway and Transportation Officials (AASHTO) approaches are considered in the modeling of time dependent material behavior. A multi-linear temperature gradient recommended by AASHTO is used in the analysis.

The cross-section adopted is composed of a precast pretensioned beam and a cast *in situ* concrete slab (Fig. 4.1.1-1c). Age of precast beam at the time of prestressing is assumed as 3 days and the age at the time of casting slab as 60 days. An initial prestressing force of 920 kips is applied. The self-weight of the girder is calculated as 1.23 kip/ft. (17.92 kN/m). Additional superimposed dead load due to the self-weight of the slab, etc., is 1.62 kip/ft. (23.68 kN/m). The modulus of elasticity of concrete of the precast beam $E_{cg}(t_1)$ = 3600 ksi (25 GPa) and $E_{cg}(t_2)$ = 5400 ksi. (37 GPa). Soon after hardening of the concrete, the composite action starts to develop gradually. The composite action occurring during first three days after casting of slab is ignored.

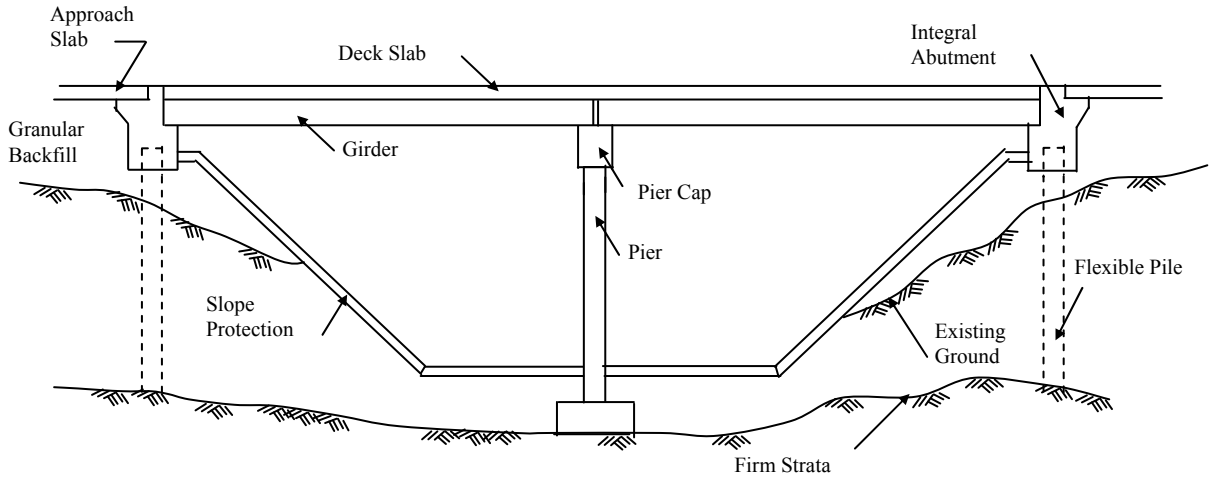

Fig. 4.1.1-1a Elevation of two-span prestressed concrete girder integral abutment bridge

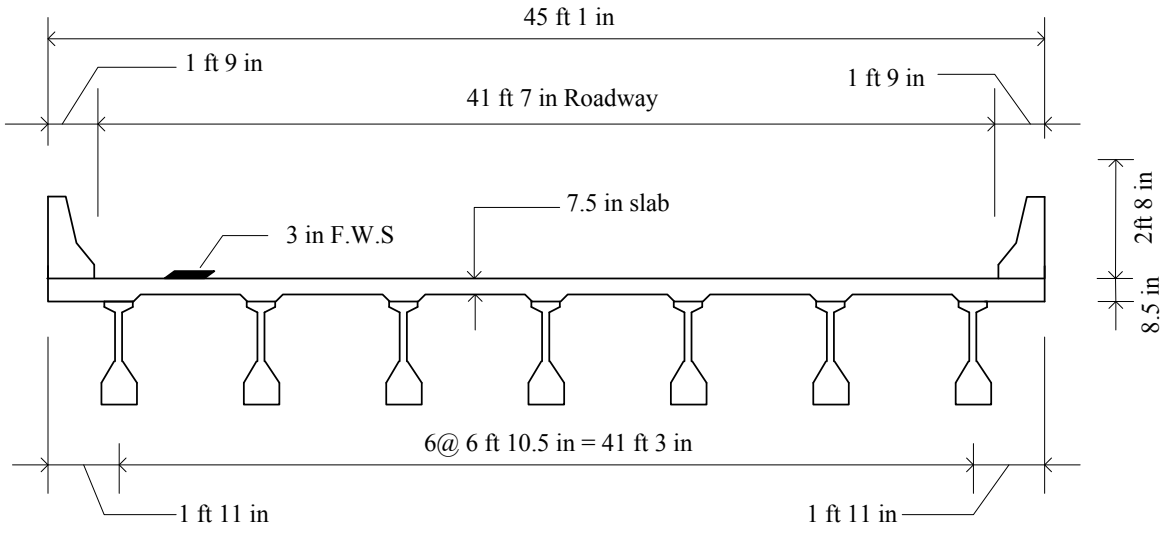

Fig. 4.1.1-1b Cross section of bridge deck

The modulus of elasticity is taken as 3,300 ksi, and 29,000 ksi, (23 GPa and 200 GPa) for concrete slab, prestressed and non-prestressed steel respectively. A bi-linear temperature gradient as recommended by AASHTO-LRFD (Table 3.12.3.1) for zone 3 is adopted as shown in Fig. 4.1.2-2.

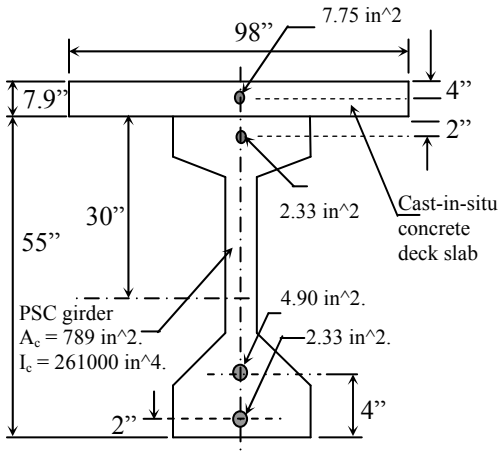

Fig. 4.1.1-1c PSC composite cross-section

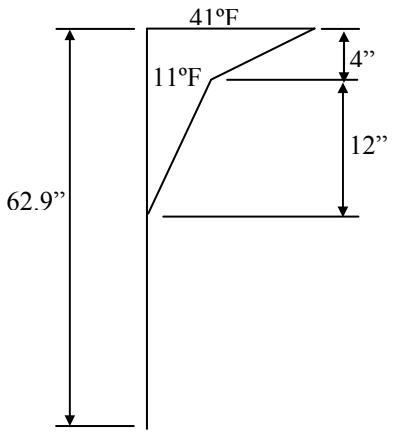

Fig. 4.1.1-2 Vertical temperature gradient in the superstructure

As described in section 3.4.3.1 the structure is analyzed in four stages as follows:

i) precast girder immediately after the transfer of prestress;

ii) precast girder prior to casting of the deck;

iii) precast girder immediately after casting of deck slab; and

iv) composite girder after the hardening of deck slab.

In stage I the instantaneous strain at any fiber across the cross-section and deflection along the span are calculated considering the PSC girder as a simply supported girder subjected to self-weight of the girder and the initial prestressing force. The strain and deflection in the simply supported PSC girder due to the creep, shrinkage, relaxation of prestressing steel, and temperature gradient are calculated in stage II. Since the composite action occurring during first three days after casting of slab is ignored, the instantaneous strain and deflection induced due to the slab weight are calculated in stage III, considering the girder as a simply supported beam.

In stage IV, the deck slab is assumed to attain strength and the girder and slab act together as a composite section. The properties of composite cross-section are considered in this stage. Since the abutment and the deck are integrally cast, the end supports are no longer simple supports. The simple support condition seizes to exist. Now the structure becomes statically indeterminate. The strain and deflection of the statically indeterminate composite section due to self-weight of the girder and slab along with the prestress P are evaluated as explained in section 3.4.3.1. The time-dependent change in the redundant forces due to creep, shrinkage, relaxation of prestress, and the temperature gradient in the composite section are also calculated. AASHTO and ACI models were used to compute the time dependent bending moment due to creep, shrinkage and temperature effects at various stages of construction.

From the computed time-dependent bending moment values, it can be seen that a redistribution of the longitudinal internal forces over a period of time occurs and the negative moment at the supports due to the continuity is redistributed due to the time-dependent effects and the moment along the span tends to approach the moment values equal to the values of the simply supported girder. Hence, it may be a conservative assumption to assume the girders as simply supported for positive moments. However, there is a considerable negative moment present at the support immediately after the cross section becomes composite due to casting of in-situ deck slab and the integral abutment. The deformations and stresses due to time-effects on continuous composite deck of a two span integral abutment bridge due to typical sustained loads are computed and presented in tables 4.1.1-1 to 4.1.1-7.

Table 4.1.1-1Moment at support and at mid-span at different times, lb-in.

Time (Days)	AASHTO		ACI	
	Support	Mid-span	Support	Mid-span
3	0.00E+00	-6.84E+06	0.00E+00	-6.84E+06
61	0.00E+00	9.53E+06	0.00E+00	9.53E+06
63	-6.35E+06	3.18E+06	-6.35E+06	3.18E+06
10284	-2.14E+06	7.39E+06	-1.34E+06	8.19E+06
Redistribution %	66.28	-132.55	78.91	-157.82

Time-dependent change in bending moment at various stages of construction at interior support with respect to time is shown in Fig. 4.1.1-3. It can be seen that the moment at the interior support reduced due to the time-dependent effects.

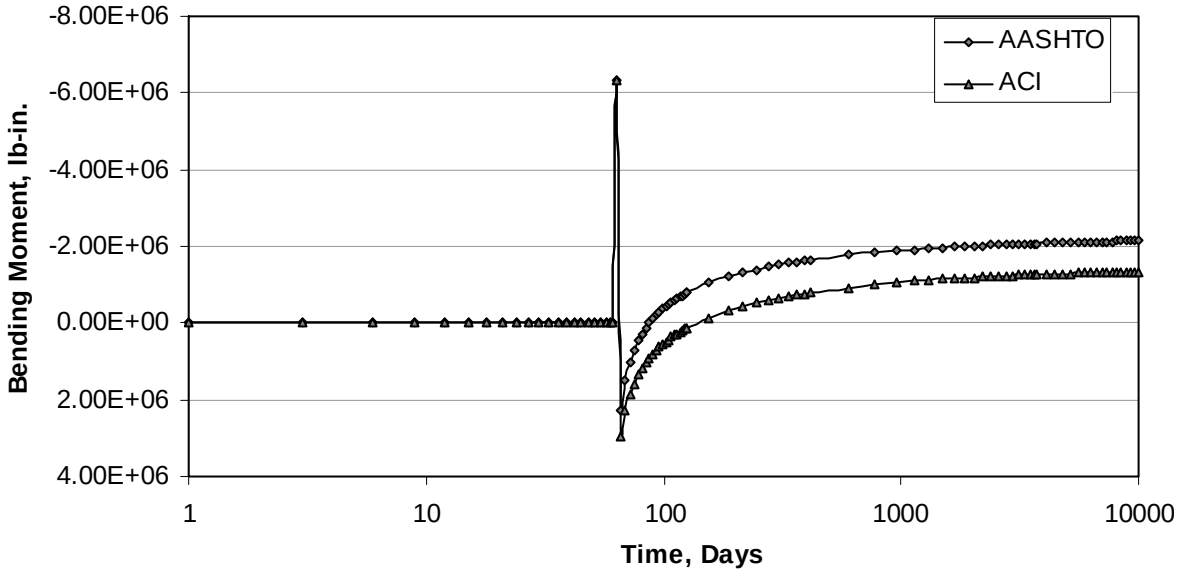

Fig. 4.1.1-3 Change in bending moments at interior support with respect to time

The time-dependent change in deflection at various stages of construction at mid-span with respect to time is shown in Fig. 4.1.1-4. It can be seen that the deflection increases over a period of time due to the time-dependent effects.

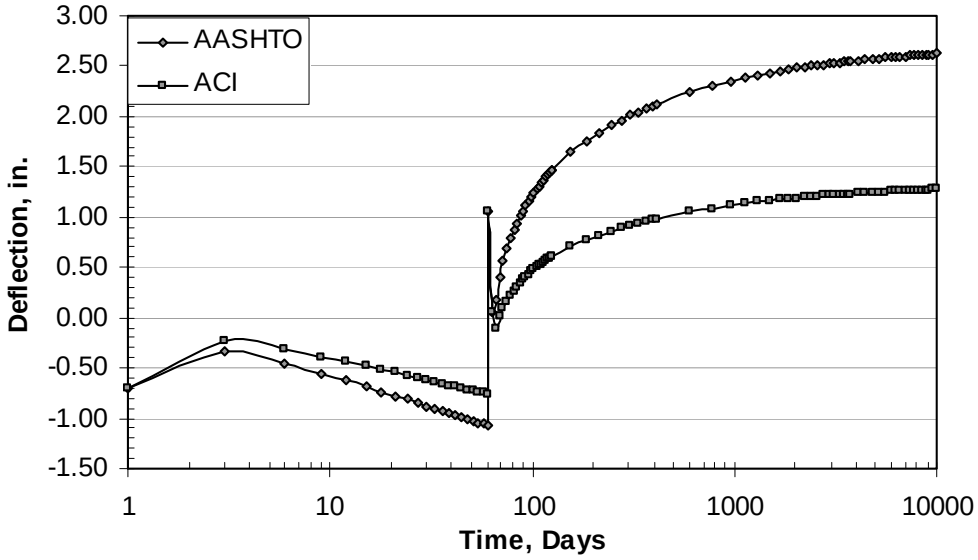

Fig. 4.1.1-4 Change in deflection at mid-span with respect to time

Time-dependent change in bending moment at various stages of construction along the span with respect to time is shown in Fig. 4.1.1-5. It can be seen that due to the time-dependent effects the moment at the mid-span tend to approach the value of a simply supported girder.

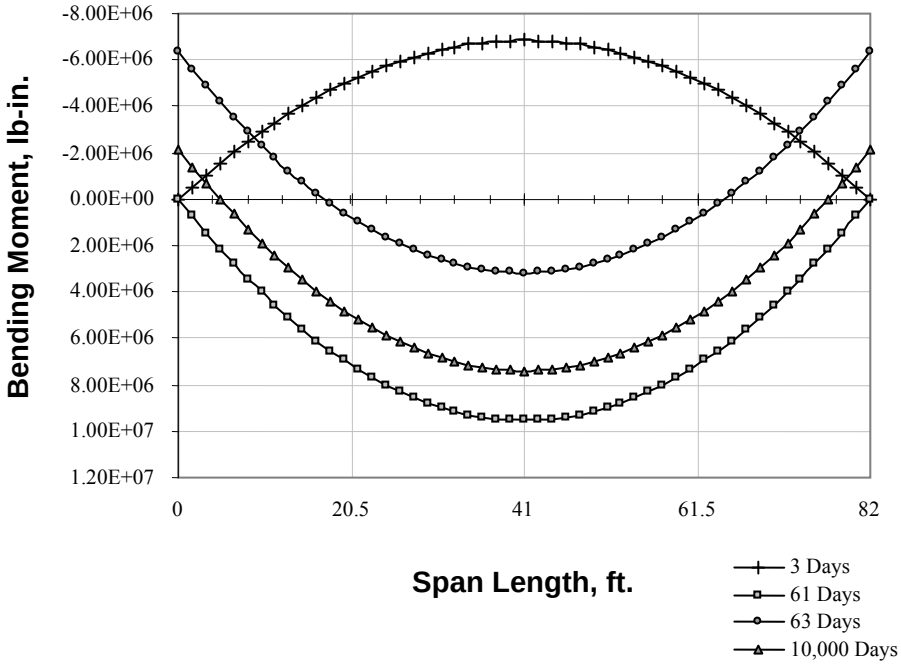

Fig. 4.1.1-5 Change in bending moments along the span with respect to time

Table 4.1.1-2 Change in stresses and forces at various times (ACI)

Time Days	Strain at the CG of the girder	Curvature /in.	Stress at the top fiber of the girder ksi	Stress at the bottom fiber of the girder ksi	Deflection at mid-span in.	Rc4 Reaction at C lb	MA4 Fixed end moment lb-in.	DelRc increase in redundant reaction lb	DelMA increase in redundant reaction lb-in.
3	-2.89E-04	-5.53E-06	-0.4392	-1.5452	-0.7124				
60	-6.25E-04	-8.95E-06	-0.4878	-1.2560	-1.4749				
61	-6.31E-04	1.57E-06	-2.2332	0.1130	-0.4123				
63	-7.89E-04	-7.62E-07	-2.6989	-1.0438	-0.3597	77482.01	-6.35E+06		
10284	-1.20E-03	-2.61E-06	-2.7351	-0.3849	0.9140	77482.01	-1.34E+06	0.00	5.01E+06

Table 4.1.1-3 Strain in various fibers at different times (ACI)

Time Days	Deck top fiber	Deck reinforcement level	Deck bottom fiber	Girder top fiber	Top reinforcement level	Prestress level	Bottom reinforcement level	Gider bottom fiber
3				-1.21E-04	-1.32E-04	-4.04E-04	-4.15E-04	-4.26E-04
60				-2.33E-04	-2.39E-04	-4.08E-04	-4.15E-04	-4.21E-04
61				-3.25E-04	-3.05E-04	2.14E-04	2.34E-04	2.55E-04
63	-6.84E-05	-7.76E-05	-8.68E-05	-8.68E-05	-9.14E-05	-2.06E-04	-2.11E-04	-2.16E-04
10284	-3.43E-04	-3.50E-04	-3.57E-04	-3.57E-04	-3.61E-04	-4.52E-04	-4.56E-04	-4.60E-04

Table 4.1.1-4 Stress in various fibers at different times, ksi (ACI)

Time Days	Deck top fiber	Deck reinforcement level	Deck bottom fiber	Girder top fiber	Top reinforcement level	Prestress level	Bottom reinforcement level	Gider bottom fiber
3	0.0000	0.0000	0.0000	-0.4392	-3.8297	-11.7297	-12.0457	-1.5452
60	0.0000	0.0000	0.0000	-0.4878	-10.7746	-23.5575	-24.0689	-1.2560
61	0.0000	0.0000	0.0000	-2.2332	-19.6078	-17.3600	-17.2702	0.1130
63	-0.2281	-2.2500	-0.2894	-2.6988	-22.2582	-23.3459	-23.3896	-1.0438
10284	-0.2245	-14.3611	-0.2213	-2.7351	-34.1373	-33.2924	-33.2587	-0.3849

Table 4.1.1-5 Strain in various fibers at different times (AASHTO)

Time Days	Deck top fiber	Deck reinforcement level	Deck bottom fiber	Girder top fiber	Top reinforcement level	Prestress level	Bottom reinforcement level	Gider bottom fiber
3				-1.21E-04	-1.32E-04	-4.04E-04	-4.15E-04	-4.26E-04
60				-3.17E-04	-3.25E-04	-5.43E-04	-5.52E-04	-5.61E-04
61				-3.25E-04	-3.05E-04	2.14E-04	2.34E-04	2.55E-04
63	-6.84E-05	-7.76E-05	-8.68E-05	-8.68E-05	-9.14E-05	-2.06E-04	-2.11E-04	-2.16E-04
10284	-5.60E-04	-5.62E-04	-5.65E-04	-5.65E-04	-5.66E-04	-5.97E-04	-5.99E-04	-6.00E-04

Table 4.1.1-6 Stress in various fibers at different times, ksi (AASHTO)

Time Days	Deck top fiber	Deck reinforcement level	Deck bottom fiber	Girder top fiber	Top reinforcement level	Prestress level	Bottom reinforcement level	Gider bottom fiber
3				-0.4392	-3.8297	-11.7297	-12.0457	-1.5452
60				-0.9370	-17.0992	-39.2171	-40.1015	-2.7174
61				-3.1802	-39.2019	-60.5070	-61.3587	-2.5207
63	-0.2281	-2.2500	-0.2894	-5.8890	-63.9549	-87.7829	-88.7352	-3.4808
10284	-0.3616	-22.7539	-0.3730	-8.6900	-106.5223	-129.2070	-130.1134	-3.6992

Table 4.1.1-7 Change in stresses and forces at various time (AASHTO)

Time Days	Strain at the CG of the girder	Curvature /in.	Stress at the top fiber of the girder ksi	Stress at the bottom fiber of the girder ksi	Deflection at mid-span in.	Rc4 Reaction at C lb	MA4 Fixed end moment lb-in.	DelRc increase in redundant reaction lb	DelMA increase in redundant reaction lb-in.
3	-2.89E-04	-5.53E-06	-0.4392	-1.5452	-0.7124				
60	-7.40E-04	-9.96E-06	-0.4978	-1.1723	-1.7857				
61	-7.46E-04	5.69E-07	-2.2432	0.1967	-0.7232				
63	-9.03E-04	-1.77E-06	-2.7088	-0.9601	-0.6706	7.75E+04	-6.35E+06		
10284	-1.49E-03	-2.41E-06	-2.8011	-0.2185	1.9515	7.75E+04	-2.14E+06	0.00E+00	4.21E+06

4.1.1.2 Substructure analysis with discrete spring modeling

The typical dimensions of the abutment wall, wing wall, the pile supports and the backfill are shown in Fig. 4.1.1-6. It is assumed that medium dense sand having a soil modulus of 360 ksf (17.2 MPa) is used as backfill in the abutment. The influence factors, which depend on the ratio of the dimension of the rectangular loaded area, usually vary from 1.0 to 3.0. Poisson's ratio is assumed as 0.3. The wingwalls are not integral with abutment, hence their stiffness contributions can be neglected. The piles are considered to have fixed head and is assumed that there is no relative movement or rotation between the piles and abutment. The width of the abutment wall is assumed as 45.1 ft. (13.75 m). Equivalent cantilever length based on stiffness criterion is used to evaluate the stiffness of the pile. The expressions for spring stiffness of the substructure system for the two dimensional problem are given by Eqns 3.2-10, 3.2-12 and 3.2-14.

The axial force and bending moment induced on the piles are evaluated by analyzing the bridge system using conventional structural analysis procedure considering the moments obtained from the time-dependent analysis applied at the superstructure-abutment joint. Moments at the abutments due to the time-dependent effects evaluated based on the AASHTO and ACI models presented in Table 4.1.1-1 show that the negative moment at the abutments tend to approach the values of moment, as if the abutments were simply supported. The maximum moment occurs at the abutments at the instant of the superstructure becoming composite. Hence, only the maximum moment at the abutment at time t = 63 days is taken as the critical moment for the substructure analysis.

A parametric study representing fixed-head prestressed concrete piles with a length/diameter ratio of 25 (Wilson, 1988) considering different abutment-wingwall sizes with zero pile stiffness showed that piles account for at least 50% of the total stiffness. Their largest contribution to translational stiffness is in vertical direction (72%) and rotational stiffness about the x and y axes (75%). Use of other more flexible pile systems might reduce the percentage of total stiffness, which is contributed by the piles. On a conservative side, assuming the stiffness of the pile system as 75%, piles of the substructure system is apportioned with seventy five percent of the calculated moment in the abutment-pile-soil system in this study.

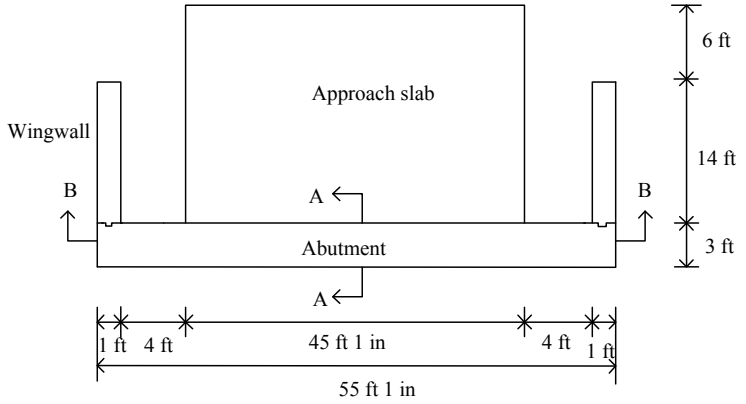

Fig. 4.1.1-6 (a) Abutment, wing wall and approach slab plan

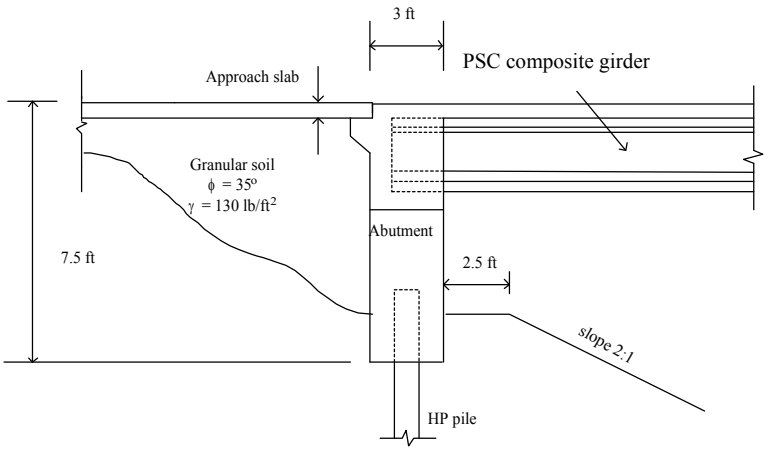

Fig. 4.1.1-6 (b) Abutment cross section

The laterally loaded piles with axial force and bending moments determined from the above procedure is then analyzed for the lateral deflection, bending moment, shear force and stress along the depth. The results of the analysis are plotted in Fig. 4.1.1-7 (a) – (d). Only about 50% of the depth from the pile head is shown in the figure for clarity. Beyond this depth the values are almost constant. The pile analysis shows that the pile lateral displacement of 0.014 in. and the stress in the pile are within the allowable limits. The lateral displacement, moment, shear and stress obtained by this approach are comparable to those of the values obtained using secondary P-Δ method for laterally loaded piles. From the results plotted, it can be seen that, the influence of the lateral soil reactions are concentrated along the top 10 ft. (3.0 m) of the pile, which is about 10 times the equivalent diameter of the pile. Beyond this depth, lateral displacement, shear force and moment are almost negligible and the lateral forces are insignificant.

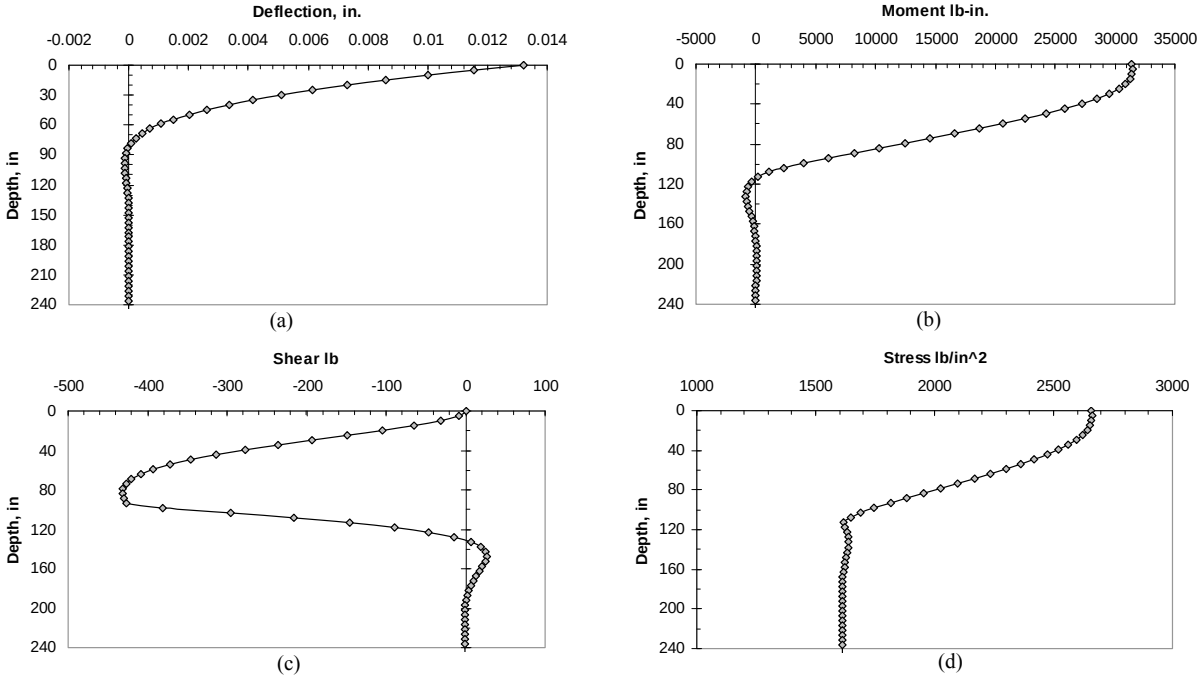

Fig. 4.1.1-7 Pile analysis results along the depth: (a) variation of horizontal displacement; (b) variation of bending moment; (c) variation of shear; (d) variation of stress

4.1.2.Steel- Composite Concrete Continuous Integral Bridges

4.1.1.1 Superstructure analysis for creep, shrinkage and temperature gradient

To illustrate the model developed under section 3.4 for analysis of continuous integral abutment bridges, a two span continuous concrete-steel composite integral abutment bridge of span 65 ft. (19.8 m) each is analyzed using the analytical procedure to determine the time-dependent redundant forces based on AASHTO and ACI models for two cases: i) with end supports having full restraints and, ii) with simply supported ends.

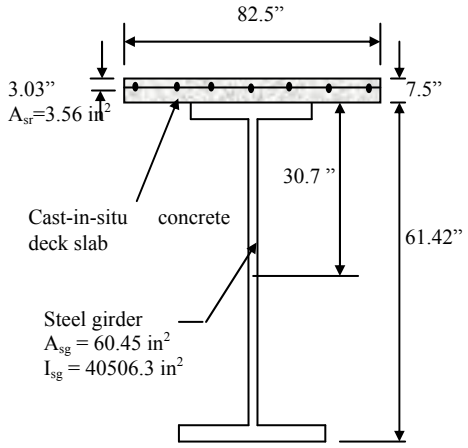

Fig. 4.1.2-1 Steel-composite cross-section

The relevant properties and dimensions are b_c = 82.5 in. (2095.5 mm), y_c = 7.5 in. (190.5 mm), y_{sr} = 3 in. (80mm), A_s = 3.56 in.^{2} (2300 mm^2), y_{gc} = 30.7 in. (780 mm), y_g = 61.5 in. (1560mm), A = 60.45 in.^{2} (39000 mm^2), I_{sg} = 40506.3 in.^{4} (16.86 x 10^9 mm^2), p = 3.22 kip/ft. (47 kN/m.), Modulus of elasticity of concrete, E_c = 3190 ksi (22,000 MPa), and that of steel, E_s =

29,000 ksi (200,000 MPa). The ultimate creep coefficient ϕ_u = 1.68, and the ultimate shrinkage strain ε_{sh} = 0.00052. A tri-linear temperature gradient as recommended by AASHTO-LRFD (Table 3.12.3.1) for zone 3 is adopted as shown in Fig. 4.1.2-2.

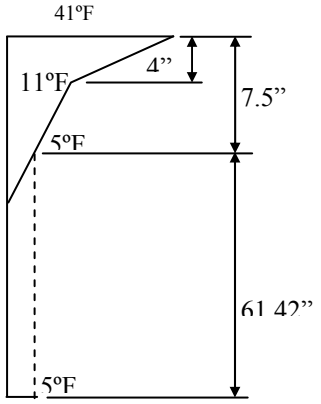

Fig. 4.1.2-2 Vertical temperature gradient in the superstructure

The iterative procedure as explained in section 3.4.3.2 is used to analyze the time dependent bending moment along the span of the superstructure due to creep, shrinkage and temperature gradient. The instantaneous moments and time dependent bending moment due to creep, shrinkage and temperature effects were computed using AASHTO and ACI models. The computed time-dependent moment values show a redistribution of the longitudinal internal forces over a period of time. An increase in the negative bending moment at supports was observed along with a reduction in the positive moments at mid-span (Table 4.1.2-1). The change in bending moment at interior support over a period of 10000 days is shown in Fig. 4.1.2-3 both for fixed end condition and for pinned end condition in order to show the advantage of using integral abutment bridges over conventional seated bridges.

Table 4.1.2-1 Bending moments at the mid-span and the interior support

Description	**Moment, (lb-in)**			
	Fixed		Simple	
	AASHTO	ACI	AASHTO	ACI
at Mid-span				
t = 0 days	7.54E+06	7.54E+06	1.08E+07	1.08E+07
t = 10000 days	-1.45E+06	5.04E+05	4.34E+06	5.87E+06
Redistribution, %	-119.26	-93.31	-59.97	-45.84
at Interior support				
t = 0 days	-1.29E+07	-1.29E+07	-1.92E+07	-1.92E+07
t = 10000 days	-2.19E+07	-1.99E+07	-3.21E+07	-2.91E+07
Redistribution, %	69.82	54.63	67.85	51.86

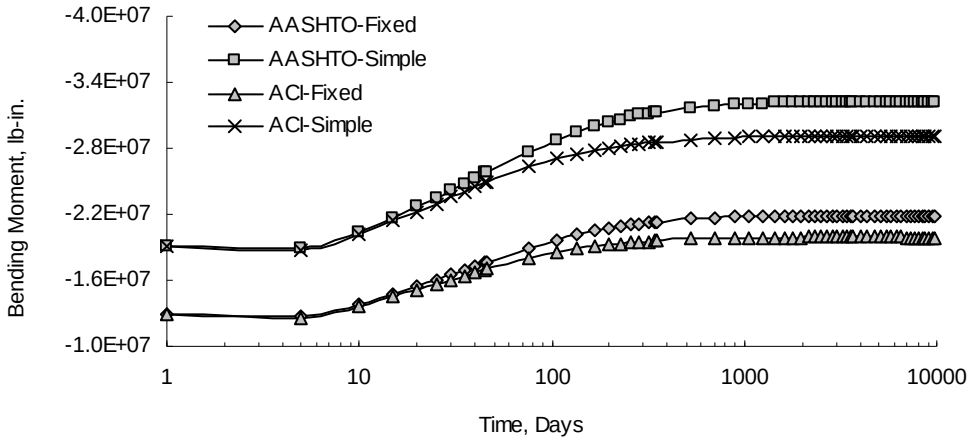

Fig. 4.1.2-3 Change in bending moments at interior support with respect to time

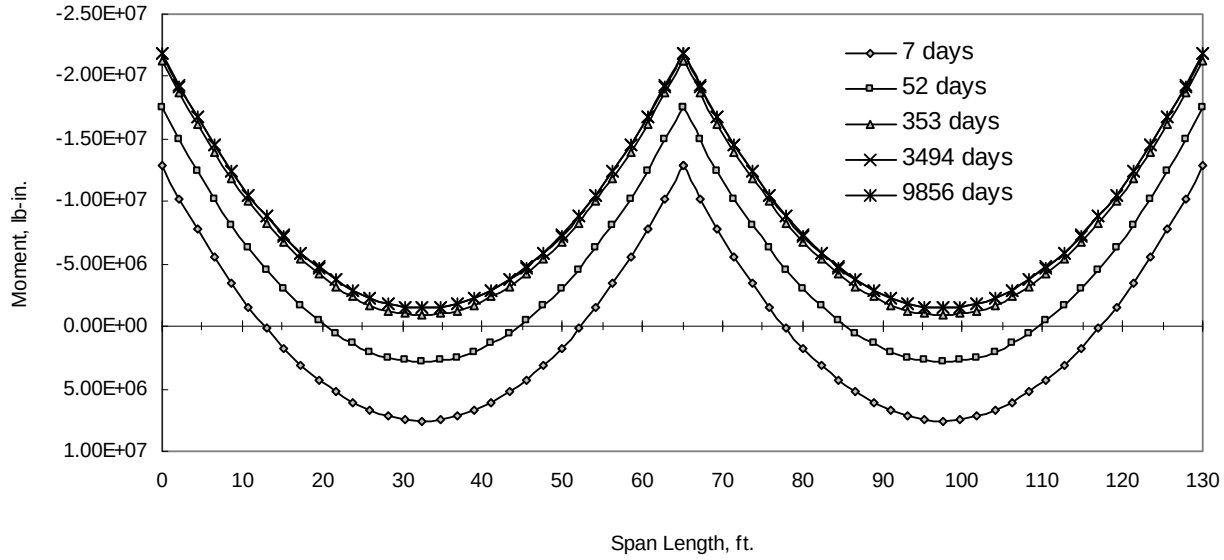

(a)

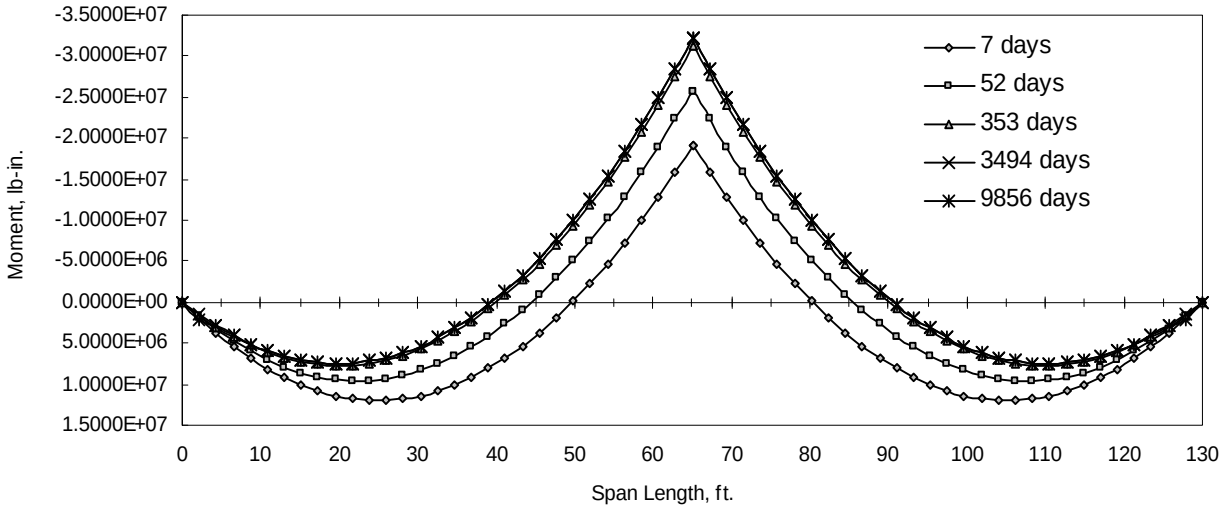

(b)

Fig. 4.1.2-4 Time dependent bending moment diagrams: (a) fixed end condition; (b) pinned support condition

The change in bending moment along the span over a period of time is shown in Fig. 4.1.2-4 both for fixed end condition and for pinned end conditions. There is considerable rate of increase in the moments in the first three months. A slow rate of increase in moment is observed after about six months in the integral abutment bridge with fixed ends. However, the rate of moment increase is insignificant after about one year in the case of integral abutment bridges with pinned end supports. There is a rapid increase in the moment along the span in the first two months period due to creep and shrinkage effects. The rate of change in moment decreases after this period. The moment value reaches a near constant value in one year. It can be seen from the resulting time dependent bending moment diagrams, that assumption of a simple support at the ends for an integral abutment bridge produces approximately twice the moment in the girder with fixed end condition. In both fixed and pinned end conditions the AASHTO model predicts higher moments than those based on the ACI model.

Fig 4.1.2-5 shows the variation of deflection over a period of time at the mid-span for the sustained loads. It can be seen that, the deflection of the girder with full restraint is considerably smaller than that with simple supports. Table 4.1.2-2 shows around hundred percent increase in deflection due to time-dependent effects. Significant changes in stresses can be observed from Table 4.1.2-3 which provides the summary of instantaneous stress values at initial time t = 0 days and stresses at 10,000 days in the concrete and steel in the mid-span and interior support sections.

Table 4.1.2-2 Deflections at the mid-span

Description	**Deflection at Mid-span, in.**			
	Fixed End		Simple Support	
	AASHTO	ACI	AASHTO	ACI
t = 0 days	0.14	0.14	0.24	0.24
t = 10000 days	0.30	0.29	0.48	0.42
deflection due to time effects	0.16	0.15	0.24	0.18
% of delayed deflection	118.26	110.43	96.93	74.15

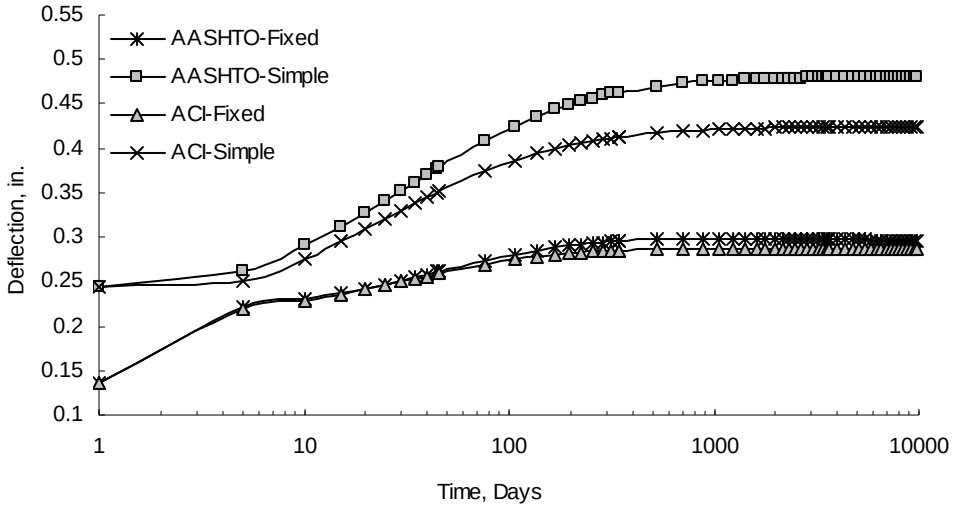

Fig 4.1.2-5 Variation of deflection over a period of time at the mid-span

Table 4.1.2-3 Stresses at the critical sections

Description	**Stressses, ksi**			
	Fixed End		Simple Support	
	AASHTO	ACI	AASHTO	ACI
at Mid-span				
Concrete top fiber				
t=0 days	-0.2030	-0.2030	-0.2915	-0.2915
t= 10000 days	0.0754	-0.0218	-0.2234	-0.2538
Concrete bottom fiber				
t=0 days	-0.1247	-0.1247	-0.1798	-0.1798
t= 10000 days	0.0551	-0.0160	-0.1653	-0.1798
Steel reinforcement				
t=0 days	-1.5620	-1.5620	-2.2451	-2.2451
t= 10000 days	0.6091	-0.1755	-1.8187	-2.0363
Girder top fiber				
t=0 days	-1.1385	-1.1385	-1.6374	-1.6374
t= 10000 days	0.5018	-0.1407	-1.4996	-1.6403
Girder bottom fiber				
t=0 days	4.6657	4.6657	6.7078	6.7078
t= 10000 days	-0.9645	0.3278	2.8789	3.8071
at Interior support				
Concrete top fiber				
t=0 days	0.3466	0.3466	*	0.5163
t= 10000 days	*	*	*	*
Concrete bottom fiber				
t=0 days	0.2146	0.2146	0.3191	0.3191
t= 10000 days	*	*	*	*
Steel reinforcement				
t=0 days	2.6672	2.6672	3.9681	3.9681
t= 10000 days	9.1690	6.9094	13.4837	10.0957
Girder top fiber				
t=0 days	1.9463	1.9463	2.8949	2.8949
t= 10000 days	7.5635	5.5649	11.1211	8.1320
Girder bottom fiber				
t=0 days	-7.9710	-7.9710	-11.8593	-11.8593
t= 10000 days	-14.5163	-12.9166	-21.3474	-18.8745

* the stress in the concrete fiber exceeds the tensile capacity of the concrete.

Figs. 4.1.2-6 to 4.1.2-8 show the variation of the stresses with time in the cross section. The evolution of stress is rapid in the initial period of about 400 days with AASHTO modeling,

it is interesting to note that reversal of stresses occurs at mid span section in the fixed end support case. The variation in the stresses both in steel reinforcement and the girder is gradual.

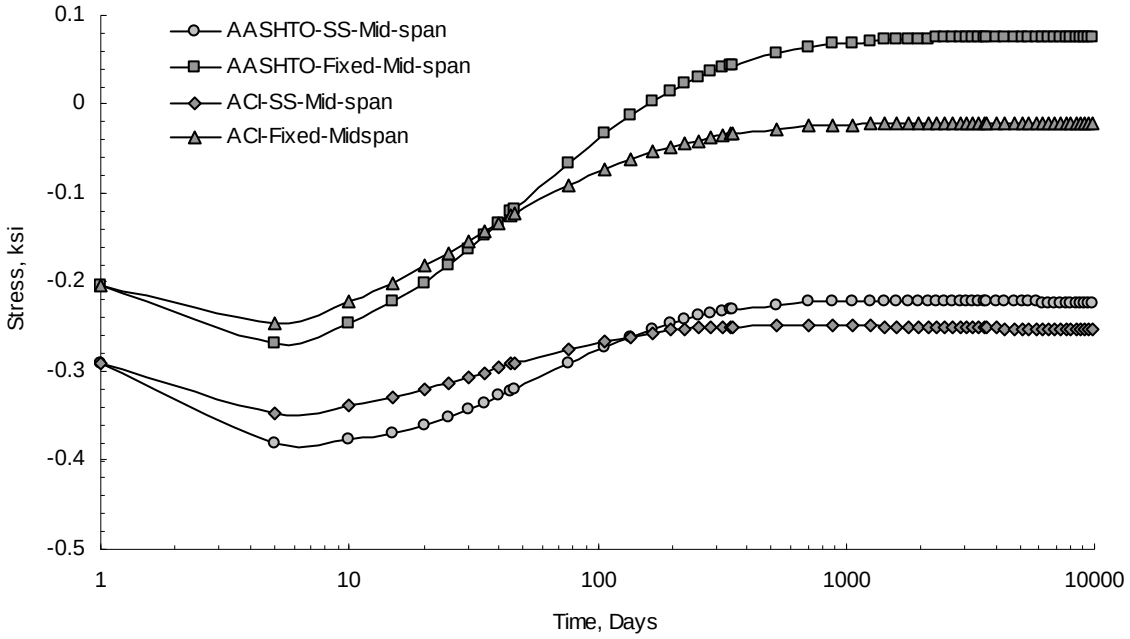

Fig. 4.1.2-6 Variation of stresses in deck slab top fiber

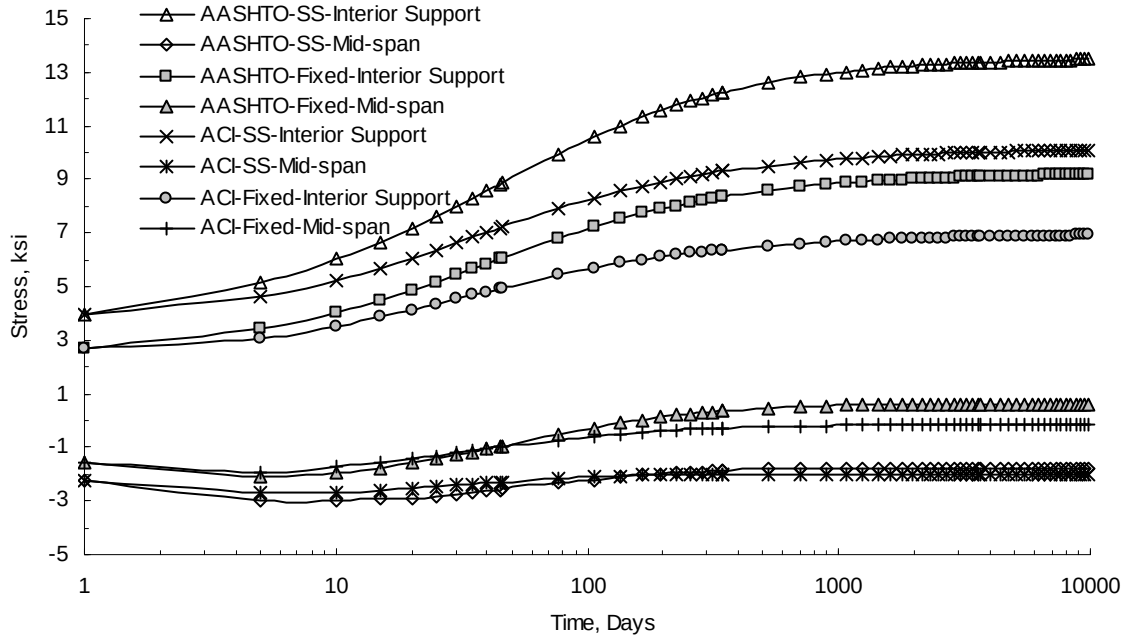

Fig. 4.1.2-7 Variation of stresses in steel reinforcement

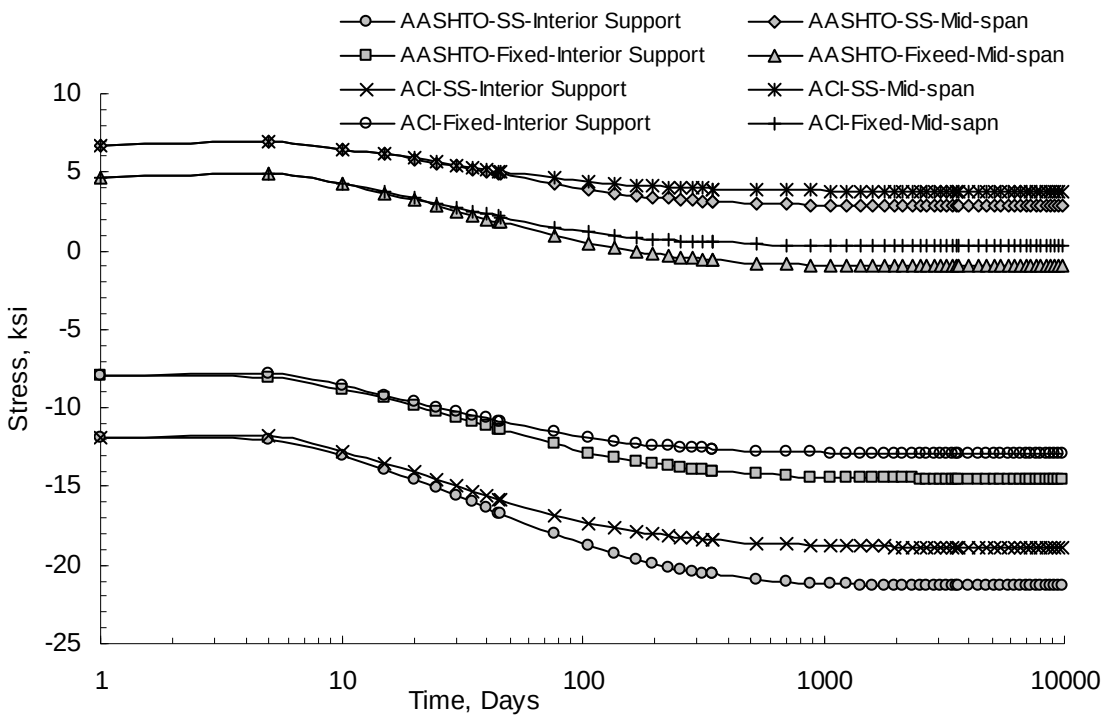

Fig. 4.1.2-8 Variation of stresses at steel girder bottom fiber

4.1.2.2 Substructure analysis with discrete spring modeling

The dimensions of the abutment wall, wing wall, the pile supports and the backfill as shown in Fig. 4.1.1-4 are also used in this example. All the assumptions - including using medium dense sand having a soil modulus of 360 ksf (17.2 MPa) as backfill in the abutment - are same as explained in section 4.1.1.2. The axial force and bending moment induced on the piles are evaluated by analyzing the bridge system using conventional structural analysis procedure considering the moments obtained from the time-dependent analysis applied at the superstructure-abutment joint.

The laterally loaded piles with axial force and bending moments determined from the above procedure are then analyzed for the lateral deflection, bending moment, shear force and stress along the depth. The results of the analysis based on the AASHTO and ACI models are plotted in Fig. 4.1.2-9 (a) – (d). Only about 50% of the depth from the pile head is shown in the figure for clarity. Beyond this depth the values are almost constant.

Similar to the results obtained in the case of PSC composite girder integral abutment bridges, the pile analysis with steel composite girder integral abutment bridge shows a lateral pile displacement of 0.05 in. The stress in the pile are within the allowable limits. The lateral displacement, moment, shear and stress obtained by this approach are comparable to those of the values obtained using secondary P-Δ method for laterally loaded piles. From the results plotted, it can be seen that, the influence of the lateral soil reactions are concentrated along the top 10 ft. (3.0 m) of the pile, which is about 10 times the equivalent diameter of the pile irrespective of different type of superstructure. Beyond this depth, lateral displacement, shear force and moment are almost negligible and the lateral forces are insignificant.

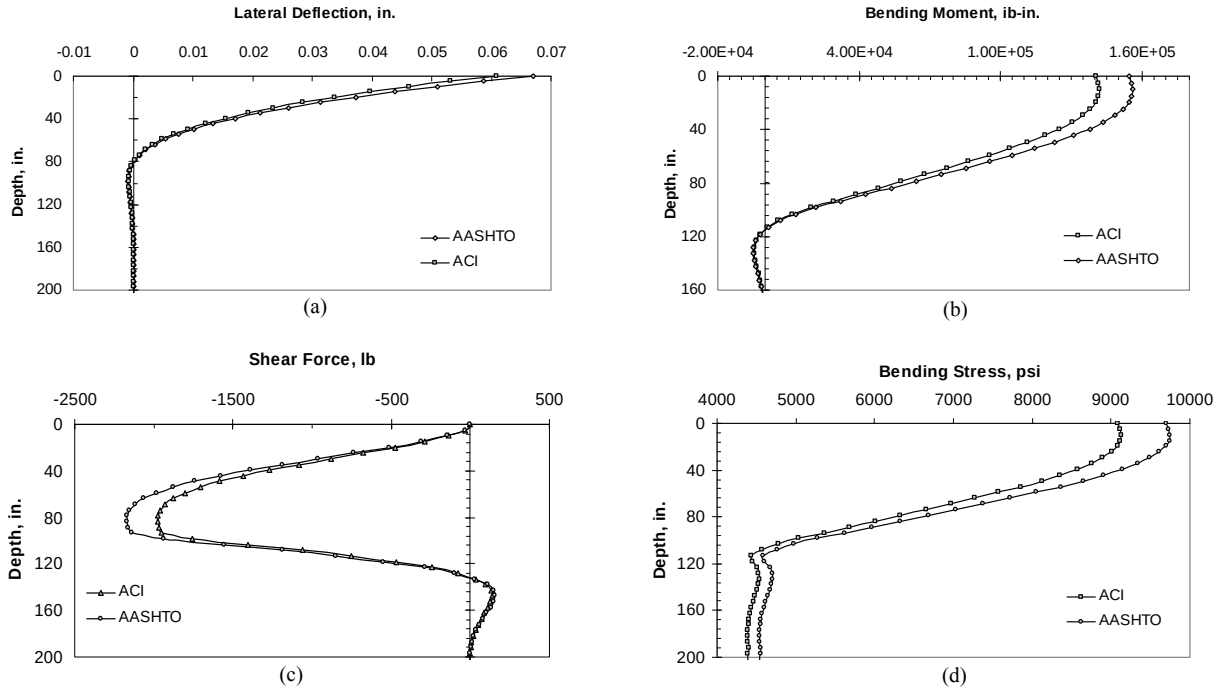

Fig. 4.1.2-9 Pile analysis results along the depth: (a) variation of horizontal displacement; (b) variation of bending moment; (c) variation of shear; (d) variation of stress

4.2 Equivalent Cantilever Idealization for Laterally Loaded Piles

4.2.1 Design data

- Two lane integral bridge (Figs. 4.2-1 and 4.2-2) with seven AASHTO Type III bridge girders (Figs. 4.2-3 and 4.2-4).
- Total length of 360 ft with five spans (60-80-80-80-60 ft).
- The coefficient of thermal expansion for concrete superstructure, $\alpha = 0.000006$ /° F (AASHTO specification).
- Load combination and load factors corresponding to AASHTO strength I are used in design.
- Approach slab of 12 in thickness. and width equal to width of deck slab (45 ft 1 in.) is assumed. The length of slab is assumed to be 20 ft. Fig. 4.2-4 shows the details of approach slab.
- Details of abutment are presented in Figs. 4.2-5.
- Total dead load of deck including the barrier and overlay is calculated as DW = 1,455.3 lb/ft.
- Vehicular live loading on the roadways of bridges or incidental structures, designated HL-93, shall consist of a combination of:
    - Design truck or design tandem
    - Design lane load
- SAP 2000 is used in the structural analysis of the intermediate pier, abutment and the pile.
- Maximum reaction on pile at abutment = 177.90 kips.

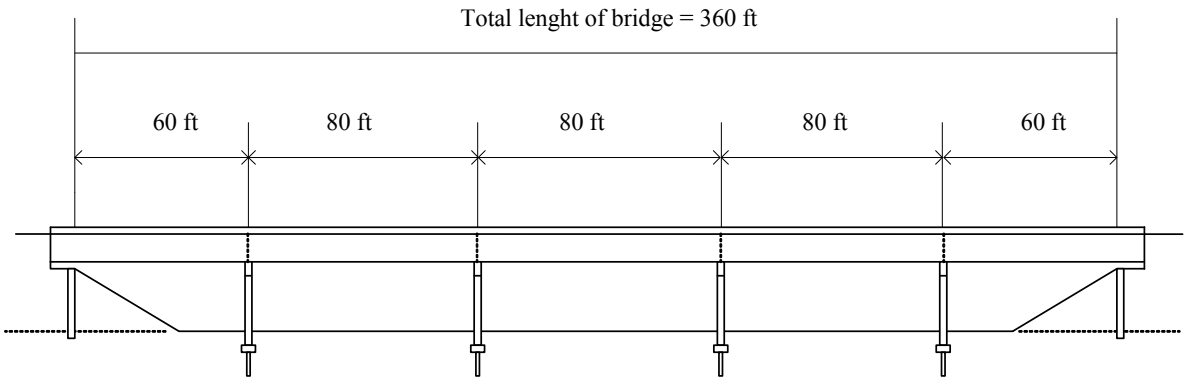

Fig. 4.2-1a Elevation of prestressed concrete girder integral abutment bridge

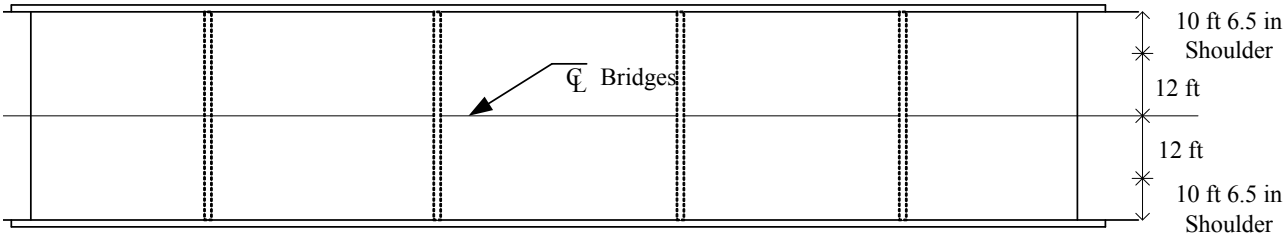

Fig. 4.2-1b Plan of prestressed concrete girder integral abutment bridge

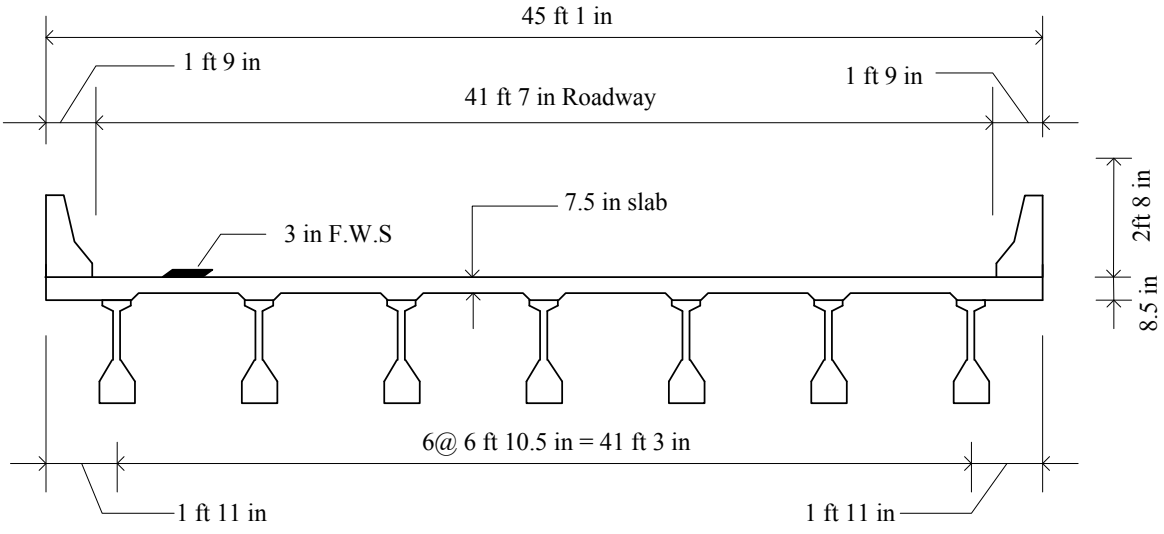

Fig. 4.2-2 Cross section of bridge deck

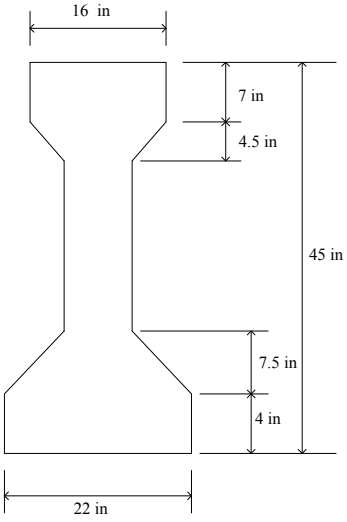

Fig. 4.2-3(a) AASHTO girder type III

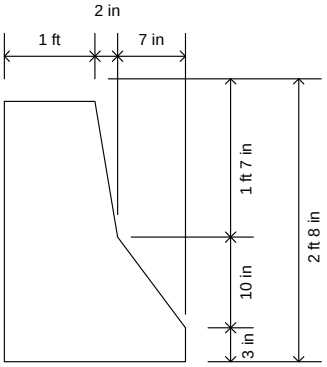

Fig. 4.2-3(b) Typical section of barrier

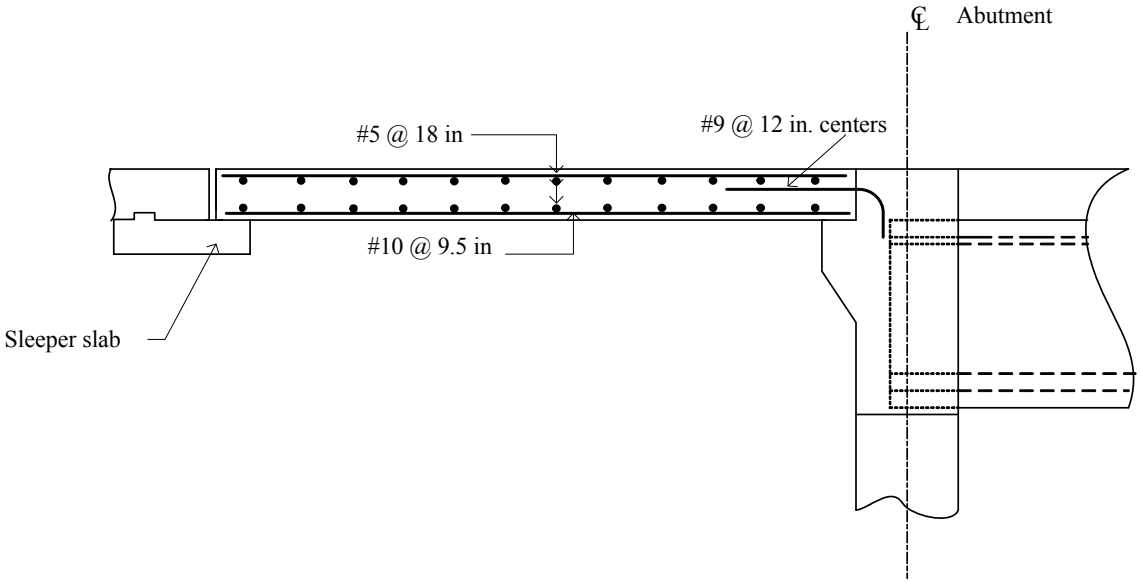

Fig. 4.2-4 Details of approach slab

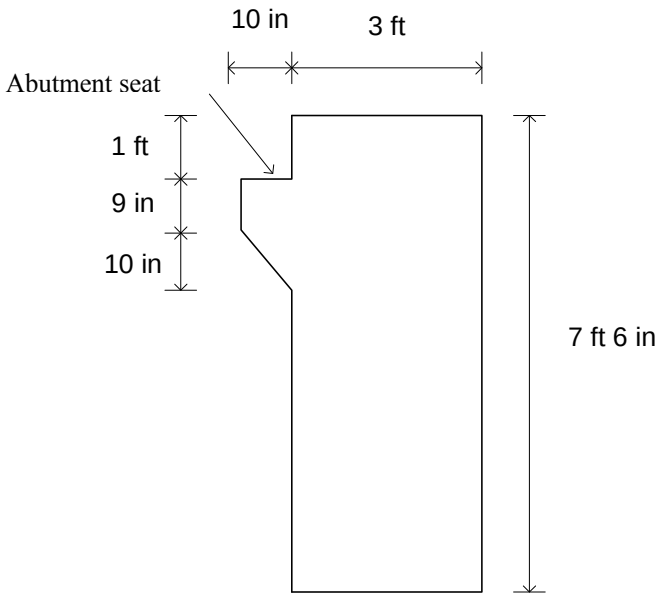

Fig. 4.2-5 (a) Abutment dimensions

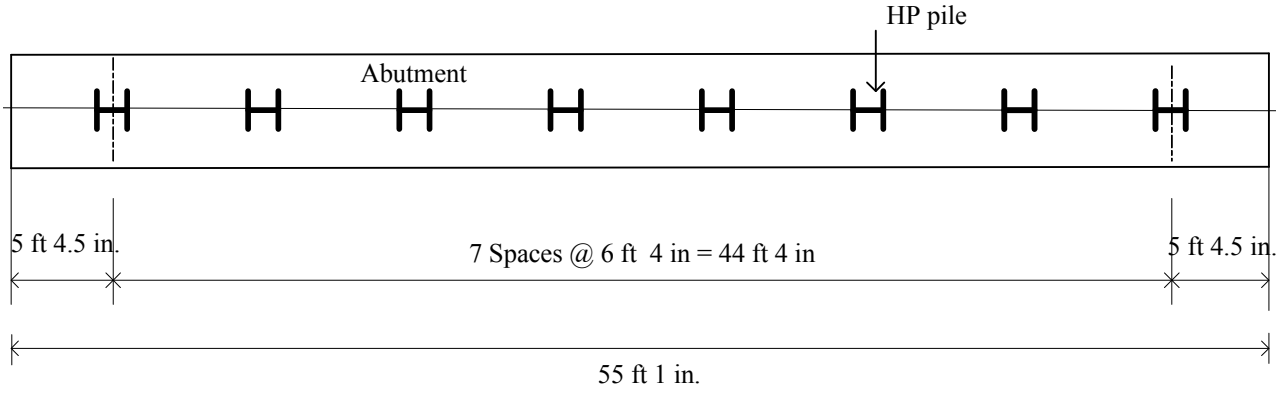

Fig. 4.2-5 (b) Abutment plan

Minimum pile length

Fig. 4.2-6 shows the soil strata consisting of stiff clay and very stiff clay. The minimum pile length required is based on the skin friction capacity of the pile. The α-method based on

total stress, is used to determine skin resistance (AASHTO 10.7.3.3.2a). An HP10 x 57 is assumed in the design and checked for adequacy.

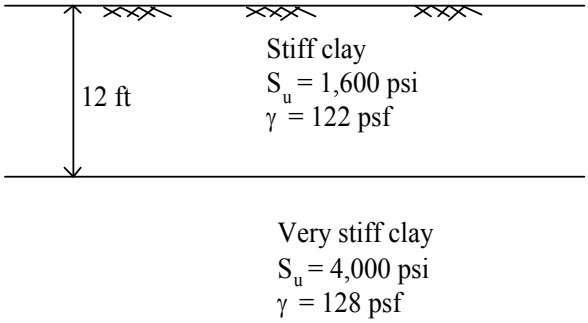

Fig. 4.2-6 Soil strata below abutment

A predrilled oversize hole filled with medium sand for a length of 8 ft from the bottom of abutment is assumed. Skin friction in predrilled hole filled with medium sand layer is neglected. Then the length of pile in the stiff clay layer becomes 8 ft (Fig. 4.2-7). Adhesion factor, α for different soil conditions can be obtained using the standard procedure described (Tomlinson, 1995). Since the top of stiff clay layer is filled with medium sand, adhesion factor, α obtained for L < 10B. [8(12) < (10)9.99] and S_u = 1.6 kip/ft^2, α = 1.

Skin friction of stiff clay per 1 ft of pile:

Friction capacity, $Q_s = f\,(L_p)$

$f = \square\ S_u$

L_p= perimeter = [(9.99/12)+(10.225/12)]2 = 3.37 ft

$Q_s = \square\ S_u\,(L_p)$

= 1 (1.6)(3.37) = 5.39 kip/ft

Skin friction of very stiff clay per 1 ft of pile:

finding α with $S_u = 4.0$ kip/ft^2

for $\frac{L}{B} = \frac{29(12)}{9.99} = 35 > 20$, the value of $\alpha = 0.53$.

$Q_s = \alpha\, S_u\, (L_p)$

$= 0.53(4.0)(3.37)$

$= 7.14$ kip/ft

The length of the embedment (neglecting bearing capacity) into the very stiff clay (l_2) is estimated by using resistance factor (AASHTO 1998, Table 10.5.5-2) □ $\phi = 0.7$.

$Q_R = \phi \Sigma Qs$

$177.90 = 0.7(5.39)(8) + 0.7(7.14)(l_2)$

$l_2 = 29.54$ ft

Using $l_2 = 29.75$ ft, the total length of pile is 29.75 + 8 +8 = 45.75 ft.

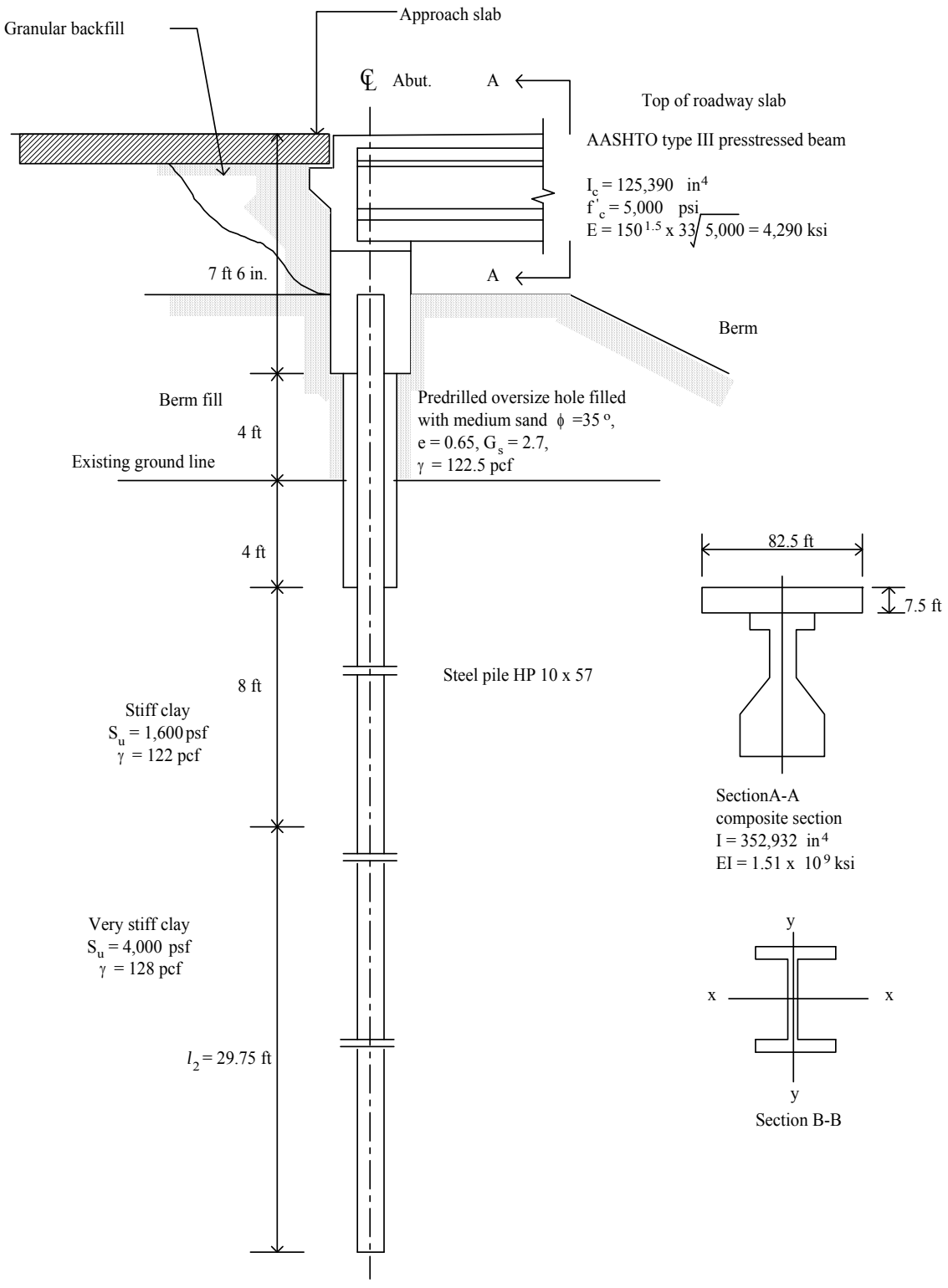

Fig. 4.2-7 Section through abutment and soil profile

4.2.2 Passive Earth Pressure

A horizontal force is induced on the back of the abutment as the bridge expands. This force can be estimated conservatively as the passive resistance of the soil behind the abutment, P_p. Passive soil pressure for a granular material is calculated as

$$P_p = \frac{1}{2}\gamma H^2 K_p$$

where

P_p = horizontal force due to passive soil pressure,

γ = soil unit weight,

H = height of abutment,

$K_p = \tan^2(45 + \frac{\phi}{2})$ (Rankine passive earth pressure coefficient), = 3.69

$$P_p = \frac{1}{2}(0.13)(7.5)^2(3.69)$$

= 13.49 kip/ft

Passive earth pressure is used to determine the bending moment in the integral abutments and hence it is conservative to assume that the maximum resistance is available, i.e., ϕ = 1.0 (AASHTO C10.5.5)

Total passive soil pressure per pile (pile spacing = 6.33ft)

P_p= 13.49(6.33) = 85.4 kips

4.2.3 Temperature and Shrinkage Effects

The horizontal displacement at each abutment due to temperature drop and shrinkage is calculated as follows:

Due to temperature drop, $\Delta_t = \alpha_t \Delta T L_b$

Due to shrinkage, $\Delta_s = \alpha_s L_b$

Creep effects are assumed to be negligible after 7 to 8 months of construction.

α_t = 0.000006 /°F (AASHTO, 5.4.2.2)

α_s = -0.0002 after 28 days,

-0.0005 after 1 year, (AASHTO, 5.4.3.2.1)

FHWA suggested using shrinkage reduction of 50%.

$\Delta = \Delta_t + 0.5\Delta_s$

= (0.000006)(40)(360)(12) + (0.5)(0.0002)(360)(12) = 1.47 in.

Displacement at each abutment = Δ/2 = 1.47/2 = 0.735 in.

4.2.4 Length of Equivalent Cantilever

4.2.4.1 Soil stiffness

Referring to Table 3.3-1 for the parameters for *p-y* curve, the initial stiffness of different soil layer are calculated as below:

Medium sand: $k_{h\ (\text{medium sand})} = \dfrac{J\gamma x}{1.35} =$

$$k_{h\ (\text{medium sand})} = \frac{600(122.5 - 62.4)8}{1.35} = 213{,}688.9\ \text{lb/ft}^2$$

Stiff clay: The smaller of the following is taken as p_u.

$p_u = 9S_uB$

$= 9(1.6)(9.99/12) = 11.99$ kip/ft

$$p_u = \left(3 + \frac{\gamma}{S_u}x + \frac{0.5}{B}x\right)S_u B$$

$$= [3 + \frac{(122 - 62.4)16}{1{,}600} + \frac{0.5(16)}{9.99/12}](1.6)(9.99/12) = 17.59\ \text{kip/ft}$$

Thus $p_u = 11.99$ kip/ft

$y_{50} = 2.5B\varepsilon_{50}$

$= 2.5(9.99/12)(0.01) = 0.0208$

$$k_{h\ (\text{stiff clay})} = \frac{p_u}{y_{50}}$$

$$k_{h\ (\text{stiff clay})} = \frac{11.99}{0.0208} = 576\ \text{kip/ft}^2$$

Very stiff clay: The smaller of the following is taken as p_u.

$p_u = 9S_uB$

$= 9(4.0)(9.99/12) = 29.97$ kip/ft

$$p_u = \left(3 + \frac{\gamma}{S_u}x + \frac{2.0}{B}x\right)S_u B$$

$$= [3 + \frac{(128 - 62.4)45.75}{4{,}000} + \frac{2(45.75)}{9.99/12}](4.0)(9.99/12) = 378.49\ \text{kip/ft}$$

Thus p_u = 29.97 kip/ft

$y_{50} = 2.0B\varepsilon_{50}$

$= 2.0(9.99/12)(0.005) = 0.0083$

$k_{h\ (very\ stiff\ clay)} = \frac{p_u}{y_{50}}$

$k_{h\ (very\ stiff\ clay)} = \frac{29.97}{0.0083} = 1{,}800$ kip/ft^2

Equivalent uniform soil stiffness: The equivalent cantilever length of the pile is calculated based on the equivalent uniform soil stiffness (Fig. 4.2-8) and critical length of the pile considerations. Two cases of soil strata are considered in arriving at the equivalent uniform soil stiffness.

- Case A. Considering the medium sand in the predrilled hole.
- Case B Neglecting the medium sand in the predrilled hole

The least value among the two is taken for design purposes.

Case A. Considering the medium sand in the predrilled hole (Fig. 4.2-9)

Equivalent uniform soil stiffness (k_e):

Step1: Assume k_e = 55 ksf

Step 2: Calculate l_o : $l_o = 2\left(\sqrt[4]{EI/k_e}\right)$

$l_o = 2\left(\sqrt[4]{\frac{29{,}000(101)}{0.382}}\right)$

= 105.24 in. (8.77 ft)

Step 3: Calculate I_k : (with l_2 = 8.77 - 8 = 0.77 ft)

$I_k = I_{k1} + I_{k2}$

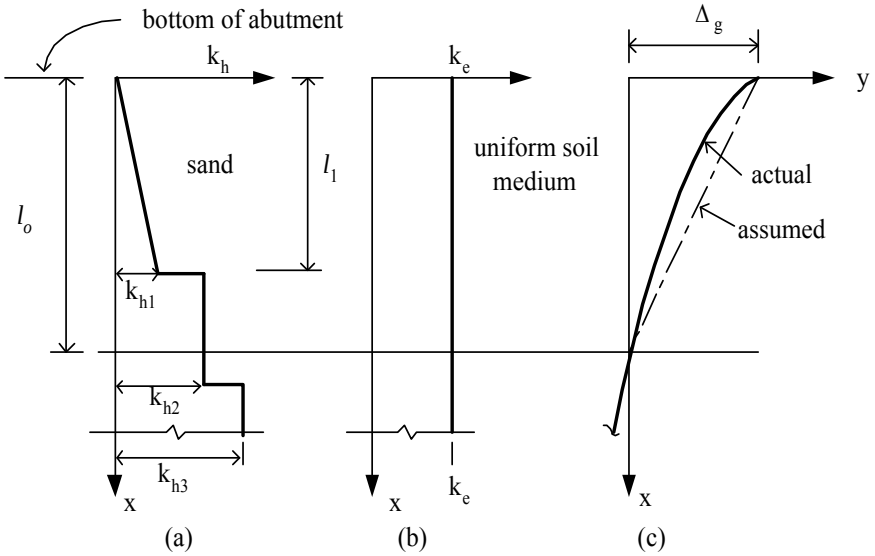

Fig. 4.2-8 Horizontal soil stiffness and displacement: (a) the variation of horizontal soil stiffness with depth, (b) an approximation of equivalent soil stiffness, (c) the displaced shape

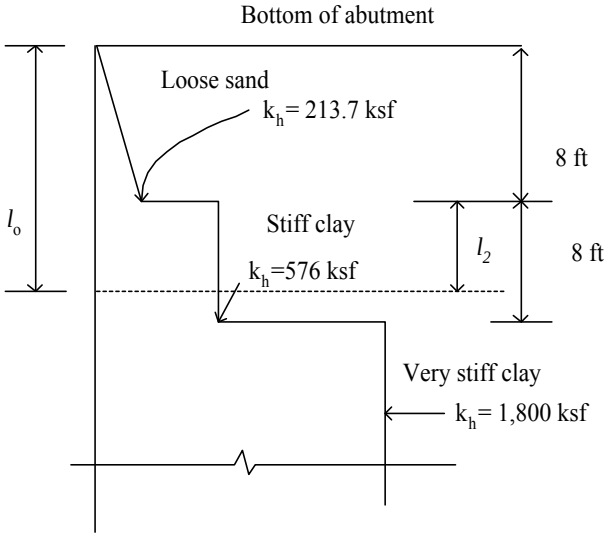

Fig. 4.2-9 Soil stiffness for case A

$$= \left\{ k_1 \left[\frac{d^3}{36} + \frac{d}{2}\left(a + \frac{2d}{3} \right)^2 \right] + k_2 \left[\frac{d^3}{36} + \frac{d}{2}\left(a + \frac{d}{3} \right)^2 \right] \right\} + k \left[\frac{d^3}{12} + dc^2 \right]$$

$$= \left\{ 0 + 213.7 \left[\frac{8^3}{36} + \frac{8}{2}\left(0.77 + \frac{8}{3} \right)^2 \right] \right\} + 576 \left[\frac{0.77^3}{12} + 0.77(0.385)^2 \right]$$

= 13,222.71 k-ft

Step 4: Determine k_e: $k_e = \frac{3I_k}{l_o^3}$

$$= \frac{3(13{,}222.71)}{(8.77)^3}$$

= 58.81 ksf (0.408 ksi)

Second Iteration

Step 2: Calculate l_o:

$$l_o = 2 \left(\sqrt[4]{\frac{29{,}000(101)}{0.408}} \right)$$

= 103.52 in. (8.63 ft.)

Step 3: Calculate I_k : (with l_2 = 8.63 – 8 = 0.63 ft.)

$$I_k = \left\{ 0 + 213.7 \left[\frac{8^3}{36} + \frac{8}{2}\left(0.63 + \frac{8}{3} \right)^2 \right] \right\} + 576 \left[\frac{0.63^3}{12} + 0.63(0.315)^2 \right]$$

= 12,377.26 k-ft

Step 4: Determine k_e

$$k_e = \frac{3(12{,}377.26)}{(8.63)^3}$$

= 57.77 ksf

Step 5: The converged value, k_e = 58 ksf (0.403 ksi)

Critical length (l_c)

Using the equivalent stiffness k_e the critical length is calculated as:

$$l_c = 4\left(\sqrt[4]{\frac{EI}{k_h}}\right)$$

$$= 4\left(\sqrt[4]{\frac{29{,}000(101)}{0.403}}\right)$$

= 207.69 in. (17.31 ft)

Fixed pile head is assumed as shown in Fig. 3.2-6. Since the top of the pile is at the ground level without any projection, l_u = 0. From Fig. 3.2-7, for l_u = 0 and l_c = 17.31 ft, the effective equivalent cantilever length l_e is obtained for stiffness, moment and buckling considerations. The values are given in Table 4.2-1.

Table 4.2-1 Total equivalent cantilever length (Case A)

	l_u/l_c	l_e/l_c (Fig. 3.2-7)	l_e (ft.)	Total length (L = l_u + l_e) (ft.)
Stiffness	0	0.50	0.5 (17.31) = 8.66	0 + 8.66 = 8.66
Moment	0	0.60	0.6 (17.31) = 10.39	0 + 10.39 = 10.39
Buckling	0	1.10	1.1 (17.31) = 19.04	0 + 19.04 = 19.04

Case B) Neglecting medium sand in predrilled hole (Fig. 4.2-10)

Step1: Assume k_e = 600 ksf (4.167 ksi)

Step 2: Calculate l_o : $l_o = 2\left(\sqrt[4]{EI / k_e}\right)$

$$= 2\left(\sqrt[4]{\frac{29{,}000(101)}{4.167}}\right)$$

= 57.91 in. (4.82 ft)

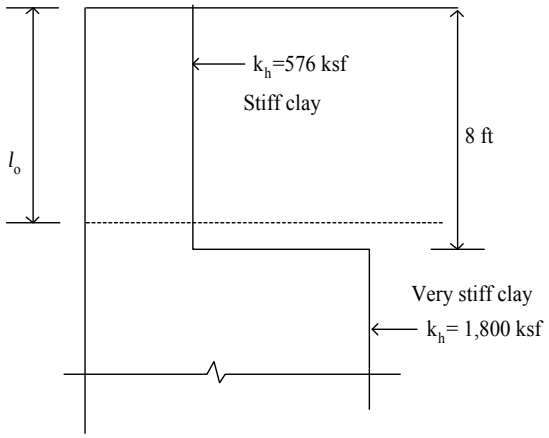

Fig. 4.2-10 Soil stiffness for case B

Step 3: Calculate I_k (with l_2 = 4.82 - 8 = -3.18 ft, however l_2 cannot be negative value and hence l_2 is taken to be zero.)

$$I_k = \frac{k_1 l_o^3}{3}$$

$$= \frac{576(4.82^3)}{3} = 21{,}500.19 \text{ k-ft}$$

Step 4: Determine k_e : $k_e = \frac{3I_k}{l_o^3}$

$$= \frac{3(21{,}500.19)}{(4.82)^3} = 576 \text{ ksf } (4.0 \text{ ksi})$$

Second Iteration

Step 2: Calculate l_o :

$$l_o = 2\left(\sqrt[4]{\frac{29{,}000(101)}{4.0}}\right)$$

= 58.5 in. (4.875 ft)

The depth of l_o is in the stiff clay layer;

hence, k_e is equal to k_h of stiff clay (k_h = 576 ksf = 4 ksi).

Critical length (l_c)

The critical length is calculated as $l_c = 4\left(\sqrt[4]{\frac{EI}{k_h}}\right)$

$$= 4\left(\sqrt[4]{\frac{29{,}000(101)}{4}}\right) = 117 \text{ in. } (9.75 \text{ ft.})$$

From Fig. 3.2-7, for l_u = 0 and l_c = 9.75 ft, the effective equivalent cantilever length l_e is obtained for stiffness, moment and buckling considerations. The values are given in Table 4.2-2.

Table 4.2-2 Total equivalent cantilever length (Case B)

	l_u/l_c	l_e/l_c (Fig. 3.2-7)	l_e (ft.)	Total length (L = l_u + l_e) (ft.)
Stiffness	8/9.75 = 0.82	0.38	9.75(0.38) = 3.71	8 + 3.701= 11.71
Moment	8/9.75 = 0.82	0.40	9.75(0.40) = 3.90	8 + 3.90 = 11.90
Buckling	8/9.75 = 0.82	0.44	9.75(0.44) = 4.29	8 + 4.29 = 12.29

4.2.4.2 Equivalent cantilever length l_e

The smaller value of the two cases, Case A and Case B, is used to determine the moment and horizontal force. Hence the effective equivalent cantilever length l_e for stiffness, moment and buckling considerations are:

$L_{stiffness}$ = 8.66 ft (104 in.)

L_{moment} = 10.39 ft (125 in.)

$L_{buckling}$ = 12.29 ft (147 in.)

4.2.5 Evaluation of Forces due to Passive Earth Pressure for Temperature and Shrinkage

The moment induced by the lateral displacement of 0.735 in. at the top of the pile due to temperature and shrinkage effect is:

$$M_T = \frac{6E_p I_p \Delta}{L_{moment}^2}$$

$$= \frac{6(29{,}000)(101)(0.735)}{(125)^2} = 826.68 \text{ kip-in.}$$

Corresponding horizontal force due to temperature and shrinkage is determined from the following:

$$H_T = \frac{12EI\Delta}{L_{stiffness}^3}$$

$$= \frac{12(29{,}000)(101)(0.735)}{(104)^3} = 23.0 \text{ kips}$$

Assuming that the bridge girder end span is simply supported, the axial force in the pile, P_T, is found by summing moments about the right end (Fig.4.2-11). Induced axial compression in the pile is determined from

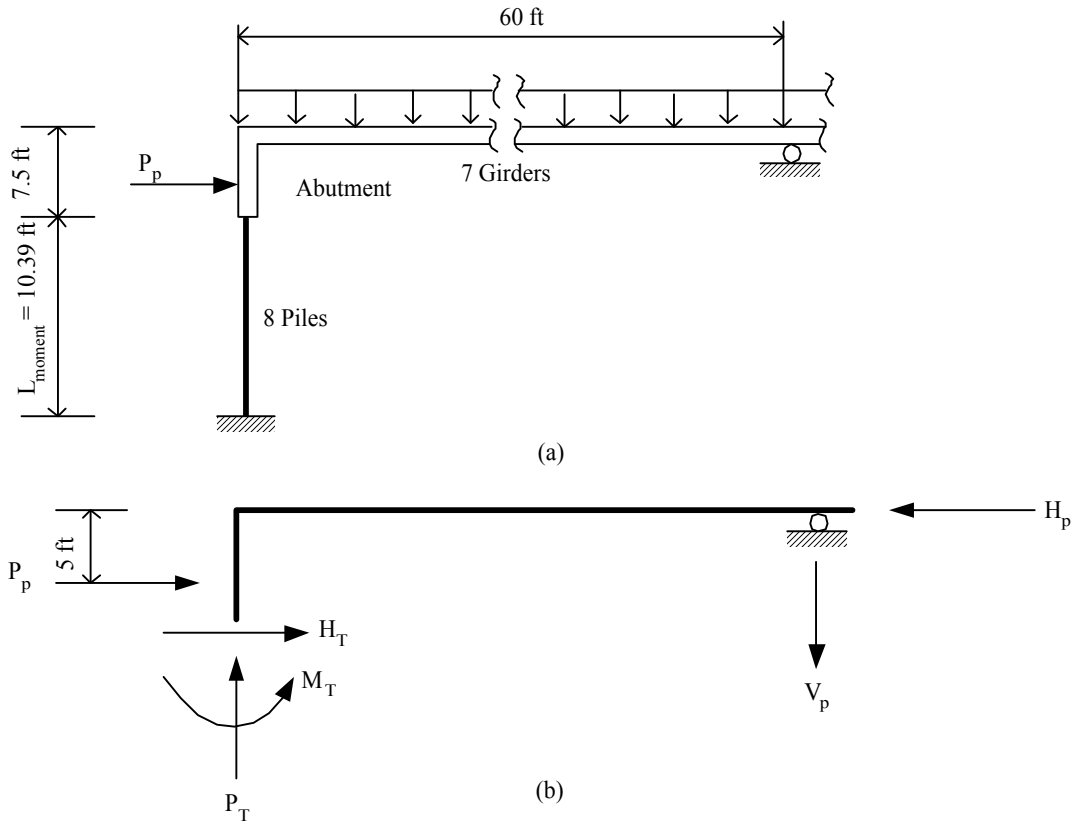

Fig.4.2-11 Idealized abutment foundation and girder endspan: (a) approximate structural model (b) free body diagram with passive soil pressure

$P_T\,(60) = P_P(5) + H_T(7.5) + M_T$

$P_T\,(60) = 85.4(5) + 23.0(7.5) + 826.68/12$

$P_T = 11.14$ kips

4.2.6 Analysis of Laterally Loaded Piles

Maximum pile reaction due to service load is obtained as 103.90 kips

Total axial force on pile including the effect of passive pressure, temperature and shrinkage

P = 103.90 + 11.14 = 115.04 kips

Secondary moment due to passive pressure, temperature and shrinkage

$M = \frac{P\Delta}{2} = (115.04)(0.735)/2 = 42.28$ k-in

H = 0 kip. (assumed as zero on conservative side)

Analysis of laterally loaded piles using LPILE

Soil properties given in Fig. 4.2-12 include effective unit weight, undrained cohesive strength, friction angle, strain corresponding to 50% of the maximum stress, ε_{50} and soil modulus parameter constant k. This constant, k has units of force per cubic length and depends on the type of soil and lateral loading imposed on the pile. Suggested values of the parameter k used for clays and sand are given in Tables 3.3-2 and 3.3-3 respectively. Tables 3.3-4 and 3.3-5 show values of strain, ε_{50} for clay and stiff clay.

The results from the LPILE analysis are given in Figs. 4.2-13 – 4.2-15. The horizontal displacement vs. depth is shown in Fig. 4.2-13. The maximum deflection is 0.0292 in. which is less than the deflection of 0.735 in. resulting from temperature and shrinkage. Figs. 4.2-14 and 4.2-15 show the variation of moment versus depth and shear versus depth respectively. The maximum stress along the pile is 9.28 ksi.

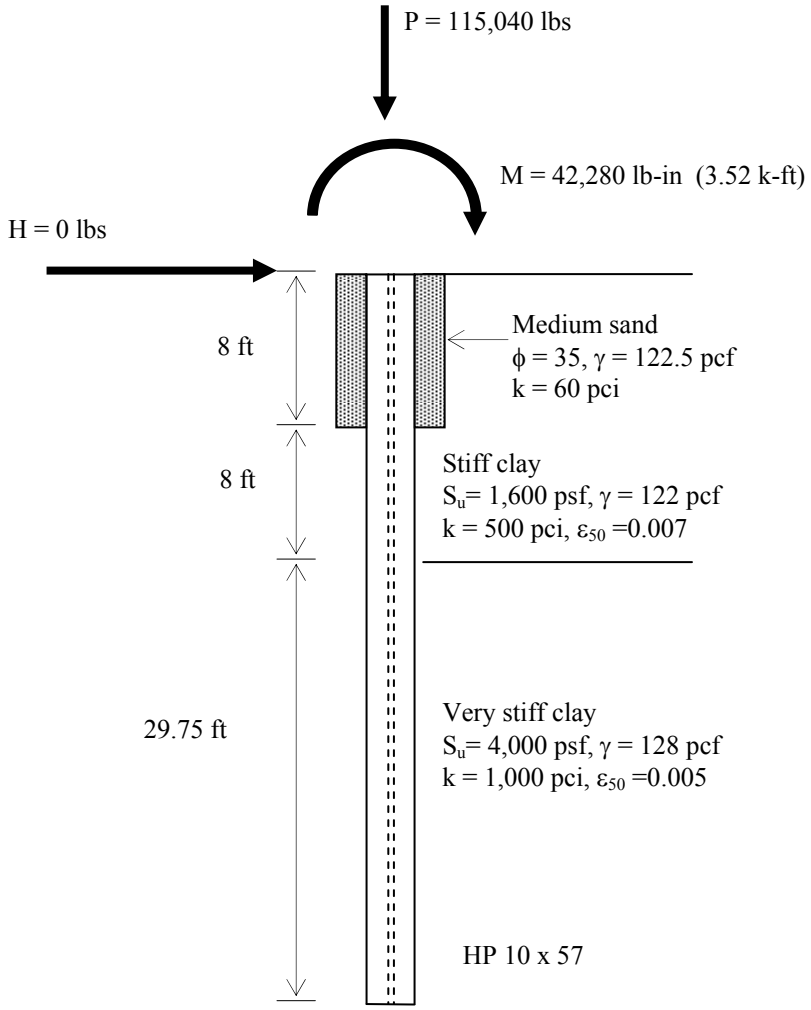

Fig. 4.2-12 Soil properties and forces on the pile

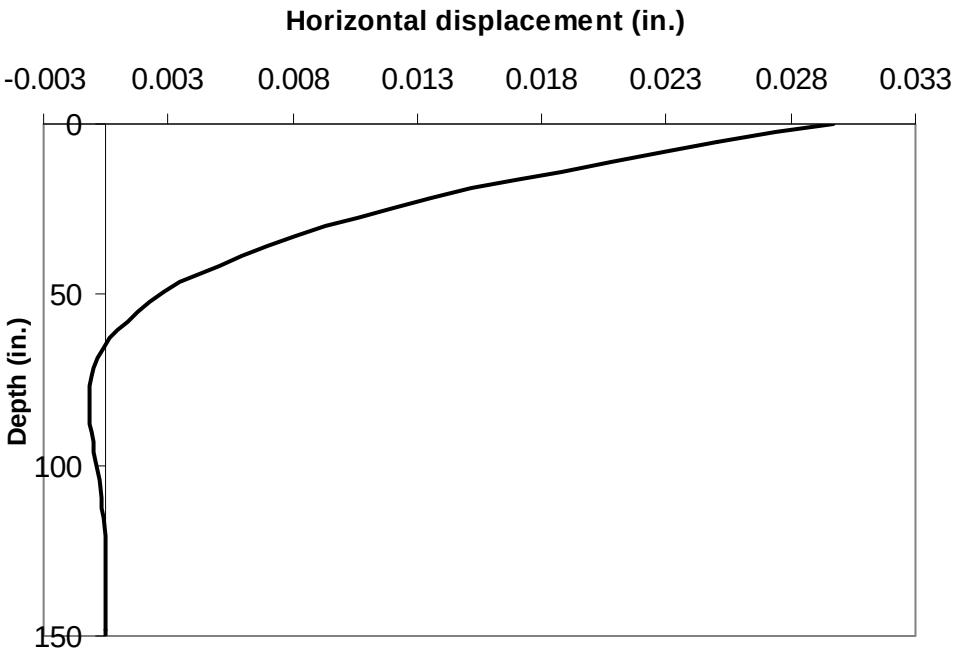

Fig. 4.2-13 Variation of horizontal displacement along the depth (LPILE)

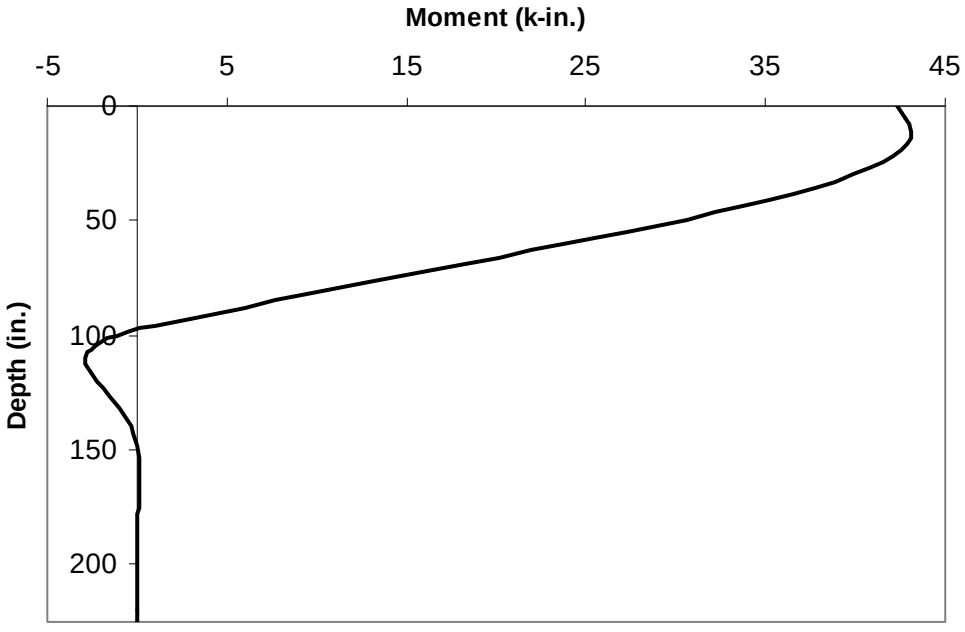

Fig. 4.2-14 Variation of bending moment along the depth (LPILE)

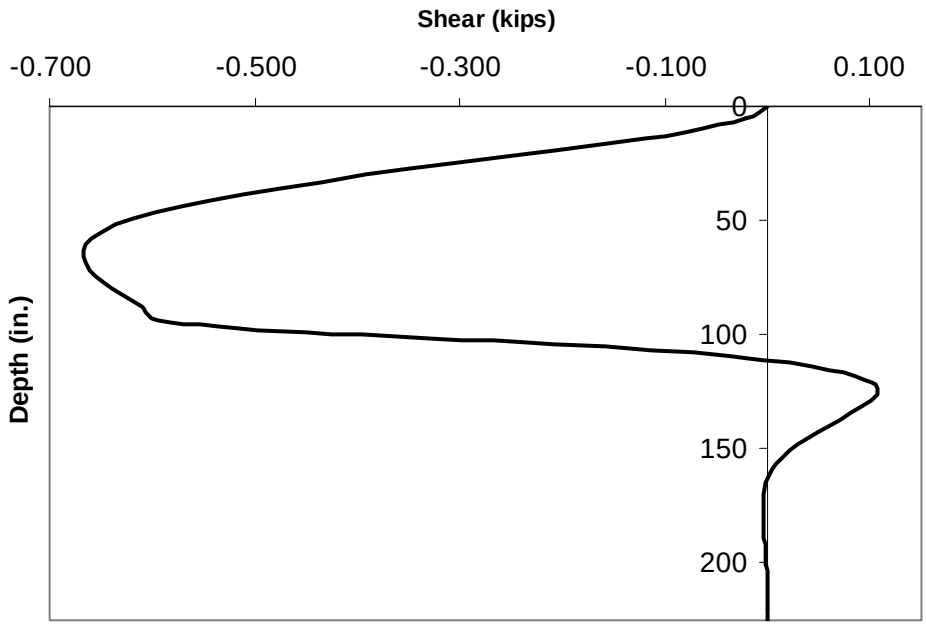

Fig. 4.2-15 Variation of shear along the depth (LPILE)

Analysis of laterally loaded piles using FB Pier

The FB-Pier v. 2.0 is also used in the analysis of laterally loaded pile. The soil data, pile properties and loading conditions are shown in Fig. 4.2-12. The maximum displacements at the top of the pile were 0.03588 in. and 0.1082 in. in the horizontal and vertical directions respectively. The shear vs. depth, and moment vs. depth are shown in Fig. 4.2-16. The maximum shear and moment in the pile are respectively 0.718 kips and 3.758 k-ft.

The maximum stress can be determined from:

Maximum stress, $\sigma_{max} = \frac{M_{max} c}{I} + \frac{P}{A}$

$$= \frac{3.758 \times 12 \times \left(\frac{10.225}{2}\right)}{101} + \frac{111.63}{16.8}$$

$$= 8.927 \text{ ksi}$$

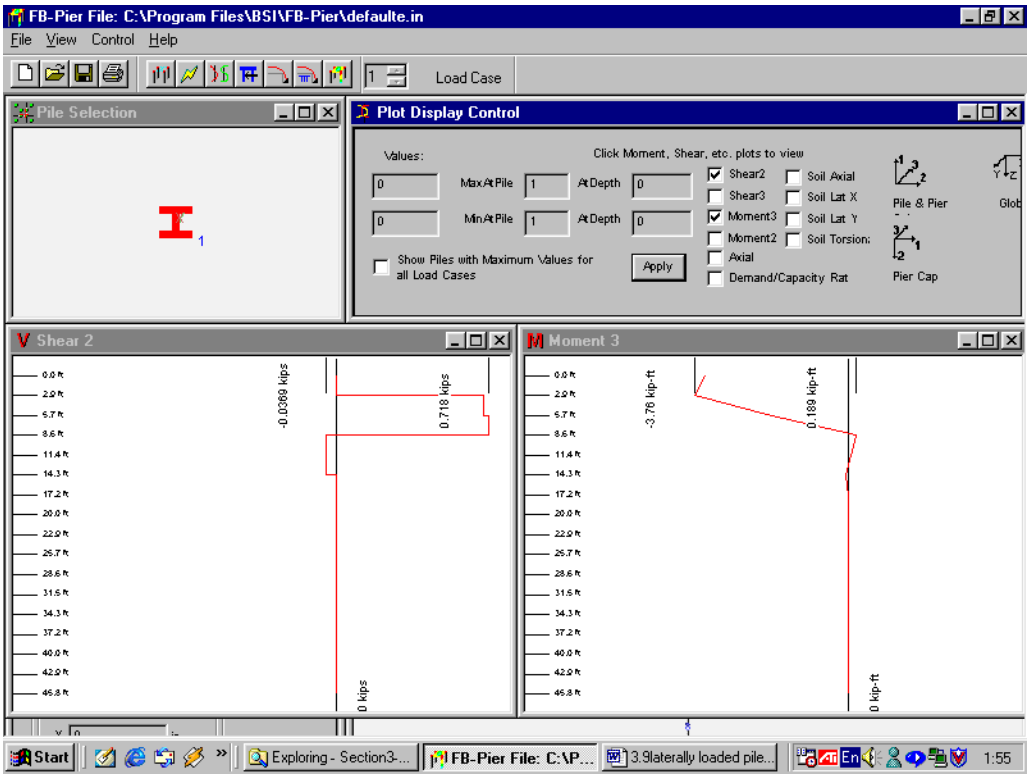

Fig. 4.2-16 Variation of shear and moment along the depth (FB-Pier)

Comparison of results

The results between LPILE and FB-Pier are compared (Table 4.2-3). The output from LPILE does not show the maximum values of axial force and vertical displacement; however, axial force can be determined using the results from LPILE analysis. The results from both programs are slightly different. LPILE gives higher values on maximum moment, shear and

horizontal displacement than FB-Pier. In contrast, the values of maximum axial force and stress from FB-Pier are higher than those based on LPILE.

Table 4.2-3 Comparison of the results based on LPILE plus 4.0 and FB-Pier v 2.0 analyses

	LPILE plus 4.0	FB-Pier v 2.0
Moment $_{max.}$ (k-in.)	43.08	45.10
Shear $_{max.}$ (kips)	0.667	0.718
Axial force $_{max}$ (kips)	115.04	111.63
Maximum horizontal displacement (in.)	0.0292	0.0359
Maximum vertical displacement (in.)	NA	0.108
Stress $_{max.}$ (ksi)	9.278	8.928

4.2.7 Parametric Study

A parametric study was carried out for the response of laterally loaded piles supporting the abutment of the integral abutment bridge under various conditions. The lateral movement of the pile is mainly a function of horizontal soil stiffness, stiffness of the pile, and presence of oversized predrilled hole filled with soil of desired stiffness (orientation of the pile). The stiffness of soil is dependent on the type of soil, depth of each soil layer, degree of compaction of the soil surround the pile, and presence of water table. The parameters considered include predrilled hole filled with sand having different degrees of compaction, different depths of predrilled hole, piles without a predrilled hole, variations in the elevation of water table, different soil types, and pile orientation. Eleven cases were considered in this study based on the identified parameters. The procedure adopted in the analysis of the pile in the *base case* is used for the

analysis of piles under various cases of the parametric study. The analytical input data are computed by considering a typical pile for an integral abutment bridge.

The results from the analyses (Table 4.2-4) including maximum moment, shear, axial force, horizontal displacement, vertical displacement and stress from LPILE and FB-Pier are synthesized and presented in Table 4.2-5 to develop a better understanding of the pile response. The results from the parametric study also serve as a guide to select, modify or revise the size of the pile for a given site condition.

Different cases of parametric study

4.2.7.1 Degrees of compaction and predrilled hole

The influence of degree of compaction, depth of predrilled hole and effect of the provision of predrilled hole are examined in *Cases I to IV*. The effect of the predrilled hole on laterally loaded pile behavior is studied based on properties of soils in the predrilled hole. Three different degrees of compaction of sand in the predrilled hole are discussed (*base case*, *Case I* and *II*) keeping the depth of predrilled hole constant. In the base case, the sand filled in the predrilled hole of 8 ft. (2.44 m) is medium compacted. The predrilled hole is filled with loose sand in *Case I*, and dense sand in *Case II*. In the parametric study, only one type of soil (sand) is considered with different degrees of compaction. However, the influence of different grades of granular fills can also be evaluated.

Two cases of different depths of predrilled hole are considered, one in the *base case* and the other in *Case III*. The degree of compaction of sand is kept constant in both cases, but the depth of predrilled hole is varied. The depth of a predrilled hole is 8 ft. (2.44 m) and 16 ft. (4.88 m) in the *base case* and *Case III*, respectively.

The influence of predrilled hole on the behavior of laterally loaded pile is examined in two different cases, *base case* in which a predrilled hole is provided, and *Case IV*, with no predrilled hole.

4.2.7.2 Water table level

Cases V, VI and *VII* examine the effect of the location of water table. In *Cases V* and *VI* water table is located at 8 ft. (2.44 m) and 16 ft. (4.88 m) below the top of the pile respectively. Water table is located below the tip of the pile in *Case VII*. The soil and pile properties for *Cases V-VII* are kept constant with the same value as used in the *base case*.

4.2.7.3 Type of soil

The behavior of laterally loaded pile is studied in different types of soil. Three cases of piles i.e., *Cases VIII, IX* and *X* are evaluated in three different soil layers – stiff clay, very stiff clay and dense sand respectively and the results are compared with the *base case*.

4.2.7.4 Pile stiffness (pile orientation)

The behavior of laterally loaded piles is examined with the orientation of pile along weak and strong axis bending while other parameters are maintained constant. In the *base case*, the pile oriented along the weak axis of bending is analyzed, whereas the pile oriented about the strong axis is analyzed in *Case XI*.

4.2.7.5 Analytical results

Horizontal displacement, variations of moment and shear along the depth of the pile for *Cases I – IV* are shown in Figs. (4.2-17) – (4.2-19). From the results shown in Table 4.2-5 (*base case, Cases I* and *II*), the horizontal displacement at the top of the pile depends on the degree of compaction of sand in the predrilled hole. The dense sand in the predrilled hole reduces the displacement at the top of the pile with a corresponding increase in stress. In the case of the pile without any predrilled hole (*Case IV*), the pile experiences a slightly higher stress compared with the piles with the predrilled hole. Hence, it may be concluded that predrilled holes with granular fill do not contribute significantly to the stress in the pile. In terms of pile length requirements, longer predrilled holes filled with medium sand (*Case III*) require longer pile lengths for a given loading condition. Although, piles without predrilled holes produce slightly higher stresses (6%), the length of the pile required is less by 11% in comparison to the piles with predrilled holes. Predrilled hole filled with sand allows pile to be more flexible, with reduction in the shear, moment and stress values.

Figs. 4.2-20 – 4.2-22 show the results from the analyses for different water table levels (*base case, Cases V, VI and VII*). Though there are variations in horizontal displacement, moment and shear along the depth of the pile, it can be seen that the variation is less than 1.5% in maximum horizontal displacement, moment, shear, and stress values among the four cases. Thus, the location of water table has very little influence on the pile response. It is, therefore, conservative to assume that the water table elevation is located at the top level of the pile in the pile analysis, which gives the maximum values among different cases.

The results from the analyses of the laterally loaded piles driven in different soil types (Figs. 4.2-23 – 4.2-25) show significant variations in maximum shear, axial force and horizontal displacement, with smaller variation in the moment. Moments are higher for piles in the order very stiff clay (*Case IX*), stiff clay (*Case VIII*), and dense sand (*Case X*) when compared to the moment for the pile driven in three different soil layers (*base case*). The axial force is low in the pile driven in dense sand and high in piles driven in very stiff clay. Very stiff clay allows a maximum displacement of 0.015 in. (0.37 mm), and the corresponding maximum displacement in dense sand is 0.066 in. (1.66 mm) (Table 4.2-5). The variation in stress between the soils seems to be about 7%. In case of pile length requirements, dense sand requires longer piles.

Significant variations in maximum shear and horizontal displacement on piles oriented along the weak and strong bending axis are observed from the analyses (*base case* and *Case XI*) shown in Figs 4.2-26 – 4.2-28. The maximum stress in the pile oriented along its strong axis is about 16% smaller than that of the pile oriented about the weak axis because of the larger section modulus. The horizontal displacement in *Case XI* is less by about 50%.

Table 4.2-4. Pile lengths and forces on the piles under service load condition

Items (1)	Base case (2)	Parametric Study Cases										
		I (3)	II (4)	*III* (5)	*IV* (6)	*V* (7)	*VI* (8)	*VII* (9)	*VIII* (10)	*IX* (11)	*X* (12)	*XI* (13)
Degree of compaction of sand in predrilled hole	Medium	Loose	Dense	Medium	N/A	Medium	Medium	Medium	N/A	N/A	N/A	Medium
Depth of predrilled hole (ft)	8	8	8	16	N/A	8	8	8	N/A	N/A	N/A	8
Pile length (ft)	45.75	45.75	45.75	63.25	40.75	45.75	45.75	45.75	47.25	21.00	93.00	45.75
Location of water table from top of pile (ft)	0	0	0	0	0	8	16	45.75	0	0	0	0
Soil type	Multiple layer	Multiple layer	Multiple layer	Multiple layer	Multiple layer	Multiple layer	Multiple layer	Multiple layer	Stiff clay	Very stiff clay	Dense sand	Multiple layer
Pile orientation	Weak axis	Weak axis	Weak axis	Weak axis	Weak axis	Weak axis	Weak axis	Weak axis	Weak axis	Weak axis	Weak axis	Strong axis
Equivalent length												
$L_{stiffness}$ (in.)	104	125	86	105	59	113	113	113	59	47	104	127
L_{moment} (in.)	125	143	103	126	70	136	136	136	70	56	125	152
$L_{buckling}$ (in.)	147	147	147	232	129	147	147	147	129	102	228	163
Service loads on pile												
Horizontal force H_T (kips)	23.00	13.35	41.26	22.16	62.15	17.78	17.78	17.78	62.15	78.15	23.06	36.89
Moment M_T (kip-in)	862.68	633.40	1225.69	809.80	1818.00	699.18	699.18	699.18	1818.0	1818.0	831.59	1624.00
Passive earth pressure P_p (kips)	85.40	85.40	85.40	85.40	85.40	85.40	85.40	85.40	85.40	85.40	85.40	85.40
Axial force due to abutment movement P_T (kips)	11.14	9.67	13.98	11.01	17.41	10.31	10.31	10.31	17.41	19.41	11.15	13.98
Axial force due to DL, LL, IM etc., P_E (kips)	103.90	103.90	103.90	103.90	103.90	103.90	103.90	103.90	103.90	103.90	103.90	103.90
Total axial force P (kips)	115.04	113.57	117.88	114.91	121.31	114.21	114.21	114.21	121.31	123.31	115.05	117.88
Secondary moment M (kip-in)	42.24	41.74	43.32	42.23	44.58	41.97	41.97	41.97	44.58	45.32	42.28	43.32
Value from interaction equation	0.254	0.253	0.256	0.298	0.257	0.254	0.254	0.254	0.257	0.252	0.303	0.228

Table 4.2-5. Summary of results from LPILE and FB-Pier analyses

Items	*Base case*	Parametric Study Cases										
		I	*II*	*III*	*IV*	*V*	*VI*	*VII*	*VIII*	*IX*	*X*	*XI*
(1)	(2)	(3)	(4)	(5)	(6)	(7)	(8)	(9)	(10)	(11)	(12)	(13)
Results from LPILE:												
Maximum moment (kip-in)	43.08	43.11	43.93	43.03	44.92	42.60	42.59	42.59	44.84	45.49	43.20	43.589
Maximum shear max (kips)	0.668	0.619	0.738	0.634	0.978	0.684	0.699	0.699	0.98	1.134	0.708	0.584
Maximum axial force (kips)	115.04	113.57	117.88	114.91	121.31	114.21	114.21	114.21	121.31	123.31	115.05	117.64
Maximum horizontal displacement (in)	0.0292	0.0466	0.0224	0.0301	0.0131	0.0245	0.0244	0.0244	0.013	0.010	0.023	0.015
Maximum stress (ksi)	9.278	9.193	9.496	9.269	9.756	9.202	9.202	9.202	9.752	9.907	9.287	7.847
Results from FB-Pier:												
Maximum moment (kip-in)	45.42	45.36	45.92	46.36	46.55	44.59	44.54	44.54	46.92	46.39	48.61	44.42
Maximum shear (kips)	0.718	0.669	0.882	0.838	1.268	0.775	0.778	0.778	1.305	1.065	0.877	0.623
Maximum axial force (kips)	111.63	110.18	114.44	110.32	118.22	110.81	109.90	109.90	117.85	119.71	106.66	113.03
Maximum horizontal displacement (in)	0.0359	0.0535	0.0292	0.019	0.019	0.031	0.031	0.031	0.022	0.015	0.066	0.018
Maximum vertical displacement (in)	0.1082	0.1065	0.1117	0.1407	0.1407	0.107	0.107	0.107	0.129	0.687	0.096	0.105
Maximum stress (ksi)	8.927	8.854	9.136	9.393	9.393	8.853	8.796	8.796	9.390	9.474	8.809	7.483

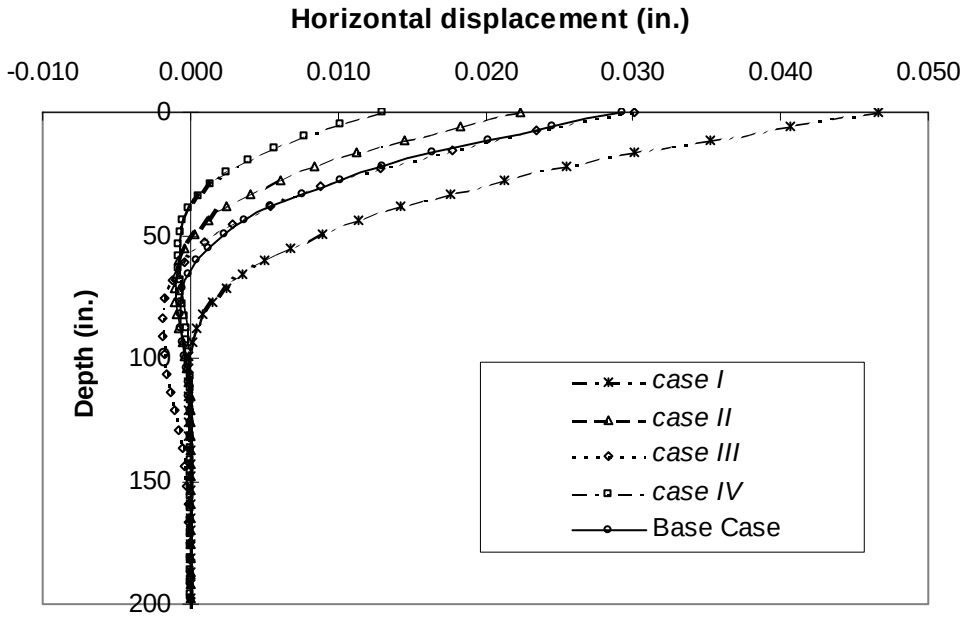

Fig. 4.2-17 Variation of horizontal displacement along the depth (Cases I-IV)

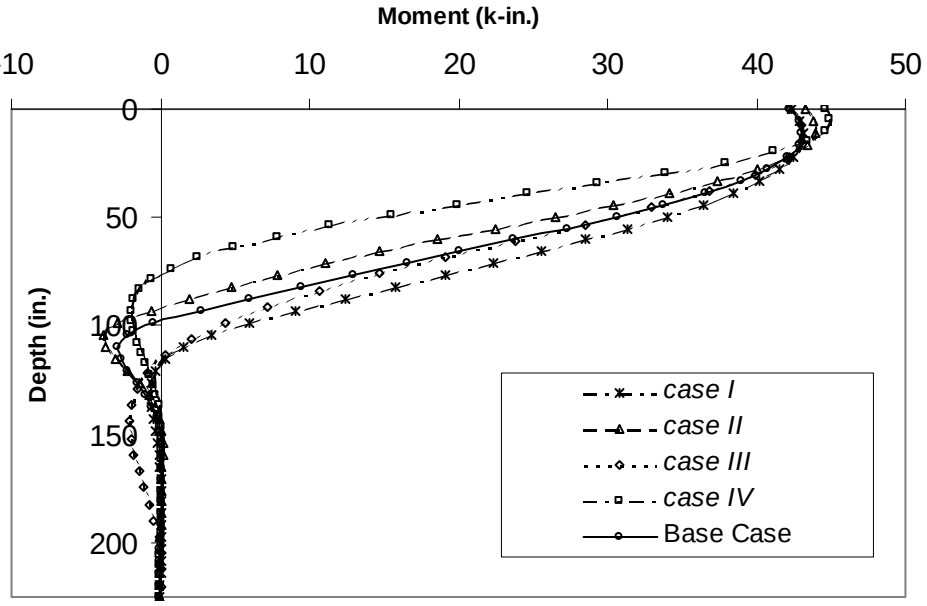

Fig. 4.2-18 Variation of bending moment along the depth (Cases I-IV)

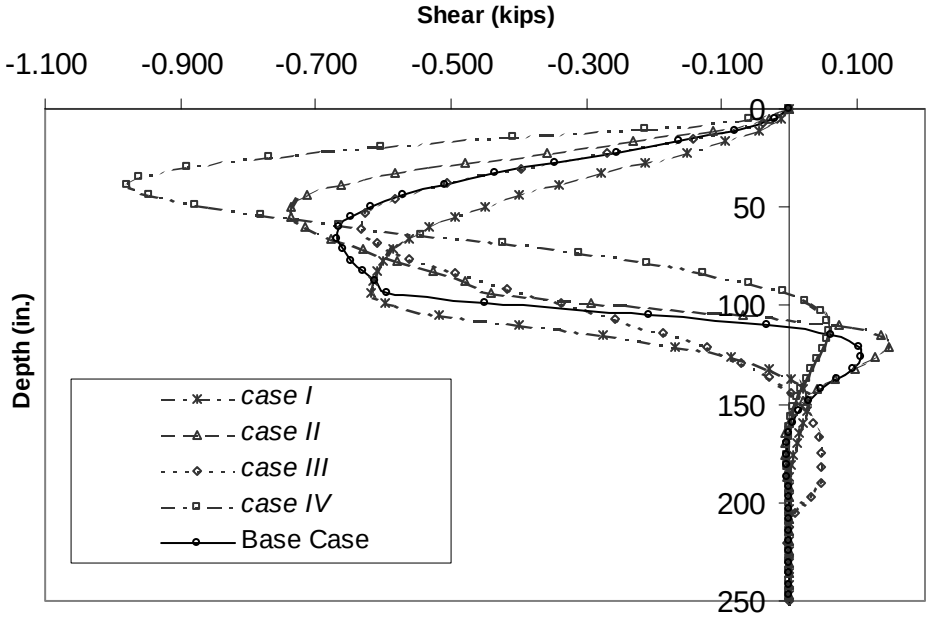

Fig. 4.2-19 Variation of shear along the depth (Cases I-IV)

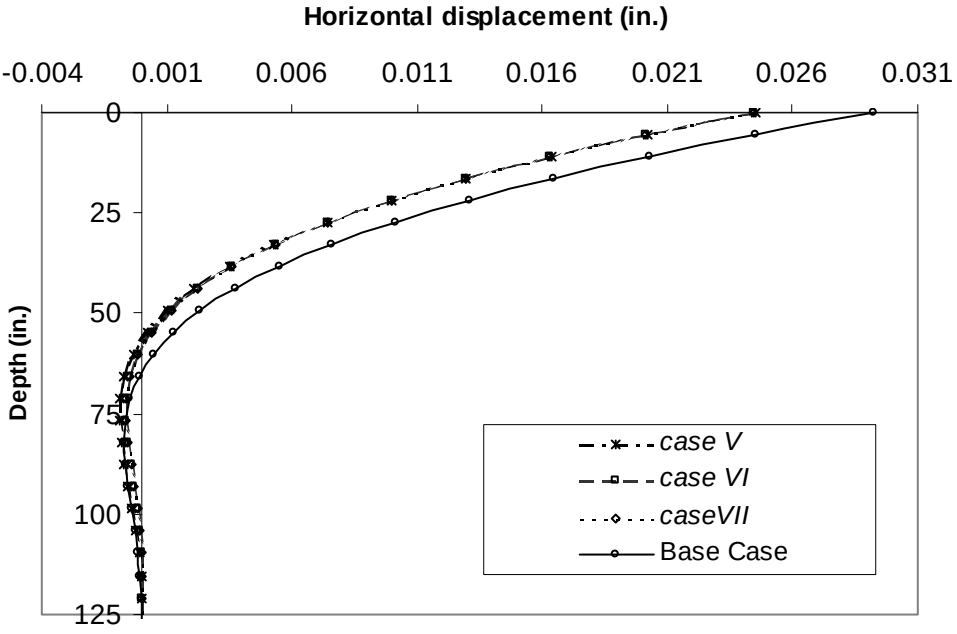

Fig. 4.2-20 Variation of horizontal displacement along the depth (Cases V-VII)

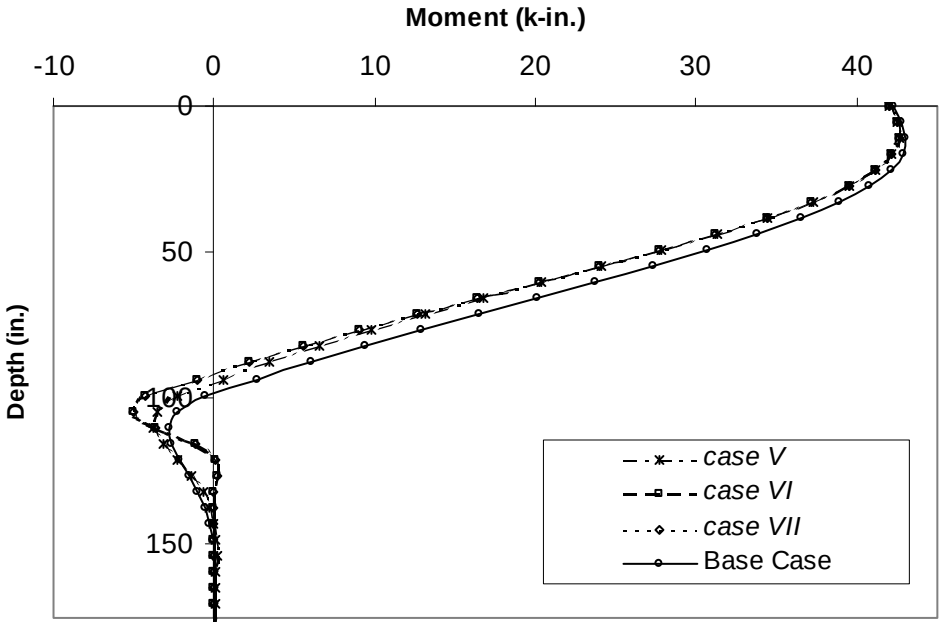

Fig. 4.2-21 Variation of bending moment along the depth (Cases V-VII)

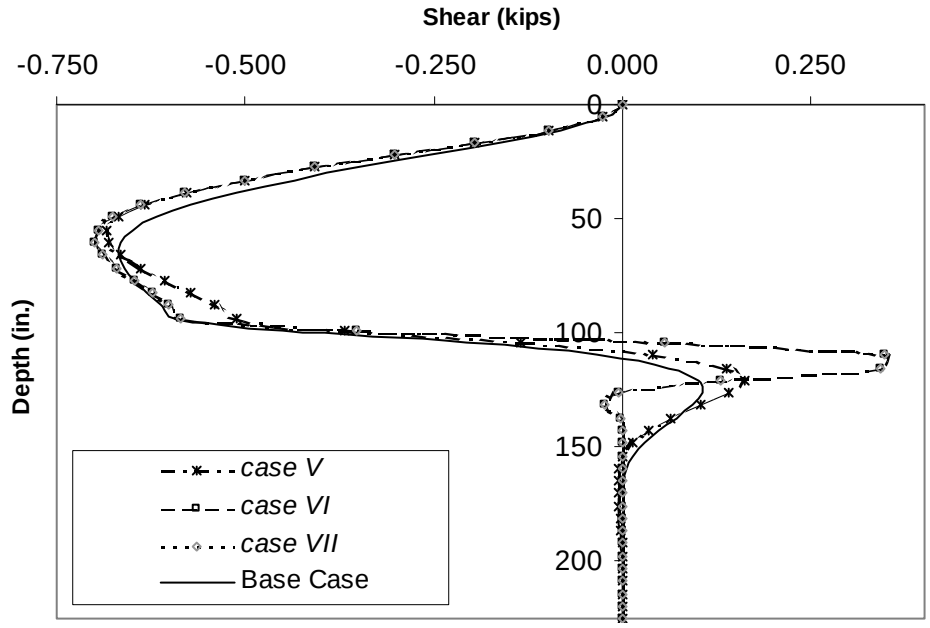

Fig. 4.2-22 Variation of shear along the depth (Cases V-VII)

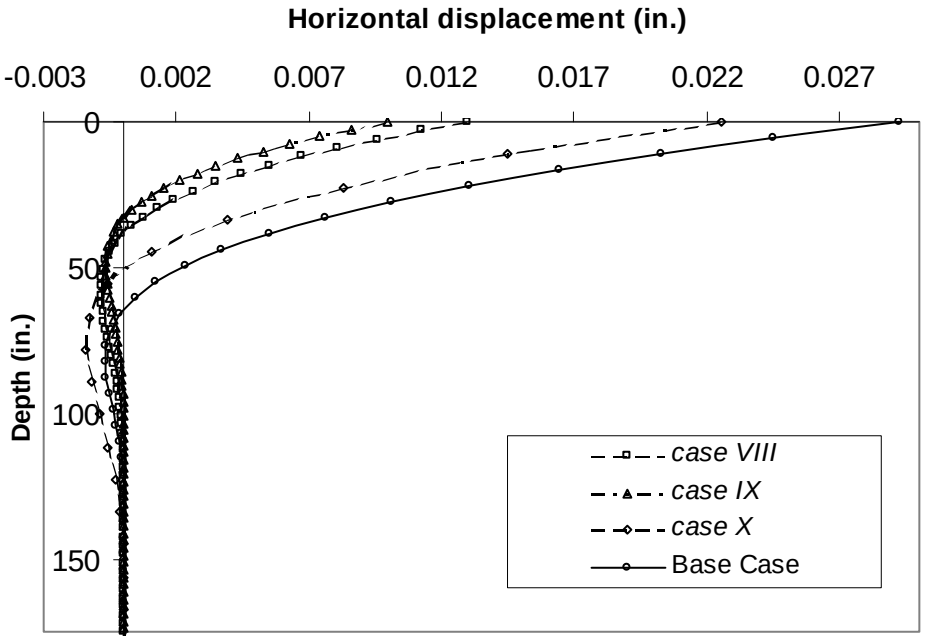

Fig. 4.2-23 Variation of horizontal displacement along the depth (Cases VIII-X)

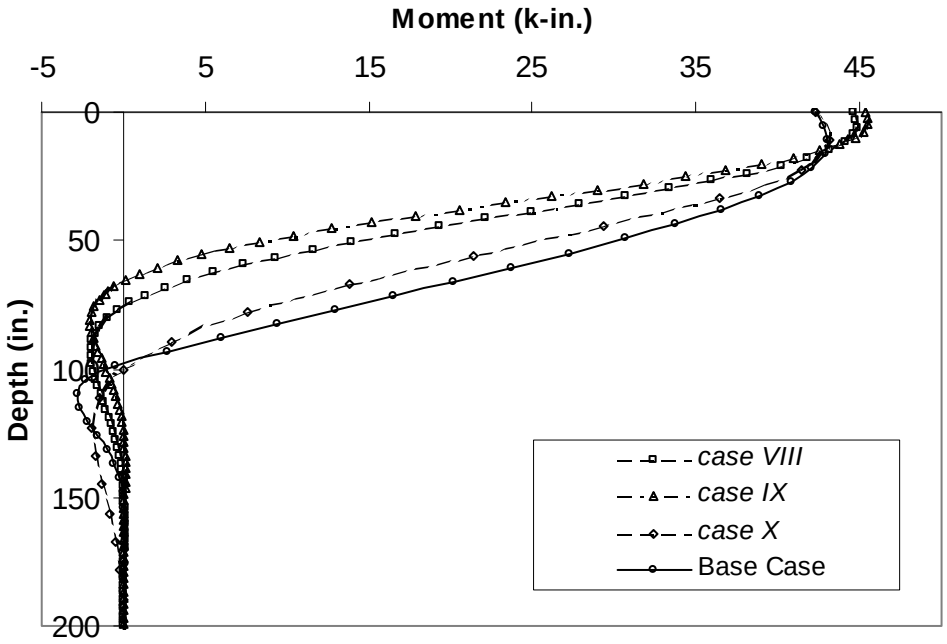

Fig. 4.2-24 Variation of bending moment along the depth (Cases VIII-X)

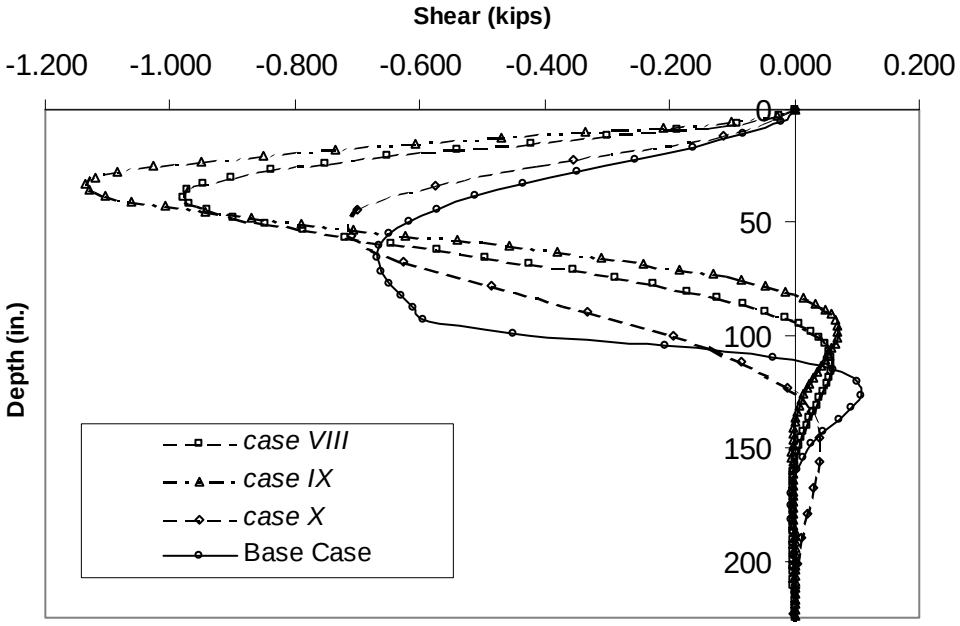

Fig. 4.2-25 Variation of shear along the depth (Cases VIII-X)

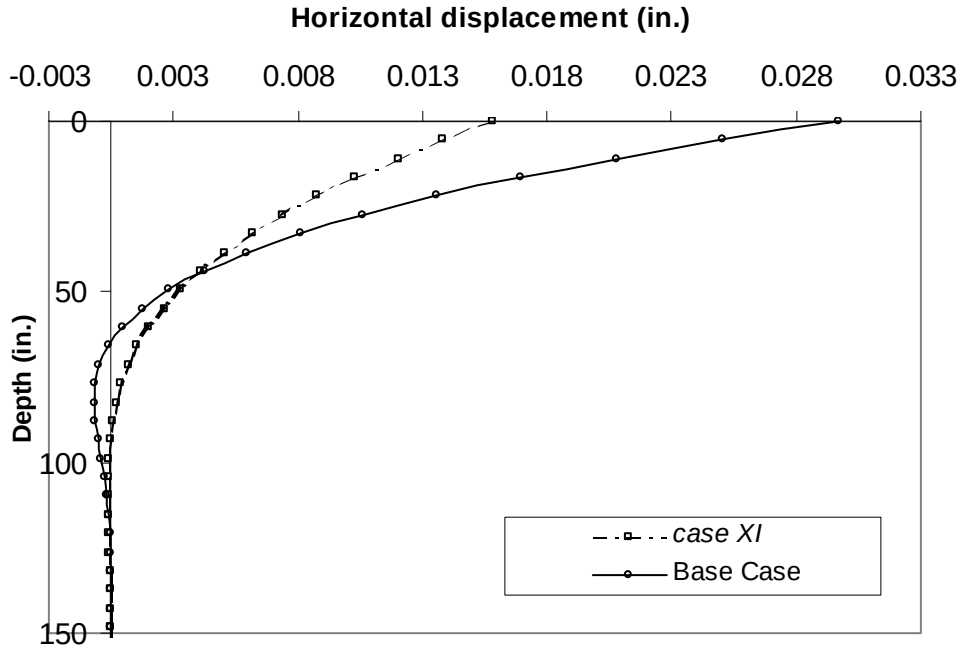

Fig. 4.2-26 Variation of horizontal displacement along the depth (Case XI)

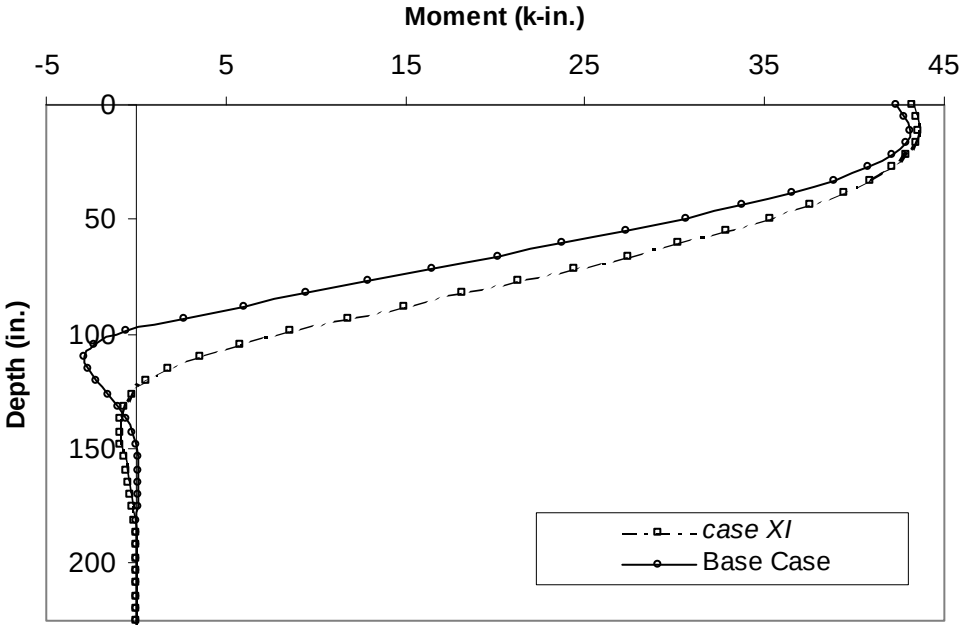

Fig. 4.2-27 Variation of bending moment along the depth (Case XI)

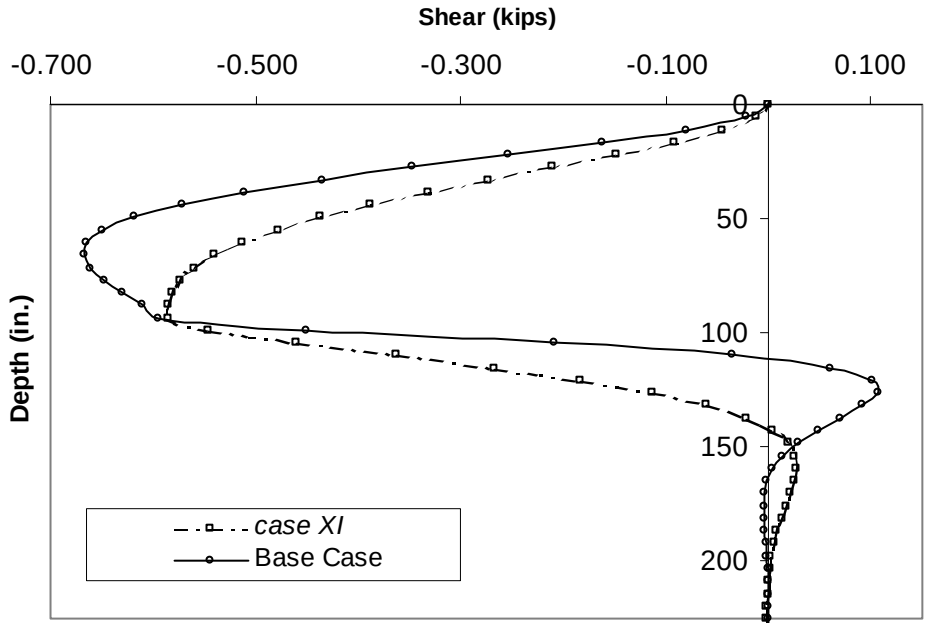

Fig. 4.2-28 Variation of shear along the depth (Case XI)

CHAPTER 5

CONCLUSIONS AND RECOMMENDATIONS

5.1 Introduction

Integral abutment type bridge structures are simple or multiple span bridges that have their superstructure cast integrally with their substructure. In the present study, the behavior of integral abutment bridges was investigated in terms of superstructure behavior due to time-dependent effects, interaction between the structural components and the soil system. A comprehensive literature review was conducted including published literature by various research institutions and current design and construction practices followed by departments of transportation.

5.2 Analysis and Design Recommendations

The recommendations for the analysis and design of integral abutment bridges are presented in the following:

5.2.1 Maximum Bridge Length

The maximum length of integral abutment bridges is determined by the soil properties, seasonal temperature variations, resistance of abutment foundations to longitudinal movements i.e., the ability of the piles supporting the abutments to withstand the bending moments and shear forces resulting from the movement of the abutments, and the type of superstructure being considered. The limiting overall lengths for steel and concrete bridges are given below:

Type of girder	Maximum structure length
Steel	640 ft. (195 m)
Caste in place or Precast Concrete	790 ft. (240 m)

5.2.2 Temperature Effects

Daily temperature variations have the greatest influence on the behavior of integral abutment bridges. Concrete, composite and all-steel superstructures can undergo daily cyclic strains in the ratio of 1:2:4.3. A temperature gradient as recommended by AASHTO can be adopted, unless site-specific temperature gradients are available. The fixed spans can be designed to accept temperature changes as internal stresses, and as a result, undergo negligible axial deformation. Consequently, the abutments can be designed to resist at-rest soil pressures. However, the amount and deformation of the wall varies depending on the relative flexural stiffness of the bridge deck, abutment wall, foundation piles and lateral stiffness of the soil behind the wall and the piles. The deformation of the abutment wall affects the limits of active and passive states. The movement associated with integral abutment bridge can also be largely

associated with seasonal thermal expansion and contraction of the superstructure. This expansion/contraction mobilizes the horizontal soil pressure. One dimensional linear thermal expansion model can be used to account for seasonal temperature effects on the superstructure, since it is simpler and requires less computation and yields reasonable accuracy for small and medium span bridges.

5.2.3 Alignment

Owing to the non-uniform distribution of loads and difficulties in establishing the movement and its direction, structures with skews greater than 35° or where an angle subtended by a 30 m arc length of the structure is greater than 5° are not considered suitable for integral abutment designs. Skews greater than 20° but not exceeding 35° may be considered, if a rigorous analysis is carried out to account for the skew effects.

The analysis for skew should consider the effects such as torsion, unequal load distribution, lateral translation, pile deflection in both longitudinal and transverse direction and increase in the length of the abutment exposed to soil pressure. The use of integral bridges can be limited to bridges with skew less than 30° to minimize the magnitude and lateral eccentricity of longitudinal forces. Curved bridges are allowed provided the stringers are straight. Beams shall be parallel to each other. All substructure units shall be parallel to each other. The maximum vertical grade between abutments shall be limited to 5%.

5.2.4 Superstructure

Adjacent prestressed box beams, prestressed concrete girders and structural steel beams may be used for integral abutment designs. The superstructure can be designed to be continuous over the intermediate supports. As a result of the structural continuity, the resulting girder design will be light and efficient. Similarly the maximum transverse stresses in the deck slab can be minimized due to continuity compared to simply supported configuration. Cracking can occur, if the continuous temperature and shrinkage reinforcement in the deck slabs over the end-diaphragms are insufficient. They shall be analyzed to determine the stresses in the beams that will result from thermal movements. Pretensioned or post tensioned concrete should have a provision for creep, shrinkage, and elastic shortening. Barrier walls above the abutments should be provided with additional reinforcement.

5.2.5 Piers

Piers for integral bridges have similar design requirements and share common design procedures with the piers of a more traditional bridge. The primary distinguishing features of the piers for an integral abutment bridge involve their ability to accommodate potentially large superstructure movements and the sharing of lateral and longitudinal forces among the substructure units. Thermal movements are usually the major concern, although superstructure movements, due to concrete creep and drying shrinkage, will also be present to some degree. As part of the overall structural system, integral abutment bridge piers will typically be required to carry a portion of the externally applied longitudinal and transverse loads on the bridge. Piers

should be flexible and supported on the flexible foundations, if made integral with the deck diaphragms.

5.2.6 Abutment

The abutment and pile design can be assumed that the girders transfer all moments and vertical and horizontal forces that are produced by the superimposed dead load, live load plus impact, earth pressure, temperature, shrinkage, creep and seismic loads. The transfer of these forces can be considered to be achieved after the rigid connection to the abutments is made. The rigid connection can be detailed to resist all applied loads. Abutments can be designed to resist the forces and end moments from the girders and transfer the loads to the foundation.

The height of the abutment should be kept as short as possible to reduce the soil pressure. Abutments of equal height are recommended to eliminate the unbalanced lateral load resulting from sidesway. The concrete abutment contains sufficient bulk to be considered as a rigid mass. A positive connection with the ends of the beams or girders is provided by rigidly connecting the beams or girders and by encasing them in reinforced concrete. This provides for full transfer of temperature variation and live load rotational displacement to the abutment piling. Forces that are induced by resistance to movements must be proportioned among all substructure units, since rotations of the superstructure induce movements in the piles.

5.2.7 Wing Walls

Wing walls may be attached to the abutment with tie rods capable of resisting lateral earth pressure. Since the wing wall attached with the abutment will move along with the movement of the bridge, the size of the wing walls may be kept as minimum as possible in order to allow the substructure to move with minimum resistance. The orientation of the wing wall may be such that it offers less resistance to the movement of the abutment, i.e., preferably parallel to the deck axis.

5.2.8 Approach Slab

Approach slabs should be provided in order to prevent vehicular traffic from consolidating the backfill adjacent to abutments, to eliminate live load surcharging of backfill, and minimize the adverse effect of consolidating backfill and approach embankment on movement of vehicular traffic. For bridges with closed decks (curbs, barriers, etc.,), approach slab should be provided with curbs to confine and carry deck drainage across backfill to the approaches and prevent erosion, or saturation and freezing of the backfill. Because of the continual cyclic movement of integral bridges, approach slabs must be anchored to the abutments; otherwise, continual bridge movement and joint infiltration will shift slabs toward flexible approach pavement, away from abutments and off the approach slab seats. Approach slabs shall be at least as long as the height of the integral abutment wall. The farther end of the approach slab shall rest on a sleeper slab. The approach slab shall be designed as a structural slab that is supported at each end. The foundation for the sleeper slab shall be founded on undisturbed

compacted material. The detailing of the joints at the ends of the approach slabs plays an essential role in the determination of its ductility and rotational capacity. In case of a skewed bridge, the end of the approach slab shall be parallel to the skew.

5.2.9 Cycle Control Joints

Cycle control joints, which facilitate longitudinal cycling of bridges and approach slabs, should be provided between approach slabs and approach pavement. For shorter bridges, the usual pavement expansion joints should be sufficient; however, for longer bridges, specially designed cycle control joints should be provided.

5.2.10 Embankments

Since integral abutment bridges receive significant support from embankments, such bridges should be built only in conjunction with stable, well-consolidated embankments. Consequently, integral bridge embankments must be constructed first to ensure that embankments and foundation soils are consolidated and stabilized before the flexible pier and abutment piles are driven.

5.2.11 Piles

Piles can be modeled using equivalent cantilever idealization approach based on Winkler soil idealization owing to its simplicity. Since the sub-soils are not always homogeneous, soil

stiffness may not be constant and vary with depth. Hence, for a non-uniform soil, equivalent soil stiffness can be assumed.

As regard to the provision of predrilled holes for the piles, the piles can be provided with predrilled holes, if the stresses developed in the laterally loaded piles are greater than the allowable stresses. Where piles are driven in dense and stiff soils, pre-augured holes filled with loose sand shall be provided to reduce resistance to lateral movement.

Steel piles are preferred due to its ductility and durability. Steel H piles in single row are generally used to support the integral abutment. The top of the piles can be embedded at least 2 ft. (600 mm) into the abutment walls and adequately reinforced to transfer the bending moments. There is no universally accepted pile orientation for steel H piles. The orientation of piles along weak or strong axis, depends on the laterally loaded pile stresses. A weak axis orientation is more flexible and allows larger lateral movements. For structures where movement and loading requirements are such that piles can be designed within the elastic range, it is suggested that the connection should be considered as fixed and piles placed with the strong axis normal to the direction of movement. If the pile resistance exceeds the elastic range, the connection may be assumed as pinned, and piles should be placed with weak axis normal to the direction of movement. Abutments will be in more jeopardy if the piles are stiff; hence, piles should be flexible and have sufficient length (say at least 15 ft.) to provide required flexibility. Where load bearing strata is near the surface or where the use of short piles, less than 15 ft. (5.0 m) in length, or caisson is planned, the site is not considered suitable for integral abutment bridges.

5.2.12 Backfill

The backfill material behind the abutment wall should accommodate the lateral movement of the bridge without producing large stresses to the bridge system. No loose backfill is allowed, since the backfill, in due course of time due to cyclic temperature loading, tends to densification and granular flow. This soil densification and granular flow increase the soil stress acting on the wall. A free-draining granular backfill can be used in order to avoid saturation and formation of ice.

5.2.13 Drainage

To ensure a successful and durable design, good drainage details must be incorporated. The goal should be to minimize the amount of water from the deck, or the approach highway that will go over the approach slab, and also ensure that joints around the approach slab are well sealed to prevent water infiltration. Even the best attempt to seal joints cannot prevent some leakage from time to time between maintenance cycles. Therefore, it is important to design a secondary system of sub-soil weeping drains to collect, channel and remove the seepage. A proper drainage of both the abutment wall and approach slab is necessary to ensure that no ice is built-up and the backfill material not washed away.

5.2.14 General Considerations

Integral abutment bridges shall be designed to resist all the vertical and lateral loads acting on them. The load effects at various stages of construction should be considered in the design. The stages at which the structure is simply supported, then made integral with abutments and backfill are of primary importance.

Caution should be exercised in the design of substructures to minimize damage in the event of an earthquake.

Rigid utility conduits, such as gas, water and sewer, are discouraged for use with integral abutments. If they are used, expansion joints in the conduits must be provided at each abutment. Sleeves through the abutment should provide at least 2 in. (50 mm) clearance all around the conduit. Flexible conduits for electrical or telephone utilities that are properly equipped with an expansion sleeve through the integral abutment are acceptable.

5.3 Future Research Needs

Integral abutment bridges provide bridge engineers an economical and attractive design alternative to the traditional design of bridges with thermal expansion joints. As a rehabilitation alternative, it is possible to convert a non-integral abutment bridge into an integral abutment bridge. Successful implementation of integral abutment bridge construction requires attention to the construction sequence by the designer and good guidance to the contractor in the contract

documents. Construction sequence should be developed suited to each application. The future research needs are described below:

- Studies on the combined effects of actual rotations, translations, skews, and horizontal curvature.
- Performance evaluation of integral bridges for its susceptibility to fatigue.
- Effects of different types of foundations, heights of the abutment, wing wall configurations.
- Procedures for rehabilitation of existing bridges to convert into integral abutment bridges.

REFERENCES

1. AASHTO, "LRFD Bridges Design Specification," *2nd ed., American Association of State Highway and Transportation Officials*, Washington, DC, 1998.

2. Abenderoth, R.E., and Greimann, L.F., "The Design of Piles in Integral Abutment Bridges," Synopsis, Bridge Engineering Center, Department of Civil and Construction Engineering, *Iowa State University*, 1983.

3. Abendorth.R.E., Greimann, L.F., and Ebner, P.B. "Abutment Pile Design for Jointless Bridges", *Journal of Structural Engineering, Vol. 115, No. 11, November 1989*, pp. 2914-2929.

4. American Concrete Institute (ACI) Report No. ACI 209R-82 on "Prediction of Creep, Shrinkage and Temperature Effects in Concrete Structures", a report by ACI Committee 209, 1982 and subsequent revisions, 1992.

5. American Iron and Steel Institute (AISI), "Integral Abutments for Steel girders," *Highway structures design handbook, Vol. II, Chapter 5*, October 1996.

6. Arockiasamy, M., Butrieng, N., and Sivakumar, M., State-of-the-art of Integral Abutment Bridges: Design and Practice, under publication in the *Journal of Bridge Engineering*, April, 2003.

7. Arsoy, S., Barker, R.M., and Duncan, J.M., "Behavior of Integral Abutment Bridges" *Virginia DOT, Report No. FHWA/VTRC 00-CR3, November 1999.*

8. Bradford, M.A., and Gilbert, R.I. “Non-Linear Behavior of Composite Beams at Service Loads”, *Structural Engineer, Journal of the Institute of Structural Engineers, Vol. 67, No 14, 1989,* pp 263-268.

9. Bradford, M.A., “Deflection of Composite Steel-Concrete Beams Subject to Creep and Shrinkage”, *ACI Structural Journal Vol. 88, No 5, 1991,* pp 610-614.

10. Bradford, M.A and Gilbert, R.I., “Composite Beams with Partial Interaction Under Sustained Loads”, *Journal of Structural Engineering, Vol. 118, No 7, 1992*, pp 1871-1883.

11. Briaud,Jean-Louis, James,R.W., and Hoffrnan,S.B., “Settlement of Bridge Approaches (The Bump at the End of the Bridge)” *National Academy Press, Washington, D.C., 1997,* pp. 75

12. Burke, M.P.Jr., “ Bridge Approach Pavements, Integral Bridges, and Cycle control Joints”, *Transportation Research Record, 1113, 1987.* Pp 54-65.

13. Burke, M.P.,Jr., “Bridge Deck Joint” *NCHRP Synthesis of Highway Practice, September, 1989.*

14. Burke, M.P.Jr., “The Design of Integral Concrete Bridges”, *Concrete International, June 1993,* pp 37-42.

15. Burke, M.P.Jr., “Integral Bridges” *Transportation Research Record, No. 1275, 1990,* pp.53-61.

16. Churchward, A., and Sokal, Y.J., “Prediction of Temperatures in Concrete Bridges” *Structural Engineering,, Vol. 107 ST11,.November. 1981,* pp. 2163-2176

17. Colorado Dept. of Transportation, “*Bridge Design Manual,*” Denver, Colorado

18. Cruz, P.J.S., Mari, A.R., and Roca, P., "Nonlinear Time Dependent Analysis of Segmentally Constructed structures", *Journal of Structural Engineering, Vol. 124, No 3, 1998,* pp 278-287.

19. Destrebecq, J.F., and Jurkiewiez, B., " A Numerical Method for the Analysis of Rheologic Effects in Concrete Bridges" *Computer Aided Civil and Infrastructure Engineering 16, 2001*, pp 347-364.

20. Dezi, L., and Tarantino, A.M., " Creep and Composite Continuous Beams. Part I Theoretical Treatment, *Journal of Structural Engineering, Vol. 119, No 7, 1993,* pp 2095-2111.

21. Dezi, L., and Tarantino, A.M., " Creep and Composite Continuous Beams, Part II, Parametric Study, *Journal of Structural Engineering, Vol. 119, No 7, 1993,* pp 2112-2133.

22. Dicleli, M., "Simplified Model for Computer-Aided Analysis of Integral Bridges", *Journal of Bridge Engineering, Vol. 5, No 3, 2000,* pp 22-30.

23. Dicleli, M., "A Rational Design Approach of Prestressed-Concrete Girder Integral Bridges", *Computer and Structures, Vol. 22, 2000,* pp 230-245.

24. Elbardy.M.M., and Ghali.A. "Temperature Variations in Concrete Bridges" *Journal of Structural Engineering, Vol. 109, No.10, October 1983*, pp.2355-2374

25. Emanuel.J.H., and Husley.J.L., "Temperature Distributions in Composite Bridges" *Structural Engineering, Vol. 104 ST1, January 1978,* pp. 65-78

26. Federal Highway Administration, "Integral, No-Joint Structures and Required Provisions for Movement," *FHWA Technical advisory T 5140.13, January 1980*.

27. *FB-Pier Users Guide and Manual*, Florida DOT and FHWA, Contract # DTF61-95-C-00157, August 2001.

28. Gangarao, H.V.S., and Zelina, T.R., "Development of Economical Low-Volume Road Bridges" *Journal of Structural Engineering, Vol. 114, No. 9, September 1988*, pp.1941-1961.

29. Gilbert, R.I and. Bradford, M.A., "Time-Dependent behavior of Continuous Composite Beams at Service Loads", *Journal of Structural Engineering, Vol. 121, No 2, 1995*, pp 319-327.

30. Girton, D.D., Hawkinson, T.R., and Greimann, L.F., "Validation of Design Recommendations for Integral Abutment Piles", *Journal of Structural Engineering, Vol. 117, No.7, July 1991*, pp. 2117-2134.

31. Greimann, L.F., et al, " Pile Design and Tests for Integral Abutment Bridges," *Final report, Iowa DOT project HR-273 ERI project 1780, Iowa State University*, Ames, Iowa, December 1987.

32. Greimann, L.F., and Wolde-Tinsae, A.M., "Abutment Pile Design for Jointless Bridges," *ASCE Journal of Structural Engineering, Vol. 114, No. 6, June 1988.*

33. Hambly, E.C., "Integral Bridge" *Proceeding of Institution Civil Engineering Transportation, February 1997*, pp. 30-38

34. Holombo, "Continuity of Precast Prestressed Spliced-Girder Bridges Under Seismic Loads" *PCI Journal, March-April 2000*, pp. 40-63.

35. Hoppe, E. J. and Gomez, J. P., "Field Study of an Integral Backwall Bridge" *Virginia Transportation Research Council, VTRC 97-R7, October 1996.*

36. Husaain, I., and Bagnariol, D., “Design and Performance of Jointless Bridges in Ontario-New Technical and Material Concepts” *Transportation Research Record, No. 1696,* pp. 109-121.

37. Husaain, I., and Bagnariol, D., “Integral Abutment Bridges” *Report SO – 96 – 01,* Ministry of Transportation, Ontario, Canada. 1996.

38. Hyo-Gyoung, K., et al., “Effects of Slab Casting Sequences and the Drying Shrinkage of Concrete Slabs on the Short-term and Long term Behavior of Composite Steel Box Girder Bridges.. Part 2”. *Engineering Structures Vol.23, 2000*, pp 1467-1480

39. Hyo-Gyoung, K. and Fillippou, F.C., “Nonlinear FE Analysis of R/C Structures under Monotonic Loads.” *Computers and Structures Vol. 65 No 1 1997*, pp 1-16.

40. Kamel, M.R., Benak, J.V., Tadros, M.K., and Jamshidi, M.“Prestressed Concrete Piles in Jointless Bridges” *PCI Journal, March-April 1996*, pp. 56-67.

41. Kunin, J., and Alampalli, S. “Behavior of Abutment Piles in an Integral Abutment, in Response to Bridge Movements” *Transportation Research Record, No. 903, 1983*, pp.72-79.

42. Kunin, J., and Alampalli, S., “Integral Abutment Bridges: Current Practice in Unites States and Canada” *Journal of Performance of Constructed Facilities, Vol. 14 No 3, 2000,* pp 104-111.

43. Lawver, A., French,C., and Shield, C.K., “Field Performance of Integral Abutment Bridge”, *Transportation Research Record, 1740, 2000,* pp 108-117.

44. Loveall, B.M. “Jointless Bridge Deck” *Civil Engineering, November 1985*, pp.64-67.

45. Ma, Z., Huo, X., Tadros, M.K., Baishya, M., " Restraint Moments in Precast/Prestressed Concrete Continuous Bridges, *PCI Journal, Nov.-Dec. 1998,* pp 40-57.

46. Mari, A.R., and Valdes, M., "Long-Term Behavior of Continuous Precast Concrete Girer Bridge Model", *Journal of Bridge Engineering, Vol. 5, No 1, 2000,* pp 22-30.

47. Moorty, S., and Roeder, C.W., "Temperature Dependent Bridge Movements" *Structural Engineering, Vol. 118, No. 4, April 1992*, pp. 1090-1105.

48. Mourad, S., and Tabsh, S.W., " Deck Slab Stresses in Integral Abutment Bridges", *Journal of Bridge Engineering, Vol. 4., No 2, 1999,* pp 125-130.

49. New Jersey Dept. of Transportation, "*Design Manual Bridges and Structures,*" Trenton, New Jersey, 1987.

50. New York Dept. of Transportation, "*Bridge Design Manual*," *2nd ed.*, Albany, New York, April, 1999.

51. Oesterle, R. G., Tabatabai, H., Lawson, T. J., Refai, T.M., Volz, J. S., and Scanlon, A. "Jointless and Integral Abutment Bridges Summary Report" CTL of Skokie, IL, to be published, under review by *FHWA, 1998.*

52. LPILE Computer Program, Reese, L.C. et al, "LPILE Plus Version 4.0 User's Guide," *Ensoft, Inc*., Austin, Texas, 2000.

53. Richart, Jr. F.E., Hall, Jr. J.R., and Woods R.D., "Vibrations of Soils and Foundations", Prentice-Hall, Inc., Englewood Cliffs, NJ, 1970, p 414.

54. Rowe, P. W. "A stress-strain Theory for Cohesionless Soil with Applications to Earth Pressure at Rest and Moving Walls" *Geotechnique, The Institution of Civil Engineers, London, Vol. 4, No. 2, 1954,* pp. 70-88.

55. Saleh., Einea, A., Tadros, M.K., " Creating Continuity in Precast Girder Bridges", *Concrete International, August 1995,* pp 27-32.

56. Samra, R.M., "Renewed Assessment of Creep and Shrinkage Effects in Reinforced Concrete Beams", *ACI Structural Journal Vol. 94,No. 6, 1997,* pp 745-751.

57. Schaefer, V.R., and Koch, J.C. "Void Development Under Bridge Approaches" Report SD90-03, South Dakota Dept. of Transportation, Office of Research, November, 1992

58. Siros K.A., and Spyrakos C.C. " Creep Analysis of Hybrid Integral Bridges", Transportation Research Record No. 1476, 1995, pp 147-154.

59. Sivakumar, M and Arockiasamy, M., Modeling of Creep, Shrinkage and Temperature Effects in Integral Abutment Bridges, Proceedings of the Ist Concrete Bridge Conference, Nashville, October 2002.

60. Soltani, A.A., and Kukreti, A.R. "Performance Evaluation of Integral Abutment Bridges" Transportation Research Record, No. 1371, 1992, pp. 17-25

61. Tabsh, S.W., " Design Consideration s for Post-Tensioned Integral Pier Caps", Proceedings of the Structural Congress, XIV, 1996, pp 444-451.

62. Tarantino, A.M., and Dezi, L., "Creep Effects in Composite Beams with Flexible Shear Connectors", Journal of Structural Engineering, Vol. 118, No 8, 1992, pp 2063-2081.

63. Thomson, Jr. T. A., and Lutenegger, A. J., "Passive Earth Pressure Tests on Integral Bridge Abutment" Proceedings of the 4th International Conference on Case Histories in Geotechnical Engineering,1998, pp. 733-739.

64. Vandewalle, L.,“Concrete Creep and Shrinkage at Cyclic Ambient Conditions”, Cement and Concrete Composites Vol. 22, 2000, pp 201-208.

65. Wasserman, E.P. and Walker, J.H., “Integral Abutments for Steel Bridges” Highway Structures Design Handbook, Vol. II, Chap. 5, October 1996. Tennessee Department of transportation.

66. Whitman, R.V., and Richart, F.E., Jr., “Design Procedures for Dynamically Loaded Foundations”, Journal of Soil Mechanics and Foundation Division, ASCE, Vol. 93, No. SM 6, Nov. 1967, pp 169-193.

67. Wilson, J. C., “Stiffness of Non-skew Monolithic Bridge Abutments for Seismic Analysis”, Earthquake Engineering and Structural Dynamics, Vol. 16, 1988, pp. 867-883.

68. Wolde-Tinsae, A.M., and Greimann, L.F., “General Design Details for Integral Abutment Bridges”, Civil Engineering Practice, fall 1988, Journal of Boston Society of Civil *Engineers Vol. 3 No 2, 1988*, pp 7-20.